AFCRL-70-0226

Research on Extremely Low Frequency Propagation with Particular Emphasis on Schumann Resonance and Related Phenomena

Part II: LOCATION OF SOURCES

by

JOHN TOOMEY and CHARLES POLK

Contractor: University of Rhode Island, Kingston, Rhode Island 02881

Contract No. AF 19(628)-4950

Project No. 5631
Task No. 563110
Work Unit 56311001

Final Report, Part II

Period Covered: 15 January 1965 to 15 November 1969

1 April 1970

Contract Monitor: Kurt Toman
Ionospheric Physics Laboratory

Prepared

for

AIR FORCE CAMBRIDGE RESEARCH LABORATORIES

Office of Aerospace Research
United States Air Force

Bedford, Massachusetts, 01730

172

DISCLAIMER NOTICE

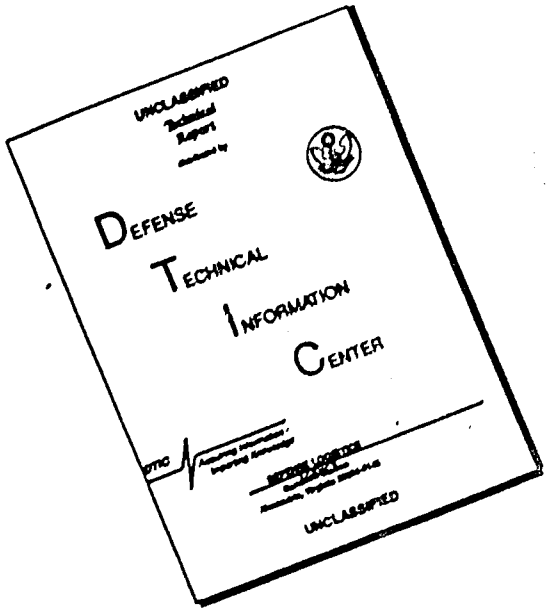

THIS DOCUMENT IS BEST QUALITY AVAILABLE. THE COPY FURNISHED TO DTIC CONTAINED A SIGNIFICANT NUMBER OF PAGES WHICH DO NOT REPRODUCE LEGIBLY.

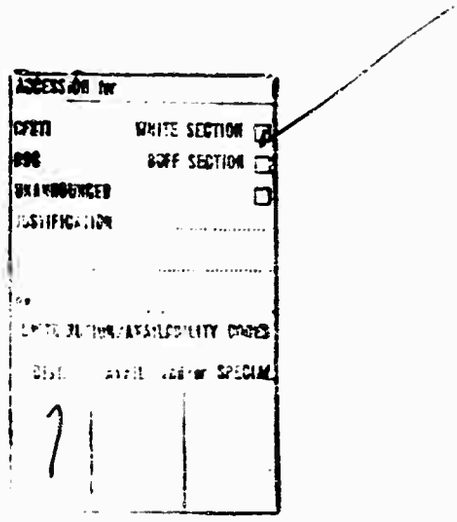

Qualified requesters may obtain additional copies from the Defense Documentation Center. All others should apply to the Clearinghouse for Federal Scientific and Technical Information.

AFCRL-70-0226

Research on Extremely Low Frequency Propagation with Particular Emphasis on Schumann Resonance and Related Phenomena

Part II: LOCATION OF SOURCES

by

John Toomey and Charles Polk

Contractor: University of Rhode Island, Kingston, Rhode Island 02881

Contract No. AF 19(628)-4950

Project No. 5631
Task No. 563110
Work Unit 56311001

Final Report (Part II)

Period Covered: 15 January 1965 to 15 November 1969

April 1, 1970

Contract Monitor: Kurt Toman
Ionospheric Physics Laboratory

Prepared

for

AIR FORCE CAMBRIDGE RESEARCH LABORATORIES

Office of Aeorspace Research
United States Air Force

Bedford, Massachusetts, 01730

Abstract

Experimental techniques for the measurement of natural extremely low frequency (ELF) electromagnetic noise are described, including methods for absolute calibration of magnetic and electric field sensors in this frequency range (3 to 30 Hz). After a review of the theory applicable to earth-ionosphere cavity resonances a method is developed which permits location of two simultaneously active, major thunderstorm regions on the surface of the earth by analysis of ELF spectra. In particular use is made of electric to magnetic field ratios and of ratios involving the power spectrum magnitudes at adjacent resonant peaks. Limitations of the method are analyzed, particularly those related to $f^{-\alpha}$ background noise (f = frequency) and to quasi-uniformly distributed, minor lightning activity which adds to the noise originating in the major thunderstorm regions. Appropriate methods of spectral analysis—appropriate frequency resolutions and integration times—are determined and the method is illustrated by experimental data. It is also indicated how the source location procedure—in conjunction with exact data ($\pm$ 0.25 Hz) describing the position of the resonant peaks—may be used to evaluate Ionospheric conductivity profiles extending downward to about 40 km.

ADMINISTRATIVE INFORMATION

Contributors:

Chapters II to X of this Final Report (Part II) are part of a thesis submitted for the Ph.D. degree by Mr. John Toomey. Other staff members who have participated in this research are:

Dr. C. Polk (project director)

Dr. M. Abbas

Dr. H. Etzold

Dr. H. König

Mr. M. Clayton

Mr. T. J. Keefe

Mr. A. Tran

Previous and related contracts

AF 19(604)-7252 (Prior to 1965)

AF 19(628)-69-C-0289 (Current, related instrumentation work)

AF 61(052)-836 (Related work at the Technical University of Munich, Germany)

Nonr-396(10) (Related ELF work, oriented towards Naval applications)

Prior Publications

Scientific Report No. 1, AFCRL-67-0236. Hydromagnetic Waves in the Ionosphere: Propagation through inhomogeneous and current carrying regions (M. Abbas)

Scientific Report No. 2, AFCRL-70-0133. Absorption of Hydromagnetic Waves in the Ionosphere (M. Abbas, Canadian Jl. of Physics, 1970, Vol. 48, No. 3, pp. 362-366)

M. Abbas: "Hydromagnetic Wave Propagation and Excitation of Schumann Resonances" Planet. and Space Sci. 1968, Vol. 16, pp. 831-844 (Based upon Scientific Report No. 1)

M. Abbas and H. Poeverlein: "Propagation of Hydromagnetic Waves in Current-Carrying Regions of the Ionosphere and Magnetosphere (Parallel Propagation)." Radio Science, 1968, Vol. 3, No. 10, pp. 1010-1019.

M. Abbas: "Coupling of Hydromagnetic to Electromagnetic Waves", IEEE Transactions on Antennas and Propagation, 1967, Vol. AP-15, No. 6, pp. 829-831.

M. Abbas: "Effect of Neglecting Hall Term on Dispersion Relation for Hydromagnetic Waves", Proceedings of the IEEE, 1968, Vol. 56, No. 1, pp. 79-80.

M. Abbas: "Propagation of Hydromagnetic Waves Normal to the Magnetic Field in the Presence of Current", Planetary and Space Science, 1969, Vol. 17, No. 2, pp. 247-254.

J. Toomey and C. Polk: "Location of Thunderstorm Regions by Analysis of ELF (Schumann) Spectra", Transactions A.G.U., 1968, Vol. 49, No. 4, p. 687.

J. Toomey and C. Polk: "ELF Spectra as a Tool for the Location of Thunderstorm Regions", EOS, 1969, Vol. 50, No. 4, p. 168.

C. Polk: "Relation of ELF Noise and Schumann Resonances to Thunderstorm Activity" in Planetary Electrodynamics, Vol. 2 (S. C. Coroniti, J. Hughes, editors), Gordon and Breach Science Publishers, 1969, pp. 55-82.

TABLE OF CONTENTS

LIST OF FIGURES

LIST OF SYMBOLS

A_n	Discrete Fourier transform at $f = nf_o$
a	Radius of earth, 6400 km
a_n	Discrete Fourier cosine transform at $f = nf_o$
b_n	Discrete sine transform at $f = nf_o$
C	A parameter measuring noise contamination of a spectrum
c	Free space phase velocity of electromagnetic waves
E	Expected value operator
E_r	Vertical electric field
E_θ	Horizontal electric field
$\mathcal{E}_n$	A quantity proportional to the squared electric field magnitude at the nth resonance produced by a thunderstorm region
f	Frequency (Hertz)
f_o	Fundamental frequency in discrete Fourier transform
G_E	Squared electric field magnitude produced by a unit area of distributed dipoles
G_H	Squared magnetic field magnitude produced by a unit area of distributed dipoles
g	Power spectrum of lightning stroke dipole moment
H	Frequency function of a linear system
H	Spectral window
h	Data window
h	Height of lower Ionosphere boundary
$\mathcal{H}_n$	A quantity proportional to the squared magnetic field magnitude at the nth resonance produced by a thunderstorm region

k	$\omega \sqrt{\mu_o \varepsilon_o}$, free space propagation constant
M	Current dipole moment of lightning stroke
N	Number of samples of a time waveform
N	Power spectrum of additive noise
n	An integer
P_n	Smoothed estimate of power spectral density at $f = nf_o$
P_n	Legendere polynomial of order n
P_ν	Legendere function of complex order ν
Q	Quality factor of a resonant cavity
Q	A parameter to be minimized
R_i	Reflection coefficient at air-ionosphere boundary
R_g	Reflection coefficient at air-earth boundary
R_x	Autocorrelation function
$R_1, R_2 \ldots$	Ratios of spectral peak powers
r	Radial spherical coordinate
$r_1, r_2 \ldots$	Ratios of spectral peak powers
S	Complex sine of angle of incidence
S	Power spectral density
S_n	Power spectral density estimate at $f = nf_o$
T	Length in seconds of a data record
T	Power spectrum of noise produced by thunderstorms
t	Time in seconds
U	Stored energy in a resonant cavity
Var	Variance operator
v	Phase velocity in earth-ionosphere waveguide

X	Fourier transform of a time function
X_a	Apparent Fourier transform
x	A time function
x_k	kth sample of a time function
α	Angle measuring inclination of receiving coil axis to east-west direction
α	Attenuation constant, nepers/meter
α	Parameter specifying frequency decay of expcnential additive noise
Δ	Range half-width of thunderstorm region
Δ_ϕ	Azimuthal half-width of thunderstorm region
Δf	Frequency resolution of power spectral density estimates
Δt	Time interval between samples of analog to digital converter
δ	A measure of the relative intensity of two thunderstorm regions
η	Characteristic impedance of free space, $\sqrt{\frac{\mu_o}{\varepsilon_o}}$
θ	Great circle distance, measured in degrees from the center of the earth, between the center of a source and the receiver.
θ	Polar angle in spherical coordinates (collatitude)
θ	Angle of incidence measured from normal to reflecting boundary
μ	Mean of a random variable
ν	Pole in Watson transformation
ρ	Surface density of lightning strokes
σ	Standard deviation of a random variable
σ_g	Conductivity of earth
τ	Lag in autocorrelation
ϕ	Bearing from receiver to center of thunderstorm region
ϕ	Azimuthal spherical angle

ψ	Potential function for fields transverse magnetic to the radial coordinate
ω	Circular frequency, radians/sec
ω_n	Radian resonant frequency at nth resonance
ω_{n_o}	Radian resonant frequency in lossless cavity

I. INTRODUCTION - OBJECTS AND OUTLINE OF THE STUDY AND SUMMARY OF EXPERIMENTAL METHODS

1.1 Objects

This project was concerned with the observation and explanation of electromagnetic noise at extremely low frequencies—approximately 3 Hz to 25 Hz—and particularly with noise near the Schumann earth-ionosphere cavity resonances at about 8, 14 and 20 Hz. Objects of the investigation were the identification of noise sources, the identification of pertinent propagation phenomena and the identification of other processes which determine properties of ELF noise such as diurnal variation of its amplitude and of its frequency spectrum.

Possible applications of the observation and analysis of ELF noise which have become apparent in the course of the work are (1) the possibility of locating the position of major thunderstorm regions on the surface of the earth, (2) identification of changes in the effective conductivity profile (i.e. electron and ion density and collision frequency profile) of the lower Ionosphere over large regions and (3) prediction of some types of Solar Proton events and associated major ionospheric disturbances.

1.2 Outline of the study

The major part of the present report is devoted to a detailed analysis of the first application—location of major thunderstorm regions (or of other ELF sources) by analysis of ELF observations at a single station. It will be shown, however, that this location

procedure is also fundamental to any determination of ionospheric conductivity profiles, since accurate information about such profiles cannot be extracted from the ELF spectra unless the relative positions of source and receiver are known (Sections V and X).

Observations indicating substantial deviations from normal ELF amplitude levels and normal ELF spectra which preceded ten Solar Proton events in 1967 and 1968 by periods between eleven and twenty-three hours will not be covered in the present report, because they are not well understood and because the number of observations is not sufficient to permit definite conclusions without further observations. Some possible source and propagation mechanisms were analyzed in "Part I" of this final report (AFCRL-70-0143).

Since much of the information obtainable from the always present natural ELF background noise is contained in its changing power spectrum, the applicable fundamentals of spectral analysis are reviewed in Section II. In Section III the characteristics of lightning strokes are discussed, because during "normal" periods—that is periods when ELF noise levels are not unusually high and "Schumann" resonances are clearly noticeable—their major source seems to be lightning activity.

The basic theory of earth-Ionosphere cavity resonances due to Schumann, Wait, Galejs, D. L. Jones, Madden and others is reviewed in section IV while details of a new ELF source location procedure are discussed in Sections V to VII.

The effects of two natural phenomena which could lead to large errors in the source location procedure are analyzed in Section VIII:

(1) Noise, possibly of extra-terrestrial or Ionospheric origin and having a $f^{-\alpha}$ power spectrum (where $1 < \alpha < 3$) is always present. In section 6.1 it is indicated how large this background noise can be before it will prevent extraction of source information from ELF data. (2) The source location procedure assumes that the major thunderstorm activity at any one time is restricted to one or two major regions such as a 10^6 km^2 area (approx. 10 by 10 degrees) between 1700 and 1900 local time at an equatorial land mass. Simultaneous with this major thunderstorm activity there are, however, many smaller thunderstorms in progress over the rest of the earth' surface. Section 8.2 considers the effect upon P spectra (and the proposed source location procedure) of various possible relative distributions of lightning activity between the major thunderstorm centers and the more uniformly distributed minor lightning activity.

In section IX the source location procedure is illustrated by the analysis of experimental ELF power spectra and in section X conclusions are drawn and directions of future work are suggested. In particular it is indicated how the source location procedure—employing the ratios of the power spectrum magnitudes at the resonant peaks—can be used, in conjunction with exact data ($\pm$ 0.25 Hz) describing the position of the resonant peaks, to evaluate Ionospheric conductivity profiles.

1.3 Experimental methods

Observations of extremely low frequency electromagnetic noise in the earth-ionosphere cavity [Schumann] resonance region are made on the Alton Jones campus of the University of Rhode Island [71° 44' 01" W, 41° 37' 53"N] in West Greenwich, R. I. The observation site is in a rural forest

location, far from sources of man-made electromagnetic and vibrational noise (approximately three miles from the nearest public road). Variations of the horizontal magnetic field and of the vertical electric field in the frequency region between approximately 3 and 40 Hz (3 dB points of input filter) are monitored continuously; the vertical electric field data cannot be used, however, during heavy local precipitation. Local lightning activity, when it occurs, contaminates both electric and magnetic field data, but thunderstorms are common in this area only between May and September and the annual average number of thunderstorm days is twenty-two.

The sensors for the horizontal magnetic field are two orthogonal 2 meter diameter coils, each consisting of four separate sections with approximately 11000 turns of number 30 wire. Both coils are electrostatically shielded by aluminum housings and are buried in the ground within a small mount (approximately 2 meter high by 10 meter in diameter) designed so as to minimize the propagation of elastic (acoustic) surface waves. The total output from each coil due to thermal noise within the coil and due to pick-up of ambient noise is approximately 4.5 microvolt measured through a 7.74 to 8.30 Hz (one-tenth octave) filter during a "quiet" period (no disturbances on the "summary record" described below and illustrated by figure 1-5).

The magnetic field equipment is calibrated at least once each week by the transmission of an 8 Hz signal from a calibrating coil for a period of 10 to 15 minutes. The calibrating coil produces a horizontal magnetic field intensity of exactly 10^{-5} ampere m^{-1} (12.56 milligamma) at the location of the receiving coil which in turn produces a 90 micro-

volt output voltage in the 7.74 to 8.30 Hz band.

The output of each receiving coil is applied to an amplifying and filter system which compensates for the rising amplitude-frequency characteristic of the coil so that the output of the system is proportional to the magnetic field and not to its derivative. The frequency response of the entire receiving system [including the receiving coil] is flat between 5 Hz and 30 Hz ($\pm$ 0.5 dB; 3 dB points are at 3 Hz and 40 Hz) for constant H-field input (constant current in the calibrating coil). The output of the amplifying system as well as timing signals are recorded AM on half-inch magnetic tape running at a speed of 0.0375 inches per second.

The vertical electric field was detected by a vertical rod antenna until August 1969 when it was supplemented by a spherical antenna. The latter is mounted approximately 30 feet (9.15 meter) above ground level and consists of a silver conductive coating painted on the interior of a plexiglass sphere. Inside the sphere is a high impedance preamplifier connected to the inner conductive walls. The entire assembly, although mounted on top of a mast, can be lowered easily to the ground for service and repair.

The design of the antenna is based upon earlier work by Ogawa (1966). Mounting of a metal antenna, which is electrically isolated from ground, at a height of 10 meters largely eliminates spurious signals due to ion motion which is particularly pronounced within the first two meters above ground. Furthermore the capacitance to ground of the small metal sphere (radius a = 7.813 inches) is rather insensitive to small changes in height since for $(a/h) < (1/10)$ its value is given by $C \approx 2\pi\varepsilon_o a(2 + a/h)$.

Consequently C and the received field intensity are rather insensitive to lateral motion or bending of the supporting mast during heavy winds. The antenna differs from Ogawa's "ball antenna" by being surrounded with a relatively thick (0.125 inch) dielectric coating which acts as a "radome" making the antenna usable even during moderate precipitation.

Since <u>absolute</u> calibration of the electric as well as the magnetic sensors is required for the type of processing described later in this report (for example the effective wave impedance $|E|/|H|$ is of interest), it was necessary to obtain means for generating a known standard, ELF field in the vicinity of the receiving antenna. This is done by feeding a 2.86 meter long vertical calibrating antenna. The vertical field generated by such an antenna can be shown to be given by

$$E_z = \frac{I_b}{4\pi\omega(H-a)\varepsilon}\left[-\frac{1}{r_1}-\frac{1}{r_2}+\frac{1}{r_3}+\frac{1}{r_o}-\frac{(z'+a)H}{r_3^3}+\frac{(z'-a)H}{r_o^3}\right] \qquad (1.1)$$

where

I_b = base current of the transmitting antenna

H = elevation of the top of the transmitting antenna above a perfectly conducting ground

a = elevation of the base of the transmitting antenna

ω = radian frequency

z' = elevation of receiving point

r_o, r_1, r_2, r_3 are defined by figure 1.1

This expression for E_z is based upon the equations given by Jordan (1950) for the near-field of a vertical antenna. In deriving (1.1) appropriate

approximations were made to take into account the extremely short length of the antenna and the extremely short observation distance in comparison with one free-space wavelength: λ is equal to $3(10^7)$ meter at 10 Hz.

It is apparent from (1.1) that for an accurate determination of the ambient field in the vicinity of a vertical ELF calibrating antenna the only quantity which must be measured, in addition to distances, is the base current. This can be done, indirectly, by evaluating the capacitance to ground, C_a, of the transmitting antenna. The antenna current is then equal to $V_a \omega C_a$ where V_a is the antenna terminal voltage.

Using a circuit suggested by H. L. König and illustrated in Figure 1.2 the antenna capacitance is given by

$$C_a = (R-1)(C_1 + C_2) \tag{1.2}$$

where R is defined by

$$R = \frac{z_2}{z_1 + z_2} \frac{(z_1 + z_p)}{z_p} \tag{1.3}$$

$$z_p = \frac{z_a z_2}{z_a + z_2} \tag{1.4}$$

For a 2.58 meter calibration antenna used on the West Greenwich field site this measurement gave C_a = 22.2pf while a calculation based upon a formula given by Watt (1967)

$$C_a' = \frac{24.16(H-a)}{\log_{10}\left[\frac{2(H-a)}{d}\right] - k} \text{ pf} \tag{1.5}$$

gave a value of 22.8 pf.

In (1.5) the quantity (H-a) is the antenna length as shown on Figure 1.2, d is the antenna diameter and k is a factor depending upon the

ratio of antenna elevation above ground to antenna length. For the value of a = 2.86 m which was used [a/(H-a)] = 1.11 and k = 0.196.

From the measured capacitance of the receiving antenna, which is normally used for the reception of ELF noise, the measured amplifier gain and the amplifier output voltage one can evaluate the receiving antenna terminal voltage. If the receiving antenna terminal voltage thus calculated agrees with the terminal voltage obtained by integrating over the length of the receiving antenna (for a linear vertical receiving antenna) the field due to the calibrating antenna calculated by (1.1), it becomes possible to translate receiving antenna voltage accurately into vertical ELF electric field values. (For a spherical receiving antenna the received voltage V during calibration must agree with the calculated voltage obtained from V = Q/C where Q is found by integrating the calculated radial component of the calibrating field over the surface of the receiving antenna: $Q = \varepsilon \int \vec{E} \cdot d\vec{s}$).

For the vertical "whip" ELF receiving antenna which has been used in 1967 and 1968 this calibration procedure (at 10 Hz) leads to the following values of terminal voltage:

From integration of the radiated calibrating field over the receiving antenna - 23.96 mV

From amplifier output voltage, amplifier gain and receiving antenna capacitance - 25.89 mV

It appears therefore that the absolute value of the received vertical electric field can be determined with a precision of at least eight percent. Employing the described calibration procedure one finds that the

vertical electric field at the West Greenwich field site near 8 Hz remained near 1.8 milli-volt/meter/$\sqrt{\text{Hz}}$ on a typical "quiet" summer day.

For rapid, visual survey of field intensity variations in the 8 Hz [first Schumann resonance] region, "summary records" are obtained as follows: the magnetic tape is replayed in the laboratory at a speed of 1.875 inches per second [50 times the recording speed] into a band-pass filter having 3 dB points at 300 Hz and 440 Hz, corresponding to 6 Hz and 8.8 Hz in the original recording. The output of this filter is passed through the rectifier and smoothing network shown in Figure 1.3. The response of this filter to application and removal of a constant 400 Hz signal at AA is shown in Figure 1.4. The charging time constant T_o of the filter [time needed for output to reach $1 - e^{-1}$ of final value] is 7.5 seconds. The measured discharge time constant T_1 is 51 seconds; the discharge function actually has the form

$$V = [T_1 - T_2]^{-1} \left[T_1 e^{-t/T_1} - T_2 e^{-t/T_2} \right],$$

but since $T_1 \gg T_2$ it follows that

$$V \approx e^{-t/T_1}. \quad [T_2 = 1.6 \text{ seconds}]$$

Since the input time constant, $T_o = 7.5$ seconds, corresponds to $[7.5(50)/60] = 6.25$ minutes of recording time, fluctuations in the input signal which are appreciably shorter than six minutes will not appear on the paper record which is produced by the output of the network in Figure 1.3. Furthermore, low level fluctuations which occur within a period of $T_1[50]/60 = 42$ minutes after a sustained large signal was received will

not appear on the output chart. The "summary records" illustrated by Figure 1.5 (and regularly published in Section 3 of the AFCRL "Geophysics and Space Data Bulletin") should therefore be used primarily to locate periods of sustained unusual activity; for such periods the original wide-band [3 Hz to 40 Hz] magnetic tape recordings may then be examined in more detail. The "summary records" can also be used for comparison with thunderstorm data and records of solar and geomagnetic activity to establish which events have significant effect upon magnetic field variations in the 8 Hz region.

Calibration signals are indicated by C on the records; periods of man-made interference or missing data are indicated by ↔; local thunderstorms (within about 25 miles of the field station) are shown by LS. The 10^{-5} amp m^{-1} 8 Hz calibrating signal saturates the amplifier of the paper chart recorder for the gain setting which is employed (although it is 10 dB below saturation level on the magnetic tape), it can therefore not be used to establish relative signal levels, except when records are reproduced at half gain. Time on the records is EST with heavy vertical lines indicating 0000 hours EST.

Fundamental considerations important in the processing for detailed spectral analysis of the wide band magnetic field and electric field data which are recorded on magnetic tape, are discussed in Chapter II and in Appendix A-1. Spectral analysis was performed by either digitizing the data and employing a "Fast-Fourier-Transform" program on an IBM 360/50, or more recently—achieving a reduction of analysis time by a factor of about 30/1—by employing a commerical ("SAICOR") special purpose analog-digital system for Fourier spectrum analysis.

II. SPECTRAL ANALYSIS

The convenience of the frequency concept in the analysis of physical phenomena is well known. In order to facilitate the comparison of theoretical with experimental results, however, a method of investigating experimental data in the frequency domain is needed. This is the tool of spectral analysis. Determining the frequency content of a time signal is by no means an easy task to accomplish and in the following paragraphs some of the problems that occur in spectral analysis, as well as methods for treating them are discussed.

The frequency content of a time function is given by its Fourier transform. A time signal, x(t), and its Fourier transform, X(f) are related by

$$X(f) = \int_{-\infty}^{+\infty} x(t)e^{-i2\pi ft}\, dt \qquad (2.1)$$

and

$$x(t) = \int_{-\infty}^{+\infty} X(f)e^{i2\pi ft}\, df \qquad (2.2)$$

provided certain mathematical conditions on x(t) and X(f) are satisfied [Weinberger, 1965]. These conditions are always satisfied by physically realizable waveforms.

Although (2.1) does give the frequency content of the signal, the result is complex, i.e. it includes the phases of the spectral components.

Usually, however, phase information is not of interest and a positive, real quantity $|X(f)|^2$ is used. The power spectral density, $S_x(f)$ can be defined as

$$S_x(f) = \lim_{T \to \infty} \frac{1}{2T} \left| \int_{-T}^{+T} x(t) e^{-i2\pi ft} dt \right|^2 \qquad (2.3)$$

It is called a power density because $S_x(f)$ df gives a measure of the power in the frequency band between f and f+df. An alternative definition of power spectral density in terms of the autocovariance function $R_x(\tau)$ is sometimes used. The autocovariance function is defined as

$$R_x(\tau) = \lim_{T \to \infty} \frac{1}{2T} \int_{-T}^{T} x(t)\, x\,(t+\tau) dt \qquad (2.4)$$

The power spectral density can then be expressed as the Fourier transform of the autocovariance function.

$$S_x(f) = \int_{-\infty}^{+\infty} R_x(\tau) e^{-2\pi f\tau}\, d\tau \qquad (2.5)$$

The definitions (2.3) and (2.5) are completely equivalent. Estimation of the power spectrum by (2.5), which until recently was the most commonly used method for estimating the power spectrum, involves two computational steps: the evaluation of the autocovariance and then the evaluation of the Fourier transform of the autocovariance. In the computation of the autocovariance, however, lags of less than or equal to only about ten percent of the total record length need be considered (Blackman and Tukey, 1958). For this reason the evaluation of the integral in (2.5) is much simpler than the evaluation of the integral in

(2.3). In the past, significant computer time savings were realized by using (2.5) since the calculation of the numerical Fourier transform was a lengthy process which could be considerably shortened by reducing the domain of the function to be transformed.

Cooley and Tukey (1965) have, however, developed a highly efficient method for numerically evaluating a Fourier transform. With the advent of this algorithm, the emphasis has shifted to using (2.3) for the evaluation of power spectra. In fact, the Cooley-Tukey algorithm or "Fast Fourier Transform" (FFT) is so fast that even if the autocovariance is desired, it is more efficient to find the power spectrum by the FFT and then to take the inverse Fourier transform via the FFT, yielding the autocovariance. The power spectral density can be efficiently estimated by evaluating (2.3) on a digital computer using the FFT.

2.1 Resolution and Bias of the Estimates

Evaluation of equation (2.1) requires knowledge of the entire history of signal, past and future. This is, of course, not possible and we must use an approximation of the form

$$X_a(f) = \int_{-T/2}^{T/2} x(t)e^{-i2\pi ft}\,dt \qquad (2.6)$$

where $[-T/2, T/2]$ is the time interval of the signal which is available. Equation (2.6) can be written as

$$X_a(f) = \int_{-\infty}^{+\infty} h(t)\,x(t)e^{-i2\pi ft}\,dt \qquad (2.7)$$

if we define $h(t)$ by

$$h(t) = \begin{cases} 1; & -T/2 \leq t \leq T/2 \\ 0; & t < -T/2 \text{ or } t > T/2 \end{cases} \qquad (2.8)$$

h(t) is often called a "data window" since it determines what portion of the data is "seen" by our analysis. Using (2.2), we can express x(t) in terms of its Fourier transform and interchange the order of integration in the resulting iterated integral to obtain

$$X_a(f) = \int_{-\infty}^{+\infty} X(f')\, H(f-f')\, df' \qquad (2.9)$$

The function H(f), called a "spectral window", is the Fourier transform of h(t), the data window, and is shown in Fig. 2.1. The effect of employing (2.6) to estimate X(f) is clear from (2.9); $X_a(f)$ is a weighted average of the actual Fourier transform. Since the width of the main lobe of H(f) is proportional to T^{-1} (Fig. 2.1), we can increase the resolution of our estimates by increasing the length of signal that we analyze. In fact, as T becomes infinite (or equivalently, h(t) = 1 for all time) H(f-f') becomes $\delta(f-f')$, the unit impulse function, (Papoulis, 1962) and $X_a(f) = X(f)$.

The estimates of X(f) can be biased by "leakage" from adjacent frequency bands due to the side lobes of H(f). This effect becomes especially troublesome if the power spectrum of x(t) contains strong sinusoidal components or large peaks (Hinich and Clay, 1968). Bendat and Piersall (1966) have approximated this additive bias of spectral estimates as

$$\frac{(\Delta f)^2}{24} \left[\frac{d^2 S_x(f)}{df^2} \right]$$

where Δf is the frequency resolution in hertz of the estimates. That this bias term is negligible for earth-ionosphere resonant cavity power spectra is shown in Appendix A.

2.2 Variability of the Estimates

To numerically estimate the Fourier transform of a time function, the integral in equation (2.6) must be calculated. An approximate formulation* is

$$A_n = A(nf_0) = \Delta t \sum_{k=0}^{N-1} x(k\Delta t) e^{-i2\pi n f_0 k \Delta t} \qquad n = 0, 1, 2, \ldots N-1 \tag{2.10}$$

where Δt is the time interval between the samples of the analog to digital converter and f_0 is the fundamental frequency, $f_0 = 1/T = 1/N\Delta t$. From (2.3) we see that

$$S_n = \frac{1}{T} |A_n|^2 \; ; \quad n = 0, 1, 2, \ldots N-1 \tag{2.11}$$

are estimates of the power spectrum. A plot of S_n versus n is called the raw periodogram. It will be shown that, unless modified, the raw periodogram is not a statistically consistent estimate of the power spectrum.

Suppose that a frequency resolution of Δf hertz is desired in the power spectrum. To achieve this resolution M + 1 values of S_n could be averaged as

$$P_n = \frac{1}{M+1} \sum_{i=-M/2}^{+M/2} S_{i+n} \tag{2.12}$$

*For convenience, we have shifted the time interval to [0, T].

where N is the nearest even integer to $(\Delta f/f_0)$. The resulting P_n would constitute an estimate of the power spectrum at $f = nf_0$ Hertz.

An expression for the variance of P_n will be derived below. We shall assume that the time signal is a member of a white stationary gaussian random process, or, in other words, that each time sample $x(k\Delta t)$ is a normally distributed random variable whose statistics are independent of k and that the power spectrum of x(t) is a constant for all frequencies. Using the notation $x_k = x(k\Delta t)$, equation (2.10) can be written

$$A_n = \Delta t \sum_{k=0}^{N-1} x_k e^{-\frac{2\pi}{N} kn} \qquad (2.13)$$

Equation (2.13) is of the form

$$A_n = a_n + ib_n$$

where

$$a_n = \Delta t \sum_{k=0}^{N-1} x_k \cos\left(\frac{2\pi}{N} kn\right)$$

$$b_n = \Delta t \sum_{k=0}^{N-1} x_k \sin\left(\frac{2\pi}{N} kn\right)$$

If x_k is assumed to be a normally distributed random variable, the a_n and b_n will also be normally distributed, since they represent linear combinations of normally distributed random variables. (Mood and Graybill, 1963). It will also be assumed that $E(x_k) = 0$, i.e. the signal is passed through a filter or some device that removes the d-c level. In digital spectral analysis, the signal is usually filtered to prevent

aliasing (Blackman and Tukey, 1958). If the gain on the data gathering equipment is adjusted we can force

$$\mathrm{Var}(a_n) = \mathrm{Var}(b_n) = 1; \quad n = 1, 2, 3, \ldots N-1 \tag{2.14}$$

so that the quantities

$$|A_n|^2 = a_n^2 + b_n^2; \quad n = 1, 2, \ldots N-1 \tag{2.15}$$

are distributed chi-square with two degrees of freedom. (Mood and Graybill, 1963). It is clear that the mean value, μ is given by

$$\mu = E[|A_n|^2]; \quad n = 1, 2, 3, \ldots N-1$$

and that the variance, σ^2 is given by

$$\sigma^2 = E[(|A_n|^2 - \mu)^2]; \quad n = 1, 2, 3, \ldots N-1$$

where E denotes expected value. Since σ^2 is a measure of power, the last equation is a result of our white noise assumption.

The variance of a chi-square variate with two degrees of freedom equals its mean. (Mood and Graybill, 1963). Thus,

$$E(P_n) = \frac{1}{M+1} \sum_{i=-M/2}^{M/2} E(|A_{i+n}|^2) = \mu \tag{2.16}$$

The random variables $|A_n|^2$ with $n = 1, 2, 3, \ldots N-1$ are independent since they are obtained by an orthogonal transformation and represent different "components" of $x(t)$. The variance of a sum of independent random variables is the sum of the variances (Mood and Graybill, 1963).

Therefore,

$$\mathrm{Var}(P_n) = \frac{1}{(M+1)^2} \sum_{i=-M/2}^{M/2} \mathrm{Var}[|A_{i+n}|^2]$$

$$\mathrm{Var}(P_n) = \frac{(M+1)\sigma^2}{(M+1)^2} \tag{2.17}$$

$$\mathrm{Var}(P_n) = \frac{\sigma^2}{M+1}$$

The reader will note that variance of the power spectrum estimates P_n can be made arbitrarily small by increasing M. Estimates obtained by (2.12) are then statistically consistent. From equations (2.16) and (2.17),

$$\frac{\mathrm{Var}(P_n)}{E^2(P_n)} = \frac{1}{M+1} \tag{2.18}$$

since $\mu = \sigma^2$. Note that if M = 0 (corresponding to the raw periodogram), the standard deviation of P_n is equal to its mean. This large variability demonstrates that the raw periodogram provides almost useless estimates of the power spectrum. Since $M \cong \frac{\Delta f}{f_0} = \Delta f T$, equation (2.18) becomes

$$\frac{\mathrm{Var}(P_n)}{E^2(P_n)} = \frac{1}{(\Delta f)T} \tag{2.19}$$

If the length of analyzed time signal and desired resolution are known, the variability of the estimates is given approximately by

equation (2.19). Although (2.19) is strictly only true for a white noise spectrum, it is a relation which applies, at least roughly, to most cases and is widely used (Blackman and Tukey, 1958).

III. THE LIGHTNING STROKE AS A SOURCE OF ELF WAVES

3.1 The Lightning Discharge Process

Upon application of an electric field, the constituent atoms and molecules of a gas become polarized. If the electric field is increased until the ionization potential is achieved, electrons will be liberated from their parent atoms and be accelerated by the applied field. Under certain conditions (Loeb, 1939), the free electrons can achieve the momentum necessary to ionize other atoms by collision. The fast moving electrons can also excite neutral atoms causing them to emit radiation which can photoionize other atoms. Hence, electron multiplication or electron avalanche can occur in an ionized gas. The lightning discharge is an example of this phenomenon.

The lightning flash is a very complex mechanism and only the general features, important to the present discussion, will be presented. If adjacent regions of air are at different temperatures convection takes place: warmer air tends to rise and cooler air descends. In a mature thunderstorm cell, convection is occurring on a large scale and a strong updraft is present. It is this updraft which carries positive charges to the top of the cloud. Negative charges, which are believed to reside on heavier particles remain in the lower regions of the cloud. The negative charges in the bottom of the thundercloud induce a positive surface charge on the conducting earth below. The

electric field in the region between the lower cloud and the earth increases as the charge separated by the updraft increases. When the breakdown potential is reached, the air below the cloud becomes ionized. The ionization will first occur where the electric field is strongest, which is usually just below the bottom of the cloud. The free electrons in the ionized air are then accelerated towards the earth by the repulsive force of the large accumulation of negative charge in the lower portions of the cloud; any motion of the positive and negative ions can be neglected since their large mass renders them immobile relative to the electrons (Schonland; 1964). The movement of the electrons takes place in a series of steps of about 50 meters in length. Hence, this first part of the lightning stroke is called the stepped leader. When the stepped leader reaches the earth, a conducting path exists between the large accumulations of charge in the cloud and the earth. The electrons in the lower part of the leader flow into the ground first, then the electrons behind them so the process appears to move up towards the cloud. The return stroke is actually an upward moving increase in the downward velocity of electrons. It is the return stroke that produces the intense light, heat, and acoustical energy of the typical lightning discharge.

It should be noted that the lightning discharge to earth consists usually of several leader-return processes in succession, with the average number being three; up to 42 strokes in a single discharge to earth have however been observed (Schonland, 1953). The leaders for strokes subsequent to the first are not stepped, but move continuously towards

the ground. These leaders are called dart leaders to distinguish them from the slower moving stepped leaders. The average period of time between strokes is about 0.05 secs.

The stepped leader travels at an effective speed of 300 km/sec. The dart leader and return stroke travel at speeds of roughly 2,000 and 10,000 km/sec respectively. The return stroke current reaches a peak value of about 30,000 amps within 6 μsecs after the leader reaches the ground. The current decays to half the peak value in an average of 24 μsecs (Chalmers, 1967).

Although only the discharge to earth has been discussed, lightning flashes that never reach the ground are quite common. These discharges do not manifest a return process but are only of the leader type (Schonland, 1953). A stroke between two different charge concentrations within the same cloud, or sheet lightning as it is commonly called, is observed frequently. Air discharges, that is, lightning flashes passing from a thundercloud into clear air (Schonland, 1956) as well as strokes from the highest regions of the cloud up to the electrosphere (workers in atmospheric electricity refer to the cosmic ray produced ionized layer as the electrosphere and to the higher conducting layers, a result of solar radiation, as the ionosphere) have been reported (Chalmers, 1967). Strokes along a path between two clouds (intercloud strokes) are also possible.

The characteristics of individual lightning discharges probably are determined to a large extent by many climatological, topographical, and geographical conditions. For example, evidence indicates that the

percentage of discharges to earth depends upon geographical latitude (Chalmers, 1967). Tropical discharges may differ significantly from those occuring in temperate zones (Watt, 1960). According to Schonland (1964), "giant" lightning flashes, with peak currents greater than 200,000 amperes have only been observed in the Swiss Alps. Lightning strokes to the Empire State Building have been observed to begin with a leader moving up towards the clouds.

The large differences in the properties of individual lightning discharges constitute a possible limitation of the methods to be reported here. It will be shown below, however, that many of these difficulties can be overcome by employing the proper characteristics of received ELF signals for the location of sources.

3.2 The Lightning Stroke as a Source of Radio Waves

Since the lightning flash consists of a time changing flow of charged particles, it must radiate electromagnetic energy. In view of the large wavelength of ELF radiation, the lightning stroke can be modeled as an infinitesimal electric dipole of current dipole moment M(t) coul-meter/sec.

According to Watt (1960) fields radiated by leader processes in lightning discharges at frequencies below 5 kHz are not significant. One might expect this to be true for the stepped leaders which are relatively short in length, but this may not be the case for the dart leaders which are as long as the return stroke and may have currents of the order of 10,000 amps (Schonland, 1956). Pierce (1963) has formulated an empirical expression for the time rate of change of lightning dipole moment

a cloud to ground stroke as

$$M(t) = 80\, h_1 \exp(-h_1^2 t^2) + 5h_2 \exp(-h_2^2 t^2) + 35\, h_3 \exp(-h_3^2 t^2) \tag{3.1}$$

where the term in h_1 accounts for leader processes, the term in h_2 accounts for the return stroke, and h_3 accounts for any continuing current after the return stroke. For a cloud discharge, only the first term applies. The spectral composition of the discharge moment can be easily shown from (3.1) to be

$$M(\omega) = 80 \exp(-\omega^2/4h_1^2) + 5 \exp(-\omega^2/4h_2^2) + 35 \exp(-\omega^2/4h_3^2) \text{ coul-km} \tag{3.2}$$

The values of h_1, h_2 and h_3 given by Pierce (1963) are 40, 40 x 10^3, and 10^3. Figure (3.1), which shows each term in equation (3.2) as well as the total, $M(\omega)$, indicates that the leader is much more significant for the first three Schumann resonances than the return stroke. It is clear that there is disagreement about which component of the discharge process is most important at ELF.

Lightning strokes can have both vertical and horizontal components. Several workers have determined from theoretical and experimental investigations that it is the vertical currents which are the major source of low frequency (ELF and VLF) electromagnetic waves in the earth ionosphere cavity. For example Williams (1959) has shown by extensive statistical

studies of thunderstorm data that the major sources of VLF waves are vertical lightning currents. Sommerfeld (1949) has analytically treated the problem of radiation from both vertical and horizontal dipoles over a flat, perfectly conducting earth assuming a homogeneous atmosphere. His results show that when the dipole height to wavelength ratio is very small (as is the case for ELF), the power radiated from a horizontal dipole is many orders of magnitude less than the power radiated by a vertical dipole of equal moment. Employing a more realistic model, Wait (1962) has shown that the ratio of the vertical electric field from a horizontal dipole to the vertical electric field from a vertical dipole is proportional to $\omega\epsilon/\sigma_g$ which for $\sigma_g = 10^{-3}$ mho/meter is equal to about 10^{-5} in the lower Schumann band. The problem of horizontal dipole excitation of the earth-ionosphere waveguide has been treated in a recent paper by Galejs (1968a). The horizontal dipole excites both TM and TE modes but all modes except the zero order TM are evanescent at ELF. The vertical dipole is, however, a much more efficient excitor of the TM_o mode than the horizontal dipole.

The reason for the poor radiation properties of the horizontal dipole seems to be intuitively clear. In order to satisfy the boundary conditions at the surface of the earth, the "image" of the source must be oppositely directed. If the source and its image are very close (in units of wavelength they are practically coincident at ELF) their fields counteract to greatly reduce their effective radiation. In view of these considerations and the experimental evidence it is generally accepted (Harris and Tanner, 1962: Galejs, 1961; Raemer, 1961) that only the vertical components of lightning current are significant in the

production of terrestrial ELF noise.

3.3 Frequency Spectrum of Lightning Stroke Dipole Moment

There are very few data available on ELF lightning spectra (Kimpara, 1965). Harris and Tanner (1962) have estimated the frequency variation of a quantity "very nearly proportional to the frequency spectrum of the square of the current moment" of the lightning stroke using the ELF data of Balser and Wagner (1960). Rycroft (1963) calculated the frequency spectrum of lightning from plausible time variations of the stroke dipole moment and Raemer (1961) estimated the power spectrum of a median return stroke employing the lightning stroke statistics compiled by Williams (1959). Galejs (1961) approximated the Raemer spectrum by the relation

$$g(\omega) = \text{const.} \exp\left[-9.1 \times 10^{-3}\omega\right] \qquad (3.3)$$

The agreement among the three lightning spectra plotted in Fig. (3.2) is surprisingly good considering that completely different methods were used in their derivation.

IV. CAVITY FIELDS FROM VERTICAL ELECTRIC DIPOLE SOURCES

4.1 The Earth-Ionosphere Cavity Model

The conductivity of the ionosphere is orders of magnitude less than the effective ground conductivity so that, in the ELF range, the ionosphere is the major contributor to wave attenuation and the earth can be assumed perfectly conducting (Galejs, 1964a).

Ionosphere models (Galejs, 1961; Jones, 1967) admitting only the vertical inhomogeneity lead to results which are in closer agreement with experiment than a sharply bounded, constant parameter model. Horizontal variations in ionospheric parameters are usually considered less important than vertical variations; but the effects of lateral ionospheric inhomogeneities have been examined by Madden-Thompson (1965) and by Nelson (1967). One important horizontal variation in ionospheric properties occurs at the boundary between the day and night hemispheres; this problem has been treated by Galejs (1964a), but his method is applicable only if the source is located along the day-night boundary.

The effect of the terrestrial static magnetic field on the propagation of ELF and VLF waves has recently received considerable attention in the literature. Galejs (1968b) has shown that there is very little change in the attenuation and phase velocity of 30 Hz waves when the propagation direction is east to west or west to east for a 45° magnetic dip angle. For other propagation directions the effect of the

magnetic field is even smaller (Galejs, 1968c). The values of attenuation and phase velocity computed by Galejs compare closely with those of Jones (1967) for propagation below an isotropic ionosphere at 30 Hz.

4.2 Cavity Fields from Vertical Electric Sources

Based upon the discussion in Chapter III, we can approximate the lightning stroke as a vertical electric dipole located at the surface of the earth. A large body of literature on radiation from dipoles in the earth-ionosphere waveguide has been published and only the salient features of the approach to the problem will be presented here. For details the reader is referred to papers by Wait (1960), and Galejs (1964a), and to books by Wait (1962) and Budden (1961).

Following the approach of Wait (1962), the fields can be obtained from a single scalar function, ψ. If the cavity has complete symmetry in the ϕ-direction the expressions for the field components are

$$E_r = \frac{i}{r} \eta \frac{1}{\sin\theta} \frac{\partial}{\partial\theta} \left(\sin\theta \frac{\partial\psi}{\partial\theta}\right) \tag{4.1}$$

$$E_\theta = -\frac{i}{r} \eta \frac{\partial^2}{\partial\theta\partial r} (r\psi) \tag{4.2}$$

$$H_\phi = -k \frac{\partial\psi}{\partial\theta} \tag{4.3}$$

$$E_\phi = H_r = H_\theta = 0 \tag{4.4}$$

The function ψ was given by Wait (1962)

$$\psi = \frac{iM(\omega)}{4kha} \frac{P_\nu(-\cos\theta)}{\sin\nu\pi} \tag{4.5}$$

The symbols in expressions (4.1) - (4.5) have the following meaning:

η = characteristic impedance of free space = $\sqrt{\mu_o/\epsilon_o}$

k = free space propagation constant = $\omega\sqrt{\mu_o\epsilon_o}$

h = height from surface of earth to "lower boundary" of ionosphere

a = radius of earth

$M(\omega)$ = source dipole moment

θ = angular separation between source and receiver

$P_\nu(-\cos\theta)$ = Legendere function of complex order, ν

The dimensionless quantity ν, which is a function of frequency, depends upon the properties of the ionosphere and will be discussed below. In essence, Ψ is proportional to the radial component of the Hertz potential.

Substituting (4.5) into (4.1), and using the fact that $P_\nu(-\cos\theta)$ must satisfy the Legendere equation,

$$\frac{1}{\sin\theta}\frac{\partial}{\partial\theta}\left[\sin\theta\frac{\partial}{\partial\theta}P_\nu(-\cos\theta)\right] + \nu(\nu+1)P_\nu(-\cos\theta) = 0$$

we obtain

$$E_r = \frac{M(\omega)\nu(\nu+1)}{4a^2\omega\epsilon_c h}\quad\frac{P_\nu(-\cos\theta)}{\sin\nu\pi} \tag{4.6}$$

The expressions (4.5) and (4.6) should be summed over all allowed values of ν, corresponding to all possible waveguide modes; but in the ELF case, only one mode, the lowest order TM mode can propagate in the earth-ionosphere waveguide. All other modes, both TM and TE, are well below their cutoff frequencies (Budden, 1961). A useful representation, called

Dougall's expansion (Magnus, et al.; 1966) of the Legendere function is

$$\frac{P_\nu(-\cos\theta)}{\sin\nu\pi} = -\frac{1}{\pi}\sum_{n=0}^{\infty}\frac{2n+1}{n(n+1)-\nu(\nu+1)}P_n(\cos\theta)$$

where the $P_n(\cos\theta)$ are the Legendere polynomials, so that the radial component of the electric field becomes

$$E_r = \frac{M(\omega)\nu(\nu+1)}{4\pi a^2\omega\varepsilon_o h}\sum_{n=0}^{\infty}\frac{2n+1}{n(n+1)-\nu(\nu+1)}P_n(\cos\theta) \qquad (4.7)$$

The quantity ν is determined by the conditions on E and H imposed by Maxwell's equations at the earth and the ionosphere. Equivalent to these boundary conditions is the modal resonance equation (Budden, 1961),

$$R_i(\theta)R_g(\theta)e^{-2ikh\cos\theta} = 1 \qquad (4.8)$$

which must be satisfied if a waveguide mode is to be self-consistent. In (4.8), θ is the complex angle of incidence (measured from the normal to the reflecting boundaries) and $R_i(\theta)$ and $R_g(\theta)$ are the Fresnel reflection coefficients at the ionosphere and earth, respectively. Wait (1962) has shown that $\nu + \frac{1}{2} = ka\sin\theta$ so that if allowed values of $\cos\theta$ are determined from (4.8), allowed values of ν are then known. It should be clear that ν, as determined by (4.8) is a function of frequency. Hence, at certain frequencies the denominator of a term in the summation in (4.7) can be very small resulting in a large value of E_r. These enhancements of the fields at certain frequencies were first predicted by Schumann (1952) and have in recent years been called "Schumann resonances".

The horizontal electric field component, E_θ is very small since at ELF the earth is a very good conductor and the electric field must be very nearly normal to the surface of the earth. For this reason, the TM mode under discussion can also be approximated as a TEM mode (Madden and Thompson, 1965).

The "horizontal" component of the magnetic field, H_ϕ is found by expanding the potential function, ψ, by Dougall's representation and substituting the result into (4.3);

$$H_\phi = \frac{iM(\omega)}{4ha\pi} \sum_{n=0}^{\infty} \frac{2n+1}{n(n+1) - \nu(\nu+1)} \frac{d}{d\theta} P_n (\cos\theta) \qquad (4.9)$$

It is apparent that H_ϕ also displays the resonant behavior.

The preceding discussion can be summarized as follows: ELF fields from a vertical dipole source consist essentially of a vertical E field and a horizontal H field. At the earth surface, the magnetic field lines are concentric circles about the source. This result is, however, only true if the cavity formed by the earth and the ionosphere is perfectly symmetric and isotropic.

4.3 Fields From A Distribution of Independent Sources

The results of the preceding section will now be generalized to include the case of a distribution of vertical dipoles on the surface of the earth which represents a reasonable model for a thunderstorm region. At this point we will no longer consider the field components themselves, but the squares of the magnitudes of the field components which are proportional to power. The relations (4.7) and (4.9) can be thought of as describing linear systems where $M(\omega)$ is the input signal

and E_r and E_ϕ are the output signals. The transfer function of this system depends on ϑ, the angular distance between source and receiver. The case of several lightning strokes can then be thought of as a multiple input linear system and it can be shown (Appendix B) that if the inputs to such a system are uncorrelated, the total power at the output is the sum of the powers due to each input. Thus if it is assumed that the lightning strokes are uncorrelated, their powers can be added.

The square of the absolute value of the E field due to a distribution of dipoles over an infinitesimal area $a^2\sin\theta d\theta d\phi$ located at a distance θ from the receiver on the earth surface is then equal to

$$|E|^2 = g(\omega)\left| \frac{\nu(\nu+1)}{4\pi a^2 \omega \varepsilon_o h} \sum_{n=0}^{\infty} \frac{2n+1}{n(n+1) - \nu(\nu+1)} P_n(\cos\theta)\right|^2 a^2\sin\theta d\theta d\phi \quad (4.10)$$

where $g(\omega)$ is the dipole moment squared per unit area, which is in the most general case a function of θ and ϕ. In a more abbreviated form,

$$|E|^2 = G_E(\theta,\phi)a^2\sin\theta d\vartheta d\phi \quad (4.11)$$

For further development we assume that the source is centered at an angular position θ, ϕ as shown on figure (4.1). The edge of the source region nearest to the receiver is at distance $(\theta-\Delta)$ and the far edge at $(\theta+\Delta)$. The azimuthal spread of the source is from $\phi-\Delta_\phi$ to $\phi+\Delta_\phi$. The square of the electric field at the receiver due to this source is then given by

$$|E|^2 = \int_{\phi-\Delta_\phi}^{\phi+\Delta_\phi} \int_{\theta-\Delta}^{\theta+\Delta} G_E(\theta',\phi)a^2\sin\theta' d\theta' d\phi' \quad (4.12)$$

The expression for the magnetic field is similar but the H field

due to each element of the source is, in general, in a different direction. If we let

$$G_H(\theta,\phi) = g(\omega)\left|\frac{1}{4ha\pi}\sum_{n=0}^{\infty}\frac{2n+1}{n(n+1)-\nu(\nu+1)}\frac{d}{d\theta}P_n(\cos\theta)\right|^2 \qquad (4.13)$$

then the square of the magnetic field at the receiver is given by

$$|H_\phi|^2 = \int_{\phi-\Delta_\phi}^{\phi+\Delta_\phi}\int_{\theta-\Delta}^{\theta+\Delta} G_H(\theta',\phi')\sin^2(\phi'-\alpha)a^2\sin\theta'\,d\theta'\,d\phi' \qquad (4.14)$$

where the factor $\sin^2(\phi'-\alpha)$ accounts for the vector summation. The angle ϕ' is defined in Figure (4.1) so that the source region extends in the azimuthal direction from $\phi' = \phi-\Delta_\phi$ to $\phi' = \phi+\Delta_\phi$; the angle α indicates the inclination of the receiving coil axis with respect to the ϕ' (and ϕ) reference line which, for example, could be the east-west direction.

V. THE RATIO METHOD FOR SOURCE LOCATION

As is evident from the discussion of the preceding chapter, the received ELF fields are dependent upon the parameter ν, which is determined by the ionosphere, and the parameter θ, the source-receiver separation. In the source location problem, it is advantageous to employ those properties of the received signal which are mainly dependent on θ and are relatively independent of ν so that precise knowledge of the state of the ionosphere is not required. It was suggested by Polk (1969) that the relative sizes of adjacent peaks in the Schumann spectra would be a useful indicator of thunderstorm location.

5.1 The Dominant Term Approximation

As introduction and to provide insight into the method, we initially make a radical approximation. Let us assume that at the n^{th} resonant frequency all terms except the n^{th} in the summations in (4.7) and (4.9) are negligible. This is equivalent to assuming that the earth-ionosphere cavity is very nearly lossless. Under this approximation, the electric field at the receiver is

$$E_r = \frac{M(\omega_n)}{4\pi a^2 \omega_n \varepsilon_o h} \frac{\nu(\nu+1)(2n+1)}{n(n+1) - \nu(\nu+1)} P_n(\cos\theta) \qquad (5.1)$$

and the magnetic field component exciting the receiving coil is

$$H_\phi = \frac{iM(\omega_n)}{4\pi h a} \frac{(2n+1)\sin(\phi-\alpha)}{n(n+1) - \nu(\nu+1)} \frac{d}{d\theta} P_n(\cos\theta) \qquad (5.2)$$

at the n^{th} resonant frequency. From (5.1) and (5.2) it readily follows that at the n^{th} resonant frequency, the vertical electric field varies as $P_n(\cos\theta)$ and the horizontal magnetic field varies as $\frac{d}{d\theta} P_n(\cos\theta)$. This behavior is illustrated in Fig. (5.1) for the first two resonances and it should be clear from Fig. (5.1) that the relative sizes of the resonances are indicative of the source-receiver distance. For example, if the receiver is 90° from the source, the ratio of the E field signal at the second resonant frequency to the E field signal at the first resonant frequency should be much larger than the corresponding ratio if the receiver is 65° from the source. For the readers' convenience expressions for the first three Legendere polynomials are listed:

$$\begin{aligned} P_1(\cos\theta) &= \cos\theta \\ P_2(\cos\theta) &= \tfrac{1}{2}(3\cos^2\theta - 1) \\ P_3(\cos\theta) &= \tfrac{1}{2}(5\cos^3\theta - 3\cos\theta) \end{aligned} \tag{5.3}$$

Equations (5.1) and (5.2) can be expressed in a more simple form in the following manner: The resonances are determined by the condition

$$\nu(\nu+1) \cong n(n+1) \tag{5.4}$$

and since

$$\nu + \tfrac{1}{2} = kaS \tag{5.5}$$

the resonant frequencies are given approximately by

$$\omega_n = \frac{c}{a}\frac{\sqrt{n(n+1)}}{ReS} \tag{5.6}$$

if $ReS \gg ImS$. If the cavity has perfectly conducting walls, $S = 1$, and the corresponding resonant frequencies are

$$\omega_{no} = \frac{c}{a}\sqrt{n(n+1)} \tag{5.7}$$

so that

$$\omega_n = \frac{\omega_{no}}{ReS} \tag{5.8}$$

Using (5.4), (5.5) and (5.8), the magnitude of the electric field at the n^{th} resonance can be expressed as

$$|E_n| = \frac{M(\omega_n)(2n+1)}{4\pi\varepsilon ha^2} \frac{Re^2S}{2\omega_{no}ImS} P_n(\cos\theta) \tag{5.9}$$

The frequency dependence of S for several different ionosphere models has been determined by Jones (1967). In Figs. (5.2) and (5.3),

$$\alpha = -0.182\, f\, ImS \text{ dB/Mm} \tag{5.10}$$

and

$$\frac{c}{v} = ReS \tag{5.11}$$

where f is the frequency in Hertz, c is the velocity of light in air, and v is the phase velocity of the field components in the earth-ionosphere waveguide. Note that if the cavity walls are perfectly conducting, the attenuation, α, should be zero which is confirmed by (5.10) since ImS = 0 for the perfect cavity. Fig. (5.2) reveals an interesting property of the earth-ionosphere waveguide: it is a "slow wave" system in the Schumann band, i.e. the phase velocity is always less than c.

The first three Schumann resonances occur at about 8, 14, and 20 Hertz with approximately 6 Hertz separating them. From Figs. (5.2) and (5.3) it is evident that ReS and ImS are fairly constant in the frequency interval between adjacent resonances. The ratio of the electric field magnitude at the N + 1 st resonance to the electric field magnitude at the n^{th} resonance is then independent of the properties of the ionosphere and is given by

$$\left| \frac{E_{n+1}}{E_n} \right| = \frac{M(\omega_{n+1})(2n+3)\omega_{no} P_{n+1}(\cos\theta)}{M(\omega_n)(2n+1)\omega_{n+1,0} P_n(\cos\theta)} \qquad (5.12)$$

Similarly, it is not difficult to show that, under the approximations that have been made, $|H_{n+1}/H_n|$ is also independent of ionospheric properties and is given by

$$\left| \frac{H_{n+1}}{H_n} \right| = \frac{M(\omega_{n+1})(2n+3)\omega_{no}^2 \frac{d}{d\theta} P_{n+1}(\cos\theta)}{M(\omega_{n+1})(2n+1)\omega_{n+1,0}^2 \frac{d}{d\theta} P_n(\cos\theta)} \qquad (5.13)$$

Another parameter which will be of interest in this report is the ratio of the E field at the n^{th} resonance to the H field at the n^{th} resonance. This can be easily shown to be

$$\left| \frac{E_n}{H_n} \right| = \eta \sqrt{n(n+1)} \quad \mathrm{Re}S \frac{1}{\sin(\phi-\alpha)} \frac{P_n(\cos\theta)}{\frac{d}{d\theta} P_n(\cos\theta)} \qquad (5.14)$$

which displays a dependence on the ionosphere model (since it involves S) but has the interesting feature that it is independent of the lightning stroke frequency spectrum.

The preceding discussion applies only to an infinitesimal point source and it is desirable to extend these results to a distributed source which is a better description of a thunderstorm region.

Following the approach in Chapter IV, and choosing the source as in Fig. (4.1) the received electric and magnetic fields in a high Q cavity can be determined as follows. If we use the notation

$$G_E(\theta,\phi) = g(\omega_n) \left| \frac{2n+1}{4\pi\varepsilon h a^2} \frac{\mathrm{Re}^2 S}{2\omega_{no} \mathrm{Im}S} \frac{d^{\circ}}{d\theta} P_n(\cos\theta) \right|^2 \qquad (5.16)$$

and

$$G_H(\theta,\phi) = g(\omega_n)\left|\frac{q^2(2n+1)}{k^3 ha^3}\,\frac{ReS}{2\omega_{no}^2\,ImS}\,\frac{d}{d\theta}\,P_n(\cos\theta)\right|^2 \qquad (5.16)$$

where, as before, $g(\omega)$ is the lightning dipole moment squared per unit area; the magnitude squared of the received electric field is

$$|E_n|^2 = \int_{\phi-\Delta_\phi}^{\phi+\Delta_\phi}\int_{\theta-\Delta}^{\theta+\Delta} G_E(\theta',\phi')a^2\sin\theta'd\theta'd\phi' \qquad (5.17)$$

and the magnitude squared of the magnetic field component exciting the receiving coil is

$$|H_n|^2 = \int_{\phi-\Delta_\phi}^{\phi+\Delta_\phi}\int_{\theta-\Delta}^{\theta+\Delta} G_H(\theta',\phi')\sin^2(\phi'-\alpha)\sin\theta'd\theta'd\phi' \qquad (5.18)$$

Assuming that $g(\omega)$ is independent of θ and ϕ, the squared electric field ratios at adjacent resonances in the high Q cavity are

$$\left|\frac{E_{n+1}}{E_n}\right|^2 = \frac{M^2(\omega_{n+1})(2n+3)^2\omega_{no}^2}{M^2(\omega_n)(2n+1)^2\omega_{n+1,0}^2}\,\frac{\int_{\theta-\Delta}^{\theta+\Delta}P_{n+1}^2(\cos\theta')\sin\theta'd\theta'}{\int_{\theta-\Delta}^{\theta+\Delta}P_n^2(\cos\theta')\sin\theta'd\theta'} \qquad (5.19)$$

and the squared magnetic field ratios are

$$\left|\frac{H_{n+1}}{H_n}\right|^2 = \frac{M^2(\omega_{n+1})(2n+3)^2\omega_{no}^4}{M^2(\omega_n)(2n+1)^2\omega_{n+1,0}^4}\,\frac{\int_{\theta-\Delta}^{\theta+\Delta}\left[\frac{d}{d\theta'}P_{n+1}(\cos\theta')\right]^2\sin\theta'd\theta'}{\int_{\theta-\Delta}^{\theta+\Delta}\left[\frac{d}{d\theta'}P_n(\cos\theta')\right]^2\sin\theta'd\theta'} \qquad (5.20)$$

The impedences or electric field to magnetic field ratios for a distributed source in the high Q cavity are given by

$$\left|\frac{E_n}{H_n}\right|^2 = \frac{\eta^2 n(n+1)Re^2 S2\Delta_\phi}{[\Delta_\phi - \frac{1}{2}\sin 2\Delta_\phi \cos 2(\phi-\alpha)]} \frac{\int_{\theta-\Delta}^{\theta+\Delta} P_n^2(\cos\theta')\sin\theta' d\theta'}{\int_{\theta-\Delta}^{\theta+\Delta}\left[\frac{d}{d\theta'} P_n(\cos\theta')\right]^2 \sin\theta' d\theta'} \tag{5.21}$$

It is evident from equations (5.19) and (5.20) that the electric field power ratios and the magnetic field power ratios are independent of the azimuthal spread, Δ_ϕ, of the source. They do depend on the distance, θ, to the center of the source and also depend on the range spread, Δ, however. The E to H power ratios, eq. (5.21), depend on $\Delta\phi$, Δ, ϕ and θ but are not a function of the lightning spectrum since they are ratios of quantities measured at the same frequency. In the next section, we dispense with the assumption of a high Q cavity and obtain more realistic expressions for the ratios.

5.2 Ratios for Distributed Sources in the Lossy Cavity

Since the quality factor of the earth-ionosphere resonant cavity is of the order of 4 (Jones, 1967) the assumption that only the resonance term in equations (4.7) or (4.9) is significant is really not justified. Relaxing this condition, the electric field ratios are given by the expression

$$\left|\frac{E_{n+1}}{E_n}\right|^2 = \frac{\int_{\phi-\Delta_\phi}^{\phi+\Delta_\phi}\int_{\theta-\Delta}^{\theta+\Delta} G_{E_{n+1}}(\theta',\phi')\sin\theta' d\theta' d\phi'}{\int_{\phi-\Delta_\phi}^{\phi+\Delta_\phi}\int_{\theta-\Delta}^{\theta+\Delta} G_{E_n}(\theta',\phi')\sin\theta' d\theta' d\phi'} \tag{5.22}$$

where

$$G_{E_n}(\theta,\phi) = g(\omega_n)\left|\frac{\nu(\nu+1)}{4\pi a^2 \omega_n \epsilon_o h}\sum_{n=0}^{\infty}\frac{2n+1}{n(n+1)-\nu(\nu+1)}P_n(\cos\theta)\right|^2 \tag{5.23}$$

and the ratios of the magnetic field squared at the n + 1 st resonance to the magnetic field squared at the nth resonance are

$$\left|\frac{H_{n+1}}{H_n}\right|^2 = \frac{\int_{\phi-\Delta_\phi}^{\phi+\Delta_\phi}\int_{\theta-\Delta}^{\theta+\Delta} G_{H_{n+1}}(\theta',\phi')\sin^2(\phi'-\alpha)\sin\theta'\,d\theta'\,d\phi'}{\int_{\phi-\Delta_\phi}^{\phi+\Delta_\phi}\int_{\theta-\Delta}^{\theta+\Delta} G_{H_n}(\theta',\phi')\sin^2(\phi'-\alpha)\sin\theta'\,d\theta'\,d\phi'} \tag{5.24}$$

where $G_{H_n}(\theta,\phi)$ is given by eq. (4.13). Finally, the electric to magnetic field ratios are given by

$$\left|\frac{E_n}{H_n}\right|^2 = \frac{\int_{\phi-\Delta_\phi}^{\phi+\Delta_\phi}\int_{\theta-\Delta}^{\theta+\Delta} G_{E_n}(\theta',\phi')\sin\theta'\,d\theta'\,d\phi'}{\int_{\phi-\Delta_\phi}^{\phi+\Delta_\phi}\int_{\theta-\Delta}^{\theta+\Delta} G_{H_n}(\theta',\phi')\sin\theta'\,d\theta'\,d\phi'} \tag{5.25}$$

Assuming that the surface distribution of dipoles is constant over the source; or equivalently, that $g(\omega)$ does not depend on θ or ϕ, it follows that

$$\left|\frac{E_{n+1}}{E_n}\right|^2 = \frac{\int_{\theta-\Delta}^{\theta+\Delta} G_{E_{n+1}}(\theta',\phi')\sin\theta'\,d\theta'}{\int_{\theta-\Delta}^{\theta+\Delta} G_{E_n}(\theta',\phi')\sin\theta'\,d\theta'} \tag{5.26}$$

$$\left|\frac{H_{n+1}}{H_n}\right|^2 = \frac{\int_{\theta-\Delta}^{\theta+\Delta} G_{H_{n+1}}(\theta',\phi')\sin\theta'd\theta'}{\int_{\theta-\Delta}^{\theta+\Delta} G_{H_n}(\theta',\phi')\sin\theta'd\theta'} \qquad (5.27)$$

$$\left|\frac{E_n}{H_n}\right|^2 = \frac{2\Delta_\phi \int_{\theta-\Delta}^{\theta+\Delta} G_{E_n}(\theta',\phi')\sin\theta'd\theta'}{[\Delta_\phi - \tfrac{1}{2}\sin 2\Delta_\phi \cos 2(\phi-\alpha)]\int_{\theta-\Delta}^{\theta+\Delta} G_{H_n}(\theta',\phi')\sin\theta'd\theta'} \qquad (5.28)$$

There are four important parameters to be determined in the thunderstorm location problem: θ, the angular distance or range to the center of the source; ϕ, the bearing or azimuth of the source center; Δ, the range spread of source; and $\Delta\phi$, the azimuthal spread of the source. The E ratios and H ratios contain information about θ and Δ but are independent of ϕ and $\Delta\phi$. The E to H ratios depend on θ, Δ, ϕ, and $\Delta\phi$. In the next chapter methods are discussed for estimating these parameters from Schumann resonance data.

Numerical results for equations (5.26) - (5.28) can be obtained by specifying an ionosphere model and a lightning spectrum. The lightning spectrum of equation (3.3) has been used successfully by Galejs (1961a) and will be employed here.

Jones (1967) has shown that the effect of heavy ions in the lower regions (below 56 km) of the ionosphere must be included in any ionosphere model to be used below 50 Hertz. Curves "c" on Figs. (5.2) and (5.3) give ReS and ImS for an ionosphere profile determined from reaction

rates of atmospheric constituent gases by Pierce and Cole (1965). This profile includes the effect of the heavy ions and values of ν can be computed from the curves "c" by $\nu = kaS - 0.5$.

The variation with source distance of the ratios of the adjacent resonant peaks in the received electric field power spectrum is shown in Fig. (5.4) for $\Delta = 20^{\circ}$. The results of calculations using both the high-Q, dominant term approximation and the full series, inhomogeneous ionosphere model are shown. Note that the relative sizes of the peaks display a marked variation with source-receiver distance. It is also evident that the ratios for the high Q cavity are not radically different from the ratios for the realistic cavity. It is also apparent from Fig. 5.1, that the results for the point source and distributed source are qualitatively the same, i.e. at $\theta = 90^{\circ}$ the second resonance is large compared to the first resonance, etc. For this reason and because the choice of the ionosphere model is not extremely critical, it is evident that eqs. (5.12, 5.13, 5.14) can yield great insight into the source location problem.

The magnetic field power spectrum ratios for both the high Q and low Q cases are shown in Fig. (5.5). Here the ionosphere model seems to have a greater effect but qualitatively the results are again the same for both ionospheres.

The expression for the electric to magnetic ratios, eq. (5.28) is fairly complicated in that it depends on all four of the source parameters. For the moment we simplify the expression by choosing the special case $\Delta\phi$ small, $\alpha = 0^{\circ}$, and $\phi = 90^{\circ}$. This effectively assumes

that the azimuthal spread is small (less than 15°) and that the receiving coil is oriented so that its maximum response is in the direction of the center of the source. Under these assumptions the coefficient multiplying the ratio of integrals in (5.28) is unity. For this special case the ratios $|F_z/H_n|^2$ are plotted as a function of θ for both the high Q and low Q cavity in Fig. (5.6). Again the qualitative results are the same for both ionosphere models.

5.3 Effect of Ionosphere Model on Ratios

It is evident from the results of the previous section that even a very drastic change in the properties of the ionosphere such as the difference between the Pierce-Cole profile and the perfectly conducting model does not fundamentally alter the variation of the ratios with source-receiver distance. To investigate this effect in a more meaningful manner, ratio calculations based upon two different inhomogeneous ionosphere profiles were performed.

The exponential conductivity profile used by Galejs (1961a) and the Pierce-Cole (1965) conductivity profile—both for day ionospheres—are shown in Fig. (5.7). The Galejs profile is based upon particle density and collision frequency data for electrons only (Galejs, 1961b); the Pierce and Cole curve, on the other hand, includes the effects of positive and negative ions which account for the fact that the two models have conductivities that differ by as much as two orders of magnitude at the lower altitudes.

A comparison of the ratios for the Pierce-Cole (or Jones) ionosphere, the Galejs ionosphere and the perfectly conducting ionosphere

is given by Figs. (5.8 - 5.14). As would be expected, the ratios for the Galejs model are closer to the results of the Pierce-Cole (Jones) model than to those for the high Q cavity. The perfectly conducting case is, of course, a very unrealistic approximation to the ionosphere and should only be used to provide initial insight into the Schumann phenomena.

If an experimental spectrum is given and the ratios are computed from it, the source distances estimated from the Jones or Galejs models would differ at most by about 10° which is an acceptable error for a source of $\Delta = 20^{\circ}$ (total source width 40°).

The relative invariance of the ratios of spectral peaks with ionosphere properties indicates that observations of these ratios might be practically useful for determining source-receiver separation. It has been pointed out by Large and Wait (1968) and by Balser and Wagner (1962) that the values of the Schumann resonant frequencies themselves depend also upon source-receiver separation; it should be noted however, that the exact values of the resonant frequencies are very strongly dependent on the properties of the ionosphere. Illustrative of this fact are Figs. (5.15 - 5.20) where the six resonant frequencies are shown as a function of source distance for the ionosphere models of Galejs and Pierce-Cole.

Suppose one were to attempt to determine source location from resonant frequency measurements: if the first resonance in the magnetic field were at 8.0 Hz (for example), the estimated source distance would be 63° based upon the Pierce and Cole model and 110° based upon the Galejs model, a difference of 47° (5000 km). If the second resonance

in the H field were at 13.7 Hz, the distances would be 28° and 75°, also a large variation. Note that for a higher or lower peak frequency only one of the models could yield a source distance; in this case, we could use the resonant frequency to choose the "best" of the two ionosphere profiles. The ionospheric dependence of the peak frequencies of the second and third resonances is strikingly illustrated by Figs. (5.17), (5.19), and (5.20) which could also be used to determine which of the two ionosphere profiles is "best".

It is clear that the resonant frequencies are determined at least equally by the ionosphere profile and the source location. In fact, for the higher resonances, the ionosphere seems to be the dominant factor in the resonant frequency variations. To obtain source-receiver information from resonant frequency measurements would require detailed knowledge of the local as well as global properties of the ionosphere; the ratio method, however, demands only fairly crude ionospheric data.

VI. PROCEDURES FOR THE LOCATION OF SOURCES BY THE RATIO METHOD

Having demonstrated that the ratios of the spectral peak powers are relatively independent of the properties of the ionosphere, we now turn to a discussion of methods for estimating the source parameters ϑ, ϕ, Δ, and Δ_ϕ from measured ratio data.

According to Jones (1969) a given spectrum corresponds to one and only one source-receiver separatior, i.e. the spectra are unique. It is reasonable, therefore, to assume what a given ordered sequence of measured ratios ($|E_2/E_1|^2$, $|E_3/E_2|^2$, $|H_2/H_1|^2$, $|H_3/H_2|^2$) can correspond to only one source distance, θ. Consequently, one would expect that unique determinations of source receiver separation from ELF spectra is possible.

6.1. General Discussion of Source Distance Estimation

Suppose we wish to find the "best match distance" between n ratios; R_1, R_2, ... R_n. For example, R_1 might be $|H_2/H_1|^2$, $R_2 = |H_3/H_2|^2$, $R_3 = |E_2/E_1|^2$, etc. It is desired to find one angle, θ, which is the solution to the n equations,

$$\begin{aligned} R_1 &= f_1(\theta) \\ R_2 &= f_2(\theta) \\ &\vdots \\ R_n &= f_n(\theta) \end{aligned} \qquad (6.1)$$

The f functions are basically the ratios of squared sums of Legendere polynomials for $|E_{n+1}/E_n|^2$, or the ratios of squared sums of derivatives of Legendere polynomials for $|H_{n+1}/H_n|^2$; hence, the functions $f_i(\theta)$ are non-linear and single valued, but the inverse functions $f_i^{-1}(R_i)$ are non-linear and multivalued.

In the discussions below, let θ_i^j be the i^{th} root for the j^{th} ratio and let N_j be the number of roots of $R_j = f_j(\theta)$, i.e. $f_j(\theta) = R_j$ at $\theta = \theta_1^j, \theta_2^j \ \ldots \ \theta_{N_j}^j$. If there are n ratios to be matched, the solutions of equations (6.1) will yield then sets of roots

$$\theta_1^1, \theta_2^1, \theta_3^1, \ \ldots \ \theta_{N_1}^1 \quad \text{by solving} \quad R_1 = f_1(\theta)$$

$$\theta_1^2, \theta_2^2, \theta_3^2, \ \ldots \ \theta_{N_2}^2 \quad \text{by solving} \quad R_2 = f_2(\theta)$$

$$\vdots$$

$$\theta_1^n, \theta_2^n, \theta_3^n, \ \ldots \ \theta_{N_n}^n \quad \text{by solving} \quad R_n = f_n(\theta)$$

a total of $(N_1 + N_2 + \ldots N_n)$ angles of which only one from each set is the desired angle. Our task is to choose the n values of θ_i^j that are mutually closest remembering that there is some measurement error in the given values of R_i. By mutually closest is meant those n values of θ_i^j for which p_j and q_n are selected such that

$$Q(p_j, q_n) = \sum_{j=1}^{n} \sum_{n \geq k > j}^{n} \left| \theta_{p_j}^j - \theta_{q_n}^k \right| \qquad (6.2)$$

is a minimum $1 \leq P_j \leq N_j \quad 1 \leq q_k \leq N_q$

The distance estimate, θ, is then specified by

$$\hat{\theta} = \frac{1}{n} (\theta^1 + \theta^2 + \ldots \theta^n) \qquad (6.3)$$

where the selected θ^j are the n mutually closest roots.

The ratio values will, of course, not be exact due to the noise like properties of ELF signals. As is discussed in Chapter II, the power spectrum estimates are random variables with standard deviation

$$\sigma = \mu \frac{1}{\sqrt{(\Delta f)T}}$$

where μ is the expected value of the power spectrum estimates. For a frequency resolution of 0.5 Hz and a time sample 15 minutes long the standard deviation is about five percent of the expected value. The probability that a normally distributed random variable is less than 2 standard deviations from its expected value is about .95. Therefore, it is quite certain that the actual ratios are within plus or minus ten percent of the estimated ratios.

If the possibility of errors in ratio estimates is included in the source location problem we define a perturbed set of ratios given by $(1 + \varepsilon_1)R_1$, $(1 + \varepsilon_2)R_2$, ... $(1 + \varepsilon_n)R_n$ where the ε_i are in the range $-.15 < \varepsilon_i < +.15$. The method is then to determine Q for all different combinations of these perturbations. The roots θ^1, θ^2, θ^3, ... θ^n which give the smallest Q are then used to determine the best match distance by (6.3).

The larger perturbations are less probable than the smaller perturbations, i.e. it is most likely that the measured ratios are equal to

the actual ratio. Because of this, it is desirable to employ a "stopping rule" as follows. Rather than searching for the absolute minimum Q as above, we stop searching for a match when the maximum of $|\theta^j_{p_j} - \theta^k_{q_j}|$ for all j and k is less than some small specified angular distance (5° for the $\Delta = 20^\circ$ model, for example). The search for the best match is done beginning with the smallest perturbations on the roots and working towards the larger perturbations. The ordering of the perturbation sequence is determined by the quantity

$$P = \sum_{i=1}^{n} |\varepsilon_i| \tag{6.4}$$

so that the perturbation vectors ($\varepsilon_1, \varepsilon_2, \ldots \varepsilon_n$) which give the smallest p are used first in the root search procedure, then the perturbation set which gives the next larger p is used and so on, until either a match is achieved or all possible perturbations (within the specified limits) have been investigated. This algorithm must, of course, be performed on a digital computer.

6.2. The Distance Estimation Procedure for Matching Two Ratios

As a simple application of the general method outlined above we consider the problem of finding the unique θ which gives the best match to two given ratios R_1 and R_2. R_1 could be $|E_2/E_1|^2$ and R_2 could be $|E_3/E_2|^2$ in the $\Delta = 20^\circ$ model, for example. The procedure requires frequent evaluation of the inverse functions $f_i^{-1}(\theta)$; i = 1, 2, ... n (n = 2 in this example) which is done by linear interpolation on tables of values of θ and R_1 and tables of values of θ and R_2. The multivalued property

of the functions $f_1(\theta)$ and $f_2(\theta)$ can be handled by dividing the tables into several piecewise singlevalued regions of θ. In the example under discussion $f_1(\theta) = |E_2/E_1|^2$ and $f_2(\theta) = |E_3/E_2|^2$ where $f_1(\theta)$ has four monotonic regions: $\theta < 55^\circ$, $55^\circ < \theta < 90^\circ$, $90^\circ < \theta < 125^\circ$, and $\theta > 125^\circ$.

The function $f_2(\theta)$ also has the same four monotonic regions: $\theta < 55^\circ$, $55^\circ < \theta < 90^\circ$, $90^\circ < \theta < 125^\circ$, and $\theta > 125^\circ$. The reader can verify these statements by refering to Figure (5.4). Hence, for a given R_1 and R_2, there will be at most four roots of $f_1(\theta)$: θ_1^1, θ_2^1, θ_3^1, θ_4^1; and four roots of $f_2(\theta)$: θ_1^2, θ_2^2, θ_3^2, θ_4^2.

The root search procedure is as follows. The smallest perturbation pair ε_1, ε_2 is chosen (these will both be zero) and the roots in each monotonic region of each ratio are found by interpolation on the tables of theoretical ratio calculations. Then, the smallest of the quantities $|\theta_i^1 - \theta_j^2|$ is found and this difference compared to 5°. If it is less than 5° it is termed a match and the distance estimate, θ is determined by

$$\hat{\theta} = \tfrac{1}{2}(\theta^1 + \theta^2)$$

where θ^1 and θ^2 are the two closest angles, the first selected from the set $(\theta_1^1, \theta_2^1, \theta_3^1, \theta_4^1)$ and the second from the set $(\theta_1^2, \theta_2^2, \theta_3^2, \theta_4^2)$. Of course, the closest two angles may be more than 5° apart. If this is the case the next larger perturbation on R_1 and R_2 is used to determine the roots, the difference between the closest two roots is compared to 5° and so on, until either there is a match or all perturbation pairs have been tried. In the latter case, the model is changed (for example a different Δ is used) and the procedure is

initiated again. A flowchart of the method for matching two ratios is shown in Figure (6.1). Refering to the flowchart, MAXEPS is the largest perturbation considered, DEPS is the increment between different perturbations, MINO is the maximum allowed distance difference for a match, MIN is the magnitude of the angular distance between the two closest roots for a given perturbation pair, and NPERTS is the total number of different perturbation pairs.

6.3. Estimation of Source Distance and Δ from Ratio Data

The source range spread can be estimated from the E ratios and/or H ratios in the following way. Suppose it is desired to choose the best distance, θ, and best match Δ from the possible models $\Delta = 0^\circ$, $\theta = 5^\circ$, $\Delta = 10^\circ$, $\Delta = 20^\circ$. The procedure is merely an extension of the method described in section 2: one determines the best θ from the $\Delta = 0^\circ$ model and stores the perturbations required for a match. Then the same is done for the other three Δ values. Whichever Δ value gives a match with the smallest perturbation is the best match Δ and the corresponding θ is the best match distance.

6.4. Determination of Azimuth and Azimuthal Spread of the Source

Refering to Figure (4.1) let the $\phi = 0$ line from the receiving site be the east-west line. A coil whose axis is along the east-west line ($\alpha = 0$) will be excited by the magnetic field component given by

$$\left|H^{EW}\right|^2 = \left[\Delta_\phi - \tfrac{1}{2}\cos 2\phi \sin 2\Delta_\phi\right] \mathcal{K}_n(\theta,\Delta) \qquad (6.5)$$

where

$$\mathcal{K}_n(\theta,\Delta) = \int_{\theta-\Delta}^{\theta+\Delta} G_{H_n}(\theta') a^2 \sin\theta' d\theta'$$

and the magnitude squared of the magnetic field component measured by a coil whose axis is along the north-south line ($\alpha = 90^\circ$) is given by

$$|H^{NS}|^2 = [\Delta_\phi + \tfrac{1}{2}\cos 2\phi \sin 2\Delta_\phi]\, \mathcal{K}_n(\theta,\Delta) \tag{6.6}$$

The electric field magnitude squared at the receiver is, as before,

$$|E_n|^2 = 2\Delta_\phi\, \mathcal{E}_n(\theta,\Delta) \tag{6.7}$$

where

$$\mathcal{E}_n(\theta,\Delta) = \int_{\theta-\Delta}^{\theta+\Delta} G_{E_n}(\theta')a^2 \sin\theta' d\theta'$$

Dividing equation (6.5) by equation (6.6) one obtains

$$\left| \frac{H_n^{EW}}{H_n^{NS}} \right|^2 = \frac{\Delta_\phi - \tfrac{1}{2}\cos 2\phi \sin 2\Delta_\phi}{\Delta_\phi + \tfrac{1}{2}\cos 2\phi \sin 2\Delta_\phi} \tag{6.8}$$

and if Δ_ϕ is small ($\Delta_\phi < 10^\circ$) this reduces to

$$\left| \frac{H_n^{EW}}{H_n^{NS}} \right|^2 = \tan^2\phi \tag{6.9}$$

A plot of $|H_n^{EW}/H_n^{NS}|^2$ against ϕ for small Δ_ϕ is shown in Figure (6.2). Note that for a fixed $|H_n^{EW}/H_n^{NS}|^2$ value there are four possible azimuthal locations, ϕ. The number of possible source bearings can be reduced to two as follows. Suppose two coils with perpendicular axes are mounted on a turntable so the angle α between the coils and the $\phi = 0$ line, see Figure (4.1), can be varied. Let $|H_1|^2$ be the magnitude squared of the magnetic field component exciting a coil whose axis makes an angle $\alpha = \alpha_1$ with $\phi = 0$ line and let $|H_2|^2$ be the magnitude squared of the magnetic field component exciting a coil whose axis is at

an angle $\alpha_2 = \alpha_1 + \pi/2$ with respect to the $\phi = 0$ line. Then it is evident from the discussion in Chapter 5 that

$$\left| \frac{H_1}{H_2} \right|^2 = \frac{\Delta_\phi - \frac{1}{2}\cos 2(\phi-\alpha)\sin 2\Delta_\phi}{\Delta_\phi + \frac{1}{2}\cos 2(\phi-\alpha)\sin 2\Delta_\phi} \cong \tan^2(\phi-\alpha) \qquad (6.10)$$

if Δ_ϕ is small. Hence, at $\alpha = \phi$ (or $\phi + \pi$) the ratio of the fields measured by the two coils must be small and by rotating the coils until $|H_1/H_2|^2$ is a minimum, the axis of coil 1 lies on the great circle path between source and receiver.

The assumption of small Δ_ϕ is not critical. Even in the highly unlikely case $\Delta_\phi = 30^\circ$, ϕ estimates based on the $\Delta_\phi = 0^\circ$ model will be in error by only about 5° or 10° as is shown in Figure (6.3) where Eq. (6.10) for various Δ_ϕ is plotted.

We have seen that estimates of θ and Δ can be obtained from the ratios $|E_2/E_1|^2$, $|E_3/E_2|^2$ and/or $|H_2/H_1|^2$, $|H_3/H_2|^2$ and that by employing a pair of orthogonal coils the azimuth of the source can be found. From either of the quantities $\left|E_n/H_n^{EW}\right|^2$ or $\left|E_n/H_n^{NS}\right|^2$ the value of Δ_ϕ can be obtained. For example,

$$\left| \frac{E_n}{H_n^{EW}} \right|^2 = \frac{2\Delta_\phi}{\Delta_\phi - \frac{1}{2}\cos 2\phi \sin 2\Delta_\phi} \frac{\mathcal{E}_n(\theta,\Delta)}{\mathcal{H}_n(\theta,\Delta)} \qquad (6.11)$$

where curves of $\mathcal{E}n(\theta,\Delta)/\mathcal{H}n(\theta,\Delta)$ versus θ for various Δ are given in Chapter 5. After having found θ, Δ, and ϕ by the methods described above eq. (6.11) contains only one unknown, Δ_ϕ, which can then be determined if measurements of $\left|E_n/H_n^{EW}\right|^2$ are available (although it is clear that (6.11) shows only a very small dependence on Δ_ϕ).

Thus, all the significant parameters of a thunderstorm source can be determined by measurements at a single receiving station. There is, however, an ambiguity of 180° in the determination of the source azimuth which could probably be resolved by the elimination of unlikely (e.g. temperate zone winter) source locations.

6.5. An Alternate Method for Source Distance Estimation from Measured Ratios

The solution of the problem posed by equations (6.1) can also be treated as a minimization of the distance between two vectors in an n dimensional vector space. Let the vector of given, experimental ratio values be denoted by

$$\overline{R} = \begin{bmatrix} r_1 \\ r_2 \\ \cdot \\ \cdot \\ \cdot \\ r_n \end{bmatrix} \tag{6.12}$$

and the vector of function values, which depend on both θ and Δ as parameters, be denoted by

$$\overline{F} = \begin{bmatrix} f_1(\theta,\Delta) \\ f_2(\theta,\Delta) \\ \cdot \\ \cdot \\ \cdot \\ f_{n_1}(\theta,\Delta) \end{bmatrix} \tag{6.13}$$

The distance between these two vectors is given by the expression

$$d = \sqrt{\sum_{i=1}^{n} [r_i - f_i(\theta,\Delta)]^2}$$

and this is a minimum for the same θ and Δ that minimize

$$Q = \sum_{i=1}^{n} [r_i - f_i(\theta,\Delta)]^2 \qquad (6.14)$$

The solution of equations (6.1) is then where $Q = 0$. There are, of course, some errors in the measurement of the quantities r_1, r_2 ... r_n so that there may not exist any (θ,Δ) pair for which $Q = 0$. One would expect, however, that useful estimates of the source distance and range extent, Δ, could be obtained by minimizing Q.

The function Q in equation (6.14) has the undesirable property that a small error in a large ratio value can be an equal or even larger contributor to the total mean squared error than a large error in a small ratio estimate. It would be preferable to weight all the errors on a percentage basis which can be accomplished by employing a minimizing function of the form

$$Q = \sum_{i=1}^{n} \left[\frac{r_i - f_i(\theta,\Delta)}{r_i}\right]^2 \qquad (6.15)$$

The standard method for determining the θ and Δ which minimize the expression in equation (6.15) would be to solve the two simultaneous non-linear equations

$$\frac{\partial Q}{\partial \theta} = 0$$

$$\frac{\partial Q}{\partial \Delta} = 0$$

for θ and Δ. The expressions for the $f_i(\theta,\Delta)$ are, however, extremely involved and the standard approach seems unwarranted. The method used here is to simply guess the θ and Δ which minimize Q. The procedure would be as follows: choose a value of Δ, say 0°. Then evaluate Q for every value of θ from 0° to 180° in steps of one degree. The value of θ for which Q is a minimum would be the best θ for that particular Δ. Next choose another value of Δ, say 5°, and repeat the above search for the minimum Q. The procedure is continued until all values of Δ have been investigated and their corresponding best match θ's have been found. The solution would be that (θ,Δ) pair for which Q is a minimum. The algorithm outlined above will always find a solution to $\overline{R} = \overline{F}(\theta)$ regardless of how poor a match is obtained. A rule to determine whether or not a solution has been found would be to test the quantity $\sqrt{Q_{min}/n}$ (average normalized deviation) against a prescribed tolerance, say .05.

6.6. Estimation of Source Distance From $|E_n/H_n|^2$ ratios

The ratio of the electric field power spectral density to the magnetic field power spectral density at their respective nth resonances is essentially independent of the lightning spectrum since the resonances of the two fields occur at very nearly the same frequency. A measurable quantity (which is not the total magnetic field magnitude squared) is determined by the addition of eqs. (6.5) and (6.6) to be

$$|H_n^{EW}|^2 + |H_n^{NS}|^2 = 2\Delta_\phi \; \mathcal{H}_n(\theta,\Delta)$$

and the electric field magnitude squared is

$$|E_n|^2 = 2\Delta_\phi \, \mathcal{E}_n(\theta,\Delta)$$

so that

$$\frac{|E_n|^2}{|H_n^{EW}|^2 + |H_n^{NS}|^2} = \frac{\mathcal{E}_n(\theta,\Delta)}{\mathcal{A}_n(\theta,\Delta)}$$

Hence, the ratios $|E_1|^2/(|H_1^{EW}|^2 + |H_1^{NS}|^2)$; $|E_2|^2/(|H_2^{EW}|^2 + |H_2^{NS}|^2)$ and $|E_3|^2/(|H_3^{EW}|^2 + |H_3^{NS}|^2)$ depend only on the source distance and distance spread, not on the lightning spectrum, the source azimuth or azimuthal spread. These remaining source parameters can be determined as described in section (6.4) and it is clear that all the parameters of the source can be estimated regardless of the lightning spectrum provided that ratios taken at the same frequency such as $|E_n/H_n|^2$, $|H_n^{EW}/H_n^{NS}|^2$, $|E_n/H_n^{EW}|^2$, or $|E_n/H_n^{NS}|^2$ are used. This suggests a method of estimating the lightning spectrum at the Schumann resonant frequencies since the ratios $|E_{n+1}/E_n|^2$ and $|H_{n+1}/H_n|^2$ do depend on the lightning frequency spectrum.

VII. LOCATION OF TWO ELF SOURCE REGIONS FROM A SINGLE RECEIVING STATION

It is probably a relatively rare occurence that only one major thunderstorm center is exciting the earth-ionosphere cavity at a given time and it is therefore desirable to have a method for locating the positions of, at least, two simultaneously active source regions.

7.1. Received ELF Spectra from Two Distinct Sources

We shall assume two sources of the type depicted in Figure (4.1): a source "A" at azimuth ϕ_A, distance θ_A and a source "B" at azimuth ϕ_B, distance θ_B from the receiving site. The range and azimuthal spreads of these two sources are denoted by Δ_A, Δ_{ϕ_A} and Δ_B, Δ_{ϕ_B} respectively. The received electric field magnitude squared is then given by

$$|E|^2 = 2\Delta_{\phi_A}\, \mathcal{E}(\theta_A, \Delta_A) + 2\Delta_{\phi_B}\, \mathcal{E}(\theta_B, \Delta_B) \tag{7.1}$$

and the power spectra in the east-west and north-south oriented coils are proportional to

$$\begin{aligned} |H^{EW}|^2 = {} & [\Delta_{\phi_A} - 1/2 \cos 2\phi_A \sin 2\Delta_{\phi_A}]\, \mathcal{H}(\theta_A, \Delta_A) \\ & + [\Delta_{\phi_B} - 1/2 \cos 2\phi_B \sin 2\Delta_{\phi_B}]\, \mathcal{H}(\theta_B, \Delta_B) \end{aligned} \tag{7.2}$$

and

$$\begin{aligned} |H^{NS}|^2 = {} & [\Delta_{\phi_A} + 1/2 \cos 2\phi_A \sin 2\Delta_{\phi_A}]\, \mathcal{H}(\theta_A, \Delta_A) \\ & + [\Delta_{\phi_B} + 1/2 \cos 2\phi_B \sin 2\Delta_{\phi_B}]\, \mathcal{H}(\theta_B, \Delta_B) \end{aligned} \tag{7.3}$$

Since there are now eight parameters which describe the location and extent of the two sources, it should be expected that estimation of these parameters would be more difficult than in the previous single source case.

7.2 Estimation of Range-Parameters for the Two Source Model

It is advantageous to employ in the location procedure those quantities which depend on the least number of independent parameters since their determination will be then greatly simplified. The electric field spectrum depends upon 6 of the 8 source parameters while each of the two magnetic field spectra is a function of the entire set of 8 parameters. This complexity can be reduced by combining equations (7.2) and (7.3) to obtain

$$|H^{EW}|^2 + |H^{NS}|^2 = 2\Delta_{\phi_A} \mathcal{H}(\theta_A, \Delta_A) + 2\Delta_{\phi_B} \mathcal{H}(\theta_B, \Delta_B) \qquad (7.4)$$

The number of variables can be further reduced if ratios of $|H^{EW}|^2 + |H^{NS}|^2$ and/or $|E|^2$ are considered. For example,

$$\left|\frac{E_{n+1}}{E_n}\right|^2 = \frac{2\Delta_{\phi_A} \mathcal{E}^A_{n+1} + 2\Delta_{\phi_B} \mathcal{E}^B_{n+1}}{2\Delta_{\phi_A} \mathcal{E}^A_{n+1} + 2\Delta_{\phi_B} \mathcal{E}^B_{n}} \qquad (7.5)$$

where $\mathcal{E}^A_{n+1} = \mathcal{E}(\theta_A, \Delta_A)$ (see eq. 6.6) is evaluated at the (n+1)st resonance of the <u>total</u> received electric field (since the total electric field is what can be measured). Equation (7.5) can be written as

$$\left|\frac{E_{n+1}}{E_n}\right|^2 = \frac{\mathcal{E}^A_{n+1} + \delta\, \mathcal{E}^B_{n+1}}{\mathcal{E}^A_{n} + \delta\, \mathcal{E}^B_{n}} \qquad (7.6)$$

where $\delta = (\Delta_{\phi_B} / \Delta_{\phi_A})$. The ratios in (7.6) thus depend on θ_A, θ_B, Δ_A, Δ_B, and δ.

We can further reduce the number of variables to three by making the assumption, $\Delta_A = \Delta_B = \Delta = 5^\circ$ corresponding to a great circle distance, 2Δ, of about 700 miles, which is probably a representative or average value for large thunderstorm areas (Kealoha, et. al., 1968; Byers, 1949). In any event, the ratios display only a second order (compared to θ) variation with Δ in the range $0^\circ \leq \Delta \leq 10^\circ$ which probably includes all realistic source sizes. As can be seen from Figures (7.1) and (7.2), a Δ value of 5° is representative for the range $0^\circ \leq \Delta \leq 10^\circ$.

The following seven ratios are then dependent only on θ_A, θ_B and δ:

$$\left| \frac{E_{n+1}}{E_n} \right|^2 = \frac{e^A_{n+1} + \delta\, e^B_{n+1}}{e^A_n + \delta\, e^B_n} \; ; \; n = 1, 2 \tag{7.7}$$

$$\frac{|H^{EW}_{n+1}|^2 + |H^{NS}_{n+1}|^2}{|H^{EW}_n|^2 + |H^{NS}_n|^2} = \frac{\mathcal{H}^A_{n+1} + \delta\, \mathcal{H}^B_{n+1}}{\mathcal{H}^A_n + \delta\, \mathcal{H}^B_n} \; ; \; n = 1, 2 \tag{7.8}$$

$$\frac{|E_n|^2}{|H^{EW}_n|^2 + |H^{NS}_n|^2} = \frac{e^A_n + \delta\, e^B_n}{\mathcal{H}^A_n + \delta\, \mathcal{H}^B_n} \; ; \; n = 1, 2, 3 \tag{7.9}$$

The above seven ratios are not all independent; the particular subset to be used will depend on the available data. Also, the ratios of the set (7.9) are independent of the lightning spectrum (provided the source spectrum at location A is the same as at location B). If the selected ratios are denoted by $f_i(\theta_A, \theta_B, \delta)$, $i = 1, 2, \ldots n$, the parameters θ_A, θ_B, and δ could be estimated by minimizing the quantity

$$Q(\theta_A, \theta_B, \delta) = \sum_{i=1}^{n} [r_i - f_i(\theta_A, \theta_B, \delta)]^2 \qquad (7.10)$$

where the r_i are the given, measured ratios. As discussed in Chapter VI, the minimization would be accomplished by repeated guesses of θ_A, θ_B, and δ; the evaluation of the f_i is again done by interpolation on tables of theoretically calculated results.

The procedure of repeated trial solutions is, however, quite time consuming. The dependence of the f_i on θ_A and θ_B is so complex that we are really forced to adopt this brute-force procedure, but the dependence of the f_i on δ is comparatively simple; the f_i are of the form

$$f_i(\delta) = \frac{A_i + \delta B_i}{C_i + \delta D_i} \qquad (7.11)$$

where A_i, B_i, C_i and D_i depend on θ_A and θ_B but we are emphasizing here the effect of δ on the ratios ($r_i = f_i$). This suggests minimizing, by conventional means, the quantity

$$Q = \sum_{i=1}^{n} \left[r_i - \frac{A_i + \delta B_i}{C_i + \delta D_i} \right]^2 \qquad (7.12)$$

for a specified θ_A and θ_B. The differentiation procedure necessitates, however, the solution of a high order polynomial in δ. A much simpler approach would be to write equation (7.11) as

$$r_i (C_i + \delta D_i) = (A_i + \delta B_i) \qquad (7.13)$$

and then to minimize the quantity

$$Q = \sum_{i=1}^{n} \left[r_i \, (C_i + \delta \, D_i) - (A_i + \delta \, B_i) \right]^2 \qquad (7.14)$$

which leads to the following linear equation for δ

$$\sum_{i=1}^{n} (C_i \, r_i - A_i) \, (D_i \, r_i - B_i) + \delta \sum_{i=1}^{n} (D_i \, r_i - B_i)^2 = 0 \qquad (7.15)$$

so that

$$\delta = \frac{\sum_{i=1}^{n} (A_i - C_i \, r_i)(D_i \, r_i - B_i)}{\sum_{i=1}^{n} (D_i \, r_i - B_i)^2} \qquad (7.16)$$

since

$$\frac{\partial^2 Q}{\partial \delta^2} = \sum_{i=1}^{n} (D_i \, r_i - B_i)^2 \geq 0 \qquad (7.17)$$

we are guaranteed that this δ minimizes Q for a specified θ_A and θ_B. The method of determining θ_A, θ_B, and δ from measured ratios can now be outlined as follows:

We investigate all values of θ_A and θ_B between 10° and 180° in steps of a prescribed increment, say 2°. The first value of θ_A, say 10°, is chosen and then a value of θ_B. All the quantities on the right hand side of (7.16) are then specified and a value of δ can be calculated. The corresponding value of Q is determined from (7.14) and stored. Then the next θ_B is chosen, δ determined, and Q calculated. If this Q is less than the previous Q, the former (along with the associated values of θ_A, θ_B, and δ) is stored in place of the latter and the next θ_B in sequence is used to determine a Q. This procedure is continued until

all possible values of θ_B are investigated. The next value of θ_A is chosen and all possible values of θ_B are used to determine a Q value and so on until the entire allowed set of θ_A, θ_B pairs have been used to evaluate the δ which yields a minimum Q. The values of θ_A, θ_B, and δ which produce the minimum of this set of minimums are the best choices of these source parameters for the given ratios.

7.3 Estimation of the Azimuthal Parameters in the Two - Source Model

There are fifteen ratios of spectral peak powers which depend upon the azimuths or bearings of the two sources; they are:

$$\left|H_n^{EW}/H_n^{NS}\right|^2 \quad ; \quad n = 1, 2, 3$$

$$\left|E_n/H_n^{EW}\right|^2 \quad ; \quad n = 1, 2, 3$$

$$\left|E_n/H_n^{NS}\right|^2 \quad ; \quad n = 1, 2, 3$$

$$\left|H_n^{NS}\right|^2 / \left(\left|H_n^{NS}\right|^2 + \left|H_n^{EW}\right|^2\right) ; \quad n = 1, 2, 3$$

$$\left|H_n^{EW}\right|^2 / \left(\left|H_n^{NS}\right|^2 + \left|H_n^{EW}\right|^2\right) ; \quad n = 1, 2, 3$$

where n denotes the ordinal number of the resonance. After examining these quantities, however it becomes clear that a knowledge of some of them implies a knowledge of the others. In fact, values for all of them are specified by measurements of any two members of the set

$$\left|H_n^{EW}/H_n^{NS}\right|^2, \left|E_n/H_n^{EW}\right|^2, \left|E_n/H_n^{NS}\right|^2$$

we shall confine our attention to the first two ratios of this set;

a different choice will not affect the arguments which follow.

By applying equations (7.1 - 7.3) these ratios are

$$\left|\frac{H_n^{EW}}{H_n^{NS}}\right|^2 = \frac{\left[\Delta_{\phi_A} - \frac{1}{2}\cos 2\phi_A \sin 2\Delta_{\phi_A}\right] \mathcal{H}_n^A + \left[\Delta_{\phi_B} - \frac{1}{2}\cos 2\phi_B \sin 2\Delta_{\phi_B}\right] \mathcal{H}_n^B}{\left[\Delta_{\phi_A} + \frac{1}{2}\cos 2\phi_A \sin 2\Delta_{\phi_A}\right] \mathcal{H}_n^A + \left[\Delta_{\phi_B} + \frac{1}{2}\cos 2\phi_B \sin 2\Delta_{\phi_B}\right] \mathcal{H}_n^B} \tag{7.18}$$

$$\left|\frac{E_n}{H_n^{EW}}\right|^2 = \frac{2\Delta_{\phi_A} \mathcal{E}_n^A + 2\Delta_{\phi_B} \mathcal{E}_n^B}{\left[\Delta_{\phi_A} - \frac{1}{2}\cos 2\phi_A \sin 2\Delta_{\phi_A}\right] \mathcal{H}_n^A + \left[\Delta_{\phi_B} - \frac{1}{2}\cos 2\phi_B \sin 2\Delta_{\phi_B}\right] \mathcal{H}_n^B} \tag{7.19}$$

n = 1, 2, 3 where

$$\mathcal{H}_n^{A,B} = \int_{\theta_{A,B}-\Delta}^{\theta_{A,B}+\Delta} G_{H_n}(\theta')\sin\theta' d\theta' \tag{7.20}$$

$$\mathcal{E}_n^{A,B} = \int_{\theta_{A,B}-\Delta}^{\theta_{A,B}+\Delta} G_{E_n}(\theta')\sin\theta' d\theta' \tag{7.21}$$

and expressions for G_H and G_E were given previously (equations (4.13) and (5.23).

A word about the geometry used in the thunderstorm location procedure is in order. Since the area of a thunderstorm region which is $2\Delta_\phi$ in azimuthal spread and 2Δ in range spread is $4a^2\Delta_\phi \sin\theta \sin\Delta$ where a is the radius of the earth (6.4×10^3 km), the area of the source depends upon the source-receiver separation θ. Hence, at very close (near 0°) or very distant (near 180°) storms the source area for a fixed Δ becomes unrealistically small. This can be accounted for, however,

by allowing Δ_ϕ to assume fairly large values, say as much as 40°. These remarks become important in determining the validity of certain approximations which are to be discussed below.

The equations (7.18) and (7.19) can be greatly simplified by making the approximation that Δ_{ϕ_A} and Δ_{ϕ_B} are small enough so that the factors $\sin 2\Delta_{\phi_A}$ and $\sin 2\Delta_{\phi_B}$ can be replaced by $2\Delta_{\phi_A}$ and $2\Delta_{\phi_B}$; this applies if Δ_{ϕ_A} and Δ_{ϕ_B} are not larger than 20°. We can preserve a representative source area of the order of at most 300,000 square miles (roughly the size of the state of Texas) in the range $10^\circ \leq \theta \leq 170^\circ$ by adjusting the Δ_ϕ's within the upper limit of 20°.

The simplified forms of eqs. (7.18) and (7.19) are

$$\left|\frac{H_n^{EW}}{H_n^{NS}}\right|^2 = \frac{\mathcal{H}_n^A \sin^2\phi_A + \delta\, \mathcal{H}_n^B \sin^2\phi_B}{\mathcal{H}_n^A \cos^2\phi_A + \delta\, \mathcal{H}_n^B \cos^2\phi_B} \tag{7.22}$$

$$\left|\frac{E_n}{H_n^{EW}}\right|^2 = \frac{\mathcal{E}_n^A + \delta\, \mathcal{E}_n^B}{\mathcal{H}_n^A \sin^2\phi_A + \delta\, \mathcal{H}_n^B \sin^2\phi_B} \tag{7.23}$$

$$n = 1, 2, 3$$

where

$$\delta = \Delta_{\phi_B}/\Delta_{\phi_A} \quad .$$

Since we have previously shown how to estimate θ_A, θ_B and δ the only unknowns in (7.22) and (7.23) are ϕ_A and ϕ_B, provided measurements of the quantities on the left hand side are available. Subsequent discussion will require some algebraic manipulation and we shall simplify the notation; let $r_1 = \left|H_1^{EW}/H_1^{NS}\right|^2$, $r_2 = \left|H_2^{EW}/H_2^{NS}\right|^2$, $r_3 = \left|H_3^{EW}/H_3^{NS}\right|^2$, $K_1 = \left|E_1/H_1^{EW}\right|^2$,

$K_2 = \left|E_2/H_2^{EW}\right|^2$, and $K_3 = \left|E_3/H_3^{EW}\right|^2$.

Using the identity $\sin^2 x + \cos^2 x = 1$ the equations (7.22) and (7.23) are seen to be six simultaneous equations which are linear in the two unknowns $\sin^2\phi_A$ and $\sin^2\phi_B$. The first three of these equations corresponding to (7.22) are

$$\mathcal{H}_n^A \sin^2\phi_A + \delta\, \mathcal{H}_n^B \sin^2\phi_B = \frac{r_n}{r_{n+1}} (\mathcal{H}_n^A + \delta\, \mathcal{H}_n^B) \tag{7.24}$$

$n = 1,2,3$ and the three equations corresponding to (7.23) are

$$\mathcal{H}_n^A \sin^2\phi_A + \delta\, \mathcal{H}_n^B \sin^2\phi_B = \frac{1}{K_n} (\mathcal{E}_n^A + \delta\, \mathcal{E}_n^B) \tag{7.25}$$

$n = 1,2,3$.

It is clear that the equations (7.24) and (7.25) are identical since it follows from

$$\frac{r_n}{r_{n+1}} (\mathcal{H}_n^A + \delta\, \mathcal{H}_n^B) = \frac{1}{K_n} (\mathcal{E}_n^A + \delta\, \mathcal{E}_n^B) = \frac{\left|H_n^{EW}\right|^2}{2\Delta_{\phi_A}} \tag{7.26}$$

hence, we need deal with only one of the two sets of equations, either (7.24) or (7.25), to determine ϕ_A and ϕ_B. Without loss of generality, we shall choose to solve equations (7.24) and shall express them in the matrix form

$$MS = C \tag{7.27}$$

where

$$M = \begin{bmatrix} \mathcal{H}_1^A & \delta\mathcal{H}_1^B \\ \mathcal{H}_2^A & \delta\mathcal{H}_2^B \\ \mathcal{H}_3^A & \delta\mathcal{H}_3^B \end{bmatrix} \tag{7.28}$$

$$S = \begin{bmatrix} \sin^2\phi_A \\ \sin^2\phi_B \end{bmatrix} \tag{7.29}$$

and

$$C = \begin{bmatrix} \frac{r_1}{r_1+1} \left(\mathcal{H}_1^A + \delta\, \mathcal{H}_1^B\right) \\ \frac{r_2}{r_2+1} \left(\mathcal{H}_2^A + \delta\, \mathcal{H}_2^B\right) \\ \frac{r_3}{r_3+1} \left(\mathcal{H}_3^A + \delta\, \mathcal{H}_3^B\right) \end{bmatrix} \tag{7.30}$$

As is well known (Hemmerle, 1967), the best solution to (7.27) in the least squares sense is obtained by solving the equation

$$M^T M S = M^T C \tag{7.31}$$

where the superscript T denotes the transpose of the matrix. The matrix equation (7.31) represents two simultaneous equations in the two unknowns $\sin^2\phi_A$ and $\sin^2\phi_B$ and can be solved by conventional means. It is instructive, however, to examine the determinant of the matrix of coefficients, $M^T M$, in (7.31). This determinant is given by the expression

$$\det\left(M^T M\right) = \delta^2 \left\{ \left[\left(\mathcal{H}_1^A\right)^2 + \left(\mathcal{H}_2^A\right)^2 + \left(\mathcal{H}_3^A\right)^2 \right] \left[\left(\mathcal{H}_1^B\right)^2 + \left(\mathcal{H}_2^B\right)^2 + \left(\mathcal{H}_3^B\right)^2 \right] - \left[\mathcal{H}_1^A \mathcal{H}_1^B + \mathcal{H}_2^A \mathcal{H}_2^B + \mathcal{H}_3^A \mathcal{H}_3^B \right] \right\} \tag{7.32}$$

which vanishes if $\theta^A = \theta^B$. Therefore if the two source centers are at equal distances from the receiver, ratios of the type shown in (7.22) or (7.23) can provide no information on the azimuthal location of the sources. This fact becomes clear if one examines the expressions for

the ratios given by (7.22) or (7.23) under the condition that $\theta_A = \theta_B$ (or $H_n^A = H_n^B = H_n$ and $e_n^A = e_n^B = e_n$) since the ratios become independent of the resonance number. In fact, if $\theta_A = \theta_B$ and $\Delta_A \cong \Delta_B$

$$|E_n|^2 = 2\Delta_{\phi_A} e_n^A + 2\Delta_{\phi_B} e_n^B = 2\Delta'_\phi e_n$$

$$\left|H_n^{EW}\right|^2 = 2\Delta_{\phi_A} \sin^2\phi_A H_n^A + 2\Delta_{\phi_B} \sin^2\phi_B H_n^B = 2\Delta'_\phi \sin^2\phi' H_n$$

$$\left|H_n^{NS}\right|^2 = 2\Delta_{\phi_A} \cos^2\phi_A H_n^A + 2\Delta_{\phi_B} \cos^2\phi_B H_n^B = 2\Delta'_\phi \cos^2\phi' H_n$$

where

$$e_n = e_n^A = e_n^B$$

$$H_n = H_n^A = H_n^B$$

$$\Delta_\phi' = \Delta_{\phi_A} = \Delta_{\phi_B}$$

and ϕ' is an equivalent - fictitious - azimuth for the two sources located at $\theta_A = \theta_B$ with $\phi_A \quad \phi_B$.

A single received spectrum is produced which is indistinguishable from the spectrum from one source.

7.4 Detecting the Presence of More Than One Major Source

If a single major source is exciting the cavity the ratios

$$\left|\frac{H_n^{EW}}{H_n^{NS}}\right|^2 = \frac{\Delta_\phi - \frac{1}{2}\cos 2\phi \sin 2\Delta_\phi}{\Delta_\phi + \frac{1}{2}\cos 2\phi \sin 2\Delta_\phi}$$

are obviously independent of the n, the ordinal number of the resonance.

For the case of two sources, however, $|H_n^{EW}/H_n^{NS}|^2$ given by equation (7.18) are clearly dependent on n unless $\theta_A = \theta_B$ and $\Delta_A \cong \Delta_B$. We can then make the following statement: if the measured quantities $|H_n^{EW}/H_n^{NS}|^2$ are different for different resonance numbers, there must be more than one source. It does not follow, however, that if these ratios are independent of n there is only one source, since as we demonstrated in the previous section, two sources at equal θ but different azimuth ϕ can imitate one source at a single receiving station.

VIII. EFFECTS OF BACKGROUND NOISE ON THE SOURCE LOCATION METHOD

Up to this point, it has been assumed that the measured ELF spectra are not contaminated by signals of an origin other than major intense thunderstorm regions. This is, of course, not always true and in this chapter the effects of various types of noise on the estimated source distances will be discussed.

8.1 Effects of Extra-Terrestrial Noise on Source Location Estimates.

Schumann spectra of the magnetic field are frequently observed to have a sharply increasing power level with decreasing frequency. This effect can be pronounced enough to cause errors in the estimates of the power levels at the lower Schumann resonant frequencies (and consequent errors in the estimation of source location) and can even be so strong as to entirely remove any evidence of resonances (see Figure 8.1). The source of this noise is probably outside the earth-ionosphere cavity and possibly involves hydromagnetic emission phenomena; it cannot be produced by distant thunderstorms since the analytical expression for the magnetic field does not contain a "zeroth" resonance term. In contrast, the electric field does have a "zeroth" resonance.

Numerical experiments were conducted to determine the effect of noise of this type on the location estimates. The frequency spectrum

of the noise can be approximated by

$$N(f) = Af^{-\alpha} \tag{8.1}$$

where α is in the range 1 to 2. It is clear that for a given A, the larger α is the less a Schumann spectrum will be contaminated. If the spectrum resulting from thunderstorm activity is designated by T(f), the total received spectrum, S(f), (including the noise) can be written as

$$S(f) = N(f) + T(f) \tag{8.2}$$

provided N and T are the power spectra of uncorrelated random processes. Assuming a source location and strength, one can then evaluate S(f) for different values of A and α and use these "noisy" spectra in the source location procedure. Figures (8.2) and (8.3) illustrate the results of these investigations. In these graphs θ_o is the true location of the thunderstorm source; the abcissa is the ratio of the spectral power at 2 Hz to the spectral power at the first resonant frequency i.e.

$$C = \frac{S(2)}{S(f_1)} \tag{8.3}$$

where f_1 is the apparent first resonant frequency. Since thunderstorm produced power at 2 Hz is negligible compared to the noise power at 2 Hz,

$$C \cong \frac{N(2)}{N(f_1) + T(f_1)} \tag{8.4}$$

C was chosen in this form so that it could be used as a criterion for accepting or rejecting a spectrum as useful for the location of thunderstorms.

Variation along the abscissa can also be roughly interpreted as variation of the percent noise power at the apparent first resonance.

The reason for this is as follows: The percent noise power, P, at the first resonance is given by

$$P = 100 \left[\frac{N(f_1)}{N(f_1) + T(f_1)} \right] \tag{8.5}$$

and since f_1 is approximately a constant (f_1 depends on A, α, and the source location and strength; but the range of variation is at most about $\pm$ 1 Hz), we have

$$P = 100 \, [N(f_1)/N(2)]C \tag{8.6}$$

so that P and C are related by a constant if α is fixed. We cannot experimentally observe P, but we can measure C. Figure (8.2) shows the variation of the estimated source distances θ for $\alpha = 1$ and varying C or P (which corresponds to varying A). The estimated source locations are plotted until the estimates are more than 10° in error. The amount of noise which is tolerable is dependent on θ_o. For example, if the source is at 120° distance, source distance estimates are unreliable if $C > .1$ ($P > 12$ %), but if the source is at 20°, $C < 4$ or P nearly 100 % does not affect the distance estimates.

Selection of $\alpha = 1$ is probably a too severe assumption about the noise frequency variation. Experimental data indicate that more often $\alpha \cong 2$. Figure (8.3) describes the effect of noise if $N(f) = A/f^2$; $\theta_o = 120^\circ$ is still the worst case but not until $C \geq 4$ ($P \geq 25$ %) must we reject a spectrum.

It can be concluded that the estimation procedure is fairly insensitive to this type of noise.

8.2 Uniform Equatorial Distribution of Low Level Thunderstorm Activity.

In this section, we examine the effect on the source location procedure of low level thunderstorm activity distributed over a large equatorial area. According to Pierce (1969a), large scale thunderstorm areas have a characteristic dimension of about 1000 Km ($\Delta = 4.5^{\circ}$) or an area of 10^6 km^2. Herman (1968) has concluded that the world's major thunderstorm regions have an area of 5×10^6 km^2 (about 1/500th of the earth's surface area). These thunderstorm regions consist of complexes 30-40 km in diameter and separated by about 100 km (Pierce, 1969b). On the average, a specific complex will contain one or two active cells which are 6 km in diameter and produce three lightning strokes per minute (Pierce, 1969b).

Using Pierce's model we can estimate the flash rate of a typical major thunderstorm area. Imagine that a typical complex is placed at the corners of a square region 100 km x 100 km. This 10^4 km^2 region then contains one complex and on the average will produce 6 flashes per minute so that one of our typical major thunderstorm regions will produce 600 flashes/minute. Assuming that two of these major regions are active at a given time, the flash rate from these two major regions would then be 1200 discharges per minute or 20 discharges per second from the world major thunderstorm regions. It is generally believed that there are three major thunderstorm regions—tropical America, Africa, and Asia; however, meteorological conditions which are favorable to thunderstorms depend on local time (late afternoon is usually considered optimum for the occurrence of thunderstorms) so that at most two major regions are likely to be active at a given time (Smith, 1961).

According to the widely accepted thunderstorm theory of atmospheric electricity, world-wide lightning activity is the generator of the atmospheric potential gradient (Chalmers, 1967) and from measurements of this potential gradient, the total world-wide lightning activity at a given time can be estimated. In this way, it can be roughly determined that there are at least 100 lightning discharges/second occurring over the entire world (Smith, 1961). Polk (1969), using a related technique, has estimated that there must be 250 "typical" discharges per second over the earth.

From these very rough estimates it seems that the amount of lightning activity concentrated in the major thunderstorm regions is only about twenty percent of the total world-wide activity. Suppose it is assumed that the other 80 percent (about 80 discharges per second) is uniformly distributed in an equatorially centered band between 30° north latitude and 30° south latitude. Then the flash rate surface density in this band (its area is exactly one-half the total surface area of the earth; about 2.58×10^{8} km^2) is 3.1×10^{-7} flashes/km^2/sec. Comparing this with the flash rate density in the major regions, 2×10^{-5} flashes/km^2/sec., we see that the source strength ($g(\omega)$) in equation (4.10) in the major regions is about two orders of magnitude larger than that in the uniform equatorial band. It remains to compare the received power levels from the uniform band of scattered "background" sources and the major regions.

Suppose there are N_A strokes uniformly distributed over an area A. Then the total dipole moment squared over this area is $N_A M^2(\omega)$ and we

have

$$N_A M^2(\omega) = \int_A \int g(\omega)\,dA \tag{8.7}$$

and if $g(\omega)$ is uniform over A,

$$g(\omega) = \frac{N_A M^2(\omega)}{A} \tag{8.8}$$

but $N_A = \rho A$ where ρ is the stroke surface density (strokes per unit area) so that

$$g(\omega) = \rho M^2(\omega) \tag{8.9}$$

We can now modify equation (3.3) to account for the stroke surface density and write

$$g(\omega) = (\text{const.})\ \rho \exp(-9.1 \times 10^{-3}\ \omega) \tag{8.10}$$

where the constant depends upon the properties of our "typical" lightning stroke. Knowledge of an absolute value for this constant is not necessary in the ratio method; only the frequency variation is important and, as was discussed in Chapter III, the frequency variation is held in fair agreement by several researchers.

It is instructive, however, to examine the likely range of values of $g(\omega)$ so that calculated signal levels can be compared with the measured levels. As mentioned in Chapter III, the average return stroke has a peak current of about 30,000 amps and a duration of about 100 micro-seconds (Pierce, 1963; Watt, 1960); assuming a stroke length of two kilometers, the peak value of the current moment of the return stroke is 6×10^7 amp-meters. The bandwidth of the pulse is of the order of the reciprocal of the pulse length or 10 KHz. Therefore, in the region $0 \leq f \leq 30$ Hz. the return stroke spectrum can be considered nearly white

and of magnitude equal to (peak amplitude) x (pulse length) or 6×10^{3} amp-meter secs. Consultation of any of the standard tables on Fourier transform pairs show that the detailed pulse shape is unimportant (e.g. see Korn and Korn, 1968) for the purposes of estimating expected signal levels. Note that this value of 6×10^{3} for $M(\omega)$, although obtained in a very rough way, compares quite favorably with the value, 5×10^{3}, given by Pierce (1963). We then can conclude that $M^2(\omega)$ for the return stroke must be in the range $10^{6} - 10^{7}$ amp^2-meter^2-sec^2 so that $g(\omega)$ would be as follows:

$g(\omega)$ for uniform low level background is $[3.1 \times 10^{-6}, 3.1 \times 10^{-7}]$

$g(\omega)$ for major thunderstorm areas is $[2 \times 10^{-4}, 2 \times 10^{-5}]$.

Using the largest $g(\omega)$ in their respective ranges, a major source ($\Delta = 5^{\circ}$, $\Delta_{\phi} = 5^{\circ}$) at a distance of 40° should produce theoretical first resonance field amplitudes as

$$|E_1| = 2\Delta_{\phi}\mathcal{E}_1(40,5) = 18\mu \text{ volts/meter}$$

$$|H_1| = 2\Delta_{\phi}\mathcal{H}_1(40,5) = .03\mu \text{ amps/meter} \quad (8.11)$$

(or .038 milligamma)

and the uniform $\pm 50^{\circ}$ band of low density "background" thunderstorm activity produces fields (at Kingston, R. I.; located at approximately 41.6°N, 71.8°W) of amplitudes

$$|E_1| = 19.3\mu \text{ volts/meter}$$

$$|H_1| = .045\mu \text{ amps/meter} \quad (8.12)$$

(or .056 milligamma)

These values are one or two orders of magnitude smaller than those reported in the literature (Polk, 1969). A possible reason for this discrepency is that the assumed value of $M(\omega)$ is one or two orders of magnitude too small. Rycroft (1965) has obtained good agreement between theoretical and experimentally measured 8 Hz field amplitudes using the dipole moment $M(\omega) = 1.4 \times 10^5$ at 8 Hz which is roughly two orders of magnitude larger than would be expected for an "average" return stroke. From "slow tail" measurements, Hughes (1967) has estimated $M(\omega)$ to be about 3×10^5 at 100 Hz and notes that this is about 40 dB larger than the estimates based upon the return stroke only (Williams, 1959). In a more recent paper, Hughes (1969) provides experimental measurements of $M(\omega)$ which if extrapolated down in frequency to the region of the first three resonances yield a value of about 10^6 amp-meters. Polk (1969) has used estimates of the vertical electrostatic field to conclude that $M(\omega)/h = 45$ amps where h is the ionospheric height. For h = 50 km, this yields a moment of $M(\omega) = 2.2 \times 10^6$ amp-meters. The empirical formula of Pierce (1963) describing time variations of the different components of a typical discharge (leader, return, and continuing currents) can be used to estimate the frequency dependence of the lightning stroke dipole moment. As was shown in Figure (3.1), the total $M^2(\omega)$ is about two orders of magnitude higher than that for only the return stroke. These discussions seem to indicate that, as was pointed out by Pierce (1963), all the processes of a lightning discharge are important in the excitation of the Schumann resonances and not exclusively the return stroke as is widely assumed. If the previously used value of $M(\omega)$ is increased by

a factor of 10, the theoretical signal levels (equations (8.11) and (8.12)) compare well with published data (Polk, 1969).

Equations (8.11) and (8.12) indicate that the signal levels from a major thunderstorm area and from the equatorial region of background noise could be of comparable size. This raises the question as to whether the "signal" from a major region can be sufficiently discriminated from the "noise" of the equatorial background so that the location of the major region can be determined.

It is reasonable to expect that the background thunderstorm noise is seasonally dependent, i.e. the background noise spectrum would be different for spring-fall, northern summer and northern winter. Estimates of the geographical distribution of the equatorial noise belt can be obtained from the literature (Smith, 1961). Assuming a distribution uniform in longitude, the extent in latitude of the noise belt for the various seasons is roughly

spring-fall	30°S to 30°N
northern summer	10°S to 60°N
northern winter	40°S to 10°N

The electric and magnetic field power spectra received in Rhode Island for these three cases are shown in Figures (8.4) and (8.5). The maximum power level variation for the different seasons is only about thirty percent; this might be expected since the source area for the three cases is fairly constant: winter area = 2.1×10^{8} km^2, spring fall area = 2.58×10^{8} km^2. summer area = 2.68×10^{8} km^2. A most important characteristic of these spectra which should be pointed out is the fact that

the peak powers at the resonances decrease with increasing resonance number, i.e. the ratios $|E_2/E_1|^2$, $|E_3/E_2|^2$, $|H_2/H_1|^2$, $|H_3/H_2|^2$ are all less than unity.

One may ask if the "real world" Schumann spectra ever depart from the estimates given by Figures (8.4) and (8.5) or if the spectra show a day to day variation during the same season. Obviously, if the spectra are the same from day to day or from week to week, the location of our hypothesized "major" regions would be impossible because either these major regions do not exist, or their level is so low that their presence cannot be detected in the background noise. Actually measured spectra do display significant day to day and even hour to hour variations.

Typical power spectra, measured in Rhode Island, are plotted in Figures (8.6) - (8.8). Figure (8.6) shows that in the space of six hours a significant change in the east-west magnetic field power spectrum occurred on February 19, 1967. Both the ratios and the resonant frequencies show marked changes. Figure (8.7) shows a similar variation. An outstanding example of spectral deviation from the background estimates of Figure (8.4) is shown in Figure (8.8) where the electric field power spectrum at 1400 EST on August 14, 1968 is plotted. Here the power level <u>increases</u> with the order of the resonance and it is clear that at this time, the background level must have been low. Spectra of this type are not at all rare occurrences and we can conclude that usually the background noise does not completely conceal the signal from the major regions.

Equations (8.11) and (8.12) indicate that the "noise" level produced by the equatorial background and that from a major source are com-

parable; however, experiment shows that significant departures from a constant ambient spectrum do occur. In the paragraphs to follow, we shall examine the problem of how much noise is tolerable in the location of the principal thunderstorm regions.

To simplify the analysis, the case of locating a single 10^6 km^2 major source in the presence of the uniform equatorial background region will be considered. The stroke densities in the major and background regions are denoted by ρ_M and ρ_B; the number of strokes per unit time in the regions are N_M and N_B. We shall use Smith's estimate of $N_W = 100$ discharges per second over the entire world and write

$$N_W = N_M + N_B \tag{8.13}$$

or

$$100 = \rho_M A_M + \rho_B A_B \tag{8.14}$$

where A_M and A_B are the areas of the major and background regions. For the purposes of computation

$$g_M(\omega) = \rho_M M^2(\omega) \tag{8.15}$$

and

$$g_B(\omega) = \rho_B M^2(\omega) \tag{8.16}$$

If the relative flash density ρ_B/ρ_M, and the areas A_M and A_B (dependent on the season) are specified the ρ_M and ρ_B can be determined from (8.14) and the spectra from the major source and the background can be calculated. Figures (8.9), (8.10), (8.11) show the effect of the background noise on the source distance estimates for northern winter. spring-fall, and northern summer. On these curves the abscissa is the relative strength of the background source ρ_B/ρ_M, the ordinate is the estimated

source distance and the curves are parametric in the actual source location, θ_o. If A_M and A_B are specified, $N_B = \rho_B A_B$ can be determined for a given value of $\rho_M \rho_B$ and the values of N_B (strokes per second in the background region) are displayed at the top of the page for the regions indicated. The curves simply display the deviation of the estimated location from the true location with increasing noise. It can be seen that there is very little seasonal dependence of noise effects, a result which might be expected since the corresponding noise spectra are very similar. We can conclude that ρ_B/ρ_M must be less than or equal to about 2×10^{-4} ($N_B \leq 5$) for the determination of precise source locations. This result is consistent with the calculations of (8.11) and (8.12) where it was found that the "noise" level and the "signal" level were about equal for the case $\rho_B/\rho_M \cong 10^{-2}$. This means the received signals are about fifty percent noise and it is not surprising that the resulting estimated source locations are very different from the true locations. This result should be contrasted with the case of the $Af^{-\alpha}$ type additive noise where almost 50 percent noise at the first resonance was tolerable; but this is due to the fact that the exponential noise contaminates only the first and second resonances of the magnetic field. Both electric and magnetic field ratios are used in the estimation procedure. On the other hand equatorial background noise contaminates all the peak powers of both the electric and magnetic field. It appears that the ratio method is quite sensitive to our hypothesized equatorial noise sources.

Figures (8.6) to (8.8) indicate, however, that the estimates used in equations (8.11) and (8.12) for the relative strengths of uniformly

distributed lightning activity as compared with activity in the major thunderstorm regions are probably erroneous. In particular, these estimates are very sensitive to the area of the major thunderstorm region; for example, if the assumed area of a major region were increased to 5×10^6 km^2 (Herman, 1968) the "signal" to noise ratio would be greatly improved. The physical parameters describing thunderstorms and lightning have large variability and are still the subject of active research. Consequently, the numerical values quoted here are at best crude estimates and are only indicative of the order of magnitude of the particular quantity. It is clear that the assumed uniform equatorial background noise must be either more restricted in area or must have a lower relative flash density than assumed in the discussion leading to (8.11) and (8.12) if ELF spectra lead to the correct determination of thunderstorm regions. To the extent to which it becomes possible therefore to confirm ELF results by direct surface or satellite observations, information is also obtained about the relative magnitude of "major" and "background" lightning activity. For example, if it should turn out that the ELF method gives consistently correct results during certain periods, but not during others, it would be possible to draw conclusions conclusions concerning the distribution in time of the "background" activity.

IX. LOCATION OF THUNDERSTORMS BY ANALYSIS OF SCHUMANN SPECTRA

In this chapter the ratio method is applied to observed spectra and estimated locations are given. Where possible, the resulting location estimates are compared with available meteorological data.

9.1 Location of a Single Active Thunderstorm Region

During the period 6-12 June, 1967 an exceptional amount of thunderstorm activity occured near Salt Lake City (Lat 40° 45'N, Long 111° 53'W) in the Rocky Mountain region of the United States and detailed records of the associated phenomena have been published (Kealoha, et al.; 1968). The power spectra of the vertical electric field and the east-west magnetic field received in central Rhode Island (71° 41' 01"W, 41° 31' 53"N) at 1730 EST to 1742 EST on June 6, 1967 are shown in Figure (9.1). This particular time was selected for analysis because simultaneous satellite cloud cover pictures and radar precipitation echo data were available (Kealoha, et al.; 1968). The radar data indicate that at this time the center of the precipitation region for this thunderstorm area was at distance $\theta = 29^\circ$, and bearing $\phi = -16^\circ$ (see Figure 4.1 for definition of angles) and had an area of about $.8 \times 10^6$ km^2, roughly corresponding to $\Delta\phi = 3.5^\circ$, $\Delta = 5^\circ$. Employing the minimization method described in section (6.5) and using the ratios computed from Figure (9.1), source locations (θ) for several different source widths (Δ) were estimated.

The source distance was estimated from the ratios $|E_2/E_1|^2$, $|E_3/E_2|^2$; $|H_2^{EW}/H_1^{EW}|^2$, and $|H_3^{EW}/H_2^{EW}|^2$. The source azimuths were obtained by rearranging equation (6.11) into the form

$$\sin^2\phi = \frac{|H_n^{EW}|^2}{|E_n|^2} \cdot \frac{\mathcal{E}_n(\theta,\phi)}{\mathcal{H}_n(\theta,\phi)} \; ; \quad n = 1, 2, 3 \qquad (9.1)$$

The right hand side of (9.1) can be evaluated from the power spectral density measurements (notice the necessity for having absolute calibration of electric and magnetic field values) and from the previously estimated θ and ϕ. Since the solution of the three equations (9.1) results in three sets of four possible angles, the corresponding angles from each set were averaged. Table I shows estimated distance, θ, and possible azimuths for $\Delta = 0^\circ$, 5°, 10°, and 20°. Also displayed in the table are the minimum values of the Q function (see equation 6.15) corresponding to the "best" values of θ for a given Δ.

Δ	θ	ϕ	Q_{min}
0°	29°	-10°, -142°, $+38^\circ$, $+170^\circ$	.065
5°	33°	-9°, -143°, $+37^\circ$, $+171^\circ$	.064
10°	32°	-9°, -143°, $+37^\circ$, $+171^\circ$	.057
20°	34°	-9°, -143°, $+37^\circ$, $+171^\circ$	.029

Table I: Source location estimates based upon the spectra of Figure (9.1).

The coil used for the magnetic field measurements near Kingston is oriented with its axis in the geomagnetic east-west direction and the ϕ

values in Table I were therefore corrected for the magnetic deviation in Rhode Island (14° west). All θ and φ values in Table I are close to the known location of the source if it is assumed that the closest azimuth estimate is the correct one. The maximum distance error is only 5° (about 300 miles) and the maximum bearing error is 7°. The fact that the θ and φ values which are closest to the known source position yield the largest Q parameter does not seem to be consistent with the development in chapter VI. In chapter VIII, however, it was shown that additive noise can cause small errors in the location estimates and this is probably the case here. The value of Δ which appears to provide the best agreement between theoretical and experimental ratios, as indicated by minimum Q, is $\Delta = 20^\circ$ which is unrealistically large. Figures (7.1) and (7.2) show, however, that for sources located at distances near 30°, the spectral ratios are nearly independent of Δ so that the ratio method can provide very little information about the areal extent of the source. The preceding example shows that, at least at this particular time (June 6, 1967), the background noise estimates suggested in chapter 8.2 are much too large and correct location of a major thunderstorm region is clearly possible.

9.2 Location of Two Simultaneously Active Sources

The power spectra of the vertical electric field, the geomagnetic north-south magnetic field and the geomagnetic east-west magnetic field measured in central Rhode Island on January 1, 1970 between 1720 and 1729 GMT are shown in Figure (9.2). Employing the methods developed in section (7.2), the distances from the receiver to

each of the two sources were estimated to be $\theta_A = 120^\circ$, $\theta_B = 162^\circ$ and the relative strength parameter, δ, was estimated to be 4.22. The possible azimuthal locations of each source were determined from the ratios $|H_n^{EW}/H_n^{NS}|^2$; n = 1, 2, 3 (see section 7.3). The eight locations listed below are derived from these calculations.

Source A

(1) 13°N, 78°E Southeastern India (2300 local time)

(2) 43°S, 20°E South African Coast (1900 local time)

(3) 64°S, 140°W Southern Pacific (0700 local time)

(4) 2°N, 132°E New Guinea (0200 local time)

Source B

(1) 28°S, 102°E West Australian Coast (2400 local time)

(2) 53°S, 90°E Southern Indian Ocean (2300 local time)

(3) 60°S, 120°E Southeastern Indian Ocean (0100 local time)

(4) 30°S, 125°E Southwestern Australia (0200 local time)

Location (3) for Source A can be eliminated since it is too far south (only about 200 miles from the Antarctic Circle). Locations (2) and (3) for Source B are also unlikely locations for thunderstorm locations. It can be concluded that Source A is either in Southeastern India, off the South African Coast, or in New Guinea; that Source B lies in Western Australia, and that the electrical intensity of Source B (total power output of the thunderstorm region) is 4.22 that of region A.

It is generally believed that the worlds major thunderstorm regions are concentrated in tropical and subtropical land masses. The above

results do not contradict this statement and curves by Smith (1961) giving the average frequency of occurrence of thunderstorms throughout the world for "December-January-February" (Smith, fig. 9-30) indicate relatively high thunderstorm activity for Southeastern India, the South-African coast, New Guinea and Western Australia. Specific surface observations for January 1, 1970 are not yet available to us at the present time.

As a further example, the analysis of the data for 1333-1343 UT July 29, 1969 resulted in the following source locations (excluding four points at extreme southern or northern latitudes, 55°S, 75°S, 55°N. 58°N):

Source A

(1) 28°N, 55°W West Central Atlantic (0900 local time)
(2) 25°N, 78°W Bahama Islands (0900 local time) (= ± 5°)

Source B

(1) 1°S, 96°E Sumatra (2000 local time)
(2) 5°S, 140°E New Guinea (2200 local time) (= ± 5°)

Although southern hemisphere surface observations were not available for this period information was available from the U.S. Weather Bureau "Northern Hemisphere Surface Charts." At 1200 UT—one and one half hours before the ELF observations—the weather conditions in the estimated storm region (20°-30°N, 73°-83°W) included cumulonimbus and towering cumulus clouds, roughly half overcast, and wind out of the southeast. At 1800 UT the amount of cumulonimbus clouds had greatly increased, precipitation was occuring and thunderstorms were observed in the northwest corner of the source region (northern Florida). It is thus likely that lightning activity developed soon after 1200 UT and then moved to the northwest of the "source region" under the influence of the prevailing winds. It is also possible, however, that lightning activity was already present at 1200 UT—although not indicated on the "surface chart"—since only seven observation stations in the source region of 10^6 km^2 area reported weather phenomena on July 29 at 1200 UT.

X. SUGGESTIONS FOR FUTURE WORK

10.1 Possible Improvements in the Thunderstorm Location Method

There are two limitations to the amount of information about thunderstorm locations and characteristics which can be obtained from a single receiving site. These are: (1) the ambiguities in the estimates of source azimuth which were explained in chapter VI and (2) the effects of equatorial background noise which could possibly (see chapter VIII) be large enough to produce serious errors in the source location estimates.

The effects of both of these difficulties could be reduced by the utilization of simultaneous measurements taken at several appropriately positioned receiving stations. It has been shown, for example, in chapter VI that, if the background noise level is sufficiently low, data from a single receiving station are sufficient to determine the source distance; bearing information is, however, ambiguous since choice among four possible angles is arbitrary. On the other hand, if spectra from two widely separated stations are known, only two possible source locations exist at the points of intersection of the constant distance loci from the two receivers. Access to measurements from three stations would remove all ambiguity.

The preceding considerations assume that data from each station are processed individually to obtain possible source locations and that the final estimates are compared. This is analogous to separately

processing the signals from each element of an antenna array; we are clearly losing information by doing this. A better method would be to collectively analyze the raw multi-station data using techniques which would be extensions of the source location methods described in this report. It would seem likely that reliable, continuous monitoring of global thunderstorm activity could be obtained in this way.

The use of multiple receiving sites could also improve the noise rejection properties of any thunderstorm location method. If the stations were placed so that the background noise spectra were different at each receiver (because of different geographical locations relative to the noise source), the effect of noise contamination could probably be reduced by cross-correlation techniques. It might also be possible to estimate the noise spectrum and analytically remove it from the received spectra. In short, there is no doubt that multiple station measurements could provide more reliable location estimates.

10.2 Estimation of the Ionospheric Conductivity Profile

As was pointed out in Chapters IV and V, Schumann spectra depend upon both the location and characteristics of the source and the properties of the cavity boundaries, particularly the ionosphere. It was shown that the relative amplitudes of the peaks in the resonant spectrum provide a measure of source location which is nearly independent of the properties of the ionosphere (see Figures 5.8 to 5.14). On the other hand, the exact spectral position of the resonant frequencies depends about equally on the source location and the ionospheric conductivity profile (see Figures 5.15 to 5.20).

It is possible therefore to first determine the location (θ) and extent (Δ) of the source from ratios of spectral peak powers and then to employ the resonant frequency values to draw conclusions concerning the conductivity profile of the ionosphere. The Schumann spectra are affected by regions of ionization extending as low as 30 to 40 km above the earth surface (Jones, 1967) and therefore should provide information which is difficult to obtain by other means. For example, if it is determined from the ratios that $\theta = 100^{\circ}$, $\Delta = 20^{\circ}$ and if the first resonant frequency in the electric field is at 8 Hertz, then Figure (5.18) suggests that the "Pierce-Cole" profile is a more appropriate ionosphere model than the Galejs profile.

A refinement of the methods for both, source location and determination of the Ionosphere profile would involve an iteration procedure. This would require the determination (from the observed, experimental ratios) of the location and extent of the source assuming first a reasonable average ionosphere profile such as the "Pierce-Cole" profile shown in Figure (5.7). Then the exact values of the observed resonant frequencies and the estimated source positions would be used to obtain a "better" ionosphere model. This model would then be used again to obtain a better estimate of the source location. The procedure would be continued until further iterations produce no change in the ionosphere profile.

10.3 Determination of Relative Contribution of Major Thunderstorm Regions to World Electrical Activity

As indicated at the end of chapter VIII, verification—or lack of verification—of ELF thunderstorm locations by ground or satellite

observations should provide information about the relative importance of the major thunderstorm regions as lightning generators in comparison with the totality of widely distributed, small thunderstorms. A systematic program of comparing the results of ELF spectral analysis with surface observations would therefore provide information about the diurnal and seasonal variability of the ratio of these two inputs to world electrical activity.

10.4 Investigation of Localized Ionospheric Perturbations on Schumann Resonances

It has been indicated in chapter VIII that the Schumann spectra are sometimes contaminated by $1/f^{\alpha}$ noise. One possible source of such noise may be hydromagnetic wave generation processes in the Magnetosphere or the Solar Wind. The $1/f^{\alpha}$ noise could, however, be also a manifestation of near-field effects, that is superposition of TE and higher order TM modes, produced by a local lateral ionospheric inhomogeneity, or it could be due to random current fluctuations in the local Ionosphere.

To determine the source of $1/f^{\alpha}$ noise comparison of ELF measurements with Ionospheric and other geophysical data such as cosmic ray count, 10.7 cm flux and micropulsation activity is necessary. Detailed investigation of analytical models describing the effect of local Ionospheric perturbations would also be required. Madden-Thompson (1965) have pointed out that the global effect at ELF of local Ionospheric perturbations would be small; higher order modes may nevertheless be appreciable at ELF within several hundred km of an inhomogeneity or discontinuity. For this reason it would be particularly useful to study the ELF spectra corres-

ponding to known Ionospheric discontinuities such as those existing at local dawn or dusk or during a Solar eclipse.

APPENDIX A

Spectral Bias for Rectangular Data Window

The quality factor for resonant cavities is defined as

$$Q = \omega_o \frac{U}{\left(-\frac{dU}{dt} \right)} \tag{A-1}$$

where U is the energy in the cavity and ω_o is the radian resonant frequency. Equation (A-1) is a differential equation for U which has the solution

$$U(t) = U_o e^{-\frac{\omega_o}{Q} t} \tag{A-2}$$

where U_o is the initial stored energy. Since power is the time derivative of the energy, the power behaves in a similar manner.

$$P(t) = P_o e^{-\frac{\omega_o}{Q} t} \tag{A-3}$$

From equation (A-3) the fields themselves oscillate as

$$E(t) = E_o e^{-\frac{\omega_o}{2Q} t} e^{i\omega_o t} \tag{A-4}$$

In the frequency domain, the behavior is described by

$$E(f) = E_o \int_o^\infty e^{-\frac{\omega_o}{2Q} t} e^{i\omega_o t} e^{-i\omega t} dt \tag{A-5}$$

if there is no energy in the cavity for $t < 0$. Integrating (A-5),

we have

$$E(f) = \frac{E_o}{\frac{\omega_o}{2Q} + i\,(\omega - \omega_o)} \qquad (A\text{-}6)$$

It is clear that (A-4) and (A-6) constitute a Fourier transform pair as in equations (2.1) and (2.2).

The power in the frequency domain is then proportional to

$$P(f) = \frac{E_o^2/4\pi^2}{\frac{f_o^2}{4Q^2} + (f - f_o)^2} \qquad (A\text{-}7)$$

where

$$f = \omega/2\pi .$$

Differentiating (A-7) twice with respect to frequency,

$$P''(f) = \frac{E_o^2}{4\pi^2} \left\{ \frac{8(f - f_o)^2 - 2\left[\frac{f_o^2}{4Q} + (f - f_o)^2 \right]}{\left[\frac{f_o^2}{4Q} + (f - f_o)^2 \right]^3} \right\} \qquad (A\text{-}8)$$

Of course, we are not interested in the absolute size of P"(f) but its size relative to P(f).

$$\frac{P''(f)}{P(f)} = \frac{8(f - f_o) - 2\left[\frac{f_o^2}{4Q^2} + (f - f_o)^2 \right]}{\left[\frac{f_o^2}{4Q^2} + (f - f_o)^2 \right]^2} \qquad (A\text{-}9)$$

For the first three Schumann modes, the resonant frequencies are approximately equal to 7.8, 14.1, 20.3 Hz and the quality factors are of the order of 4 (Jones, 1967). Employing these values, we can evaluate (A-9)

in the region of each resonance and determine the importance of the additive bias term $\frac{(\Delta f)^2}{24} S''(f)$. The power and the power spectrum are approximately related by

$$P(f) = S(f)\Delta f \qquad \text{(A-10)}$$

so that the normalized additive bias term for spectral density estimates is

$$\frac{(\Delta f)^2}{24} \frac{S''(f)}{S(f)} = \frac{(\Delta f)^2 P''(f)}{24P(f)} \qquad \text{(A-11)}$$

The frequency variation of this bias term in the region about each of the first three cavity resonances is shown in Figure (A-1) for a frequency resolution f = 1 Hz. It can be seen from Figure (A-1) that near the first resonance the additive bias of the estimates is about -18 percent of power spectral density at that point. This rather large error can be reduced by decreasing the resolution to 0.5 Hz or 0.25 Hz, which reduces the bias to about -4 percent and -1 percent respectively. From the preceeding discussion it is clear that if resolutions of 0.5 or less are used, the bias produced by employing a rectangular data window is negligible.

An intuitive argument, verifying qualitatively the mathematical results presented above, is provided by Figure (A-2) where a very high Q resonance is shown. The procedure outlined in Chapter II uses the average power over a bandwidth Δf as the estimate of the power spectrum at the center of the band. In Figure (A-2) the average power in the bandwidth Δf is schematically represented by point A; on the other hand,

the actual power at the center of the band is given by point B. It is clear that approximating the power spectrum by the average power in a band Δf can be very misleading if the spectrum is rapidly varying with frequency.

This problem can be eliminated by decreasing Δf, but this will increase the variance of the power spectral density estimates as is indicated by equation (2.19). There is then an optimum range of Δf which must be used: Δf must be chosen large to minimize the variance of the estimates; but it should be made small to minimize the bias of the estimates. This appendix, together with Chapter II has shown that a Δf of 0.25 Hz or 0.5 Hz provides acceptable levels of estimate bias and variance.

It is not to be construed from the above that the lower the Q of the resonances (or equivalently, the less the frequency variation of the spectrum) the better the information contained in the spectrum. Obviously if the spectrum is white ($Q = 0$) the bias is zero but there is no information provided by the spectrum. The purpose of this appendix is merely to demonstrate that for a frequency spectrum of the Schumann type, where the quality factors of the resonances are of the order of 4 or less, a frequency resolution of 0.25 Hz or 0.5 Hz gives good estimates of the actual spectrum.

APPENDIX F

Linear Stationary Systems with Uncorrelated Inputs

If a linear system is driven by a source at radian frequency ω, the Fourier transforms of the output $y(t)$ and input $x(t)$ are related by the transfer function $H(j\omega)$ as

$$Y(j\omega) = H(j\omega)\, X(j\omega) \tag{B-1}$$

$H(j\omega)$ is the Fourier transform of the impulse response of the system. It can be shown (Davenport and Root, 1958) that the output power spectrum is given by

$$S_y(\omega) = |H(j\omega)|^2\, S_x(\omega) \tag{B-2}$$

If we generalize this to a multiple input system, the single output $y(t)$ is related to the N inputs $X_k(t)$; $k = 1, 2, \ldots N$ by

$$y(t) = \sum_{n=1}^{N} y_n(t) \tag{B-3}$$

where $y_k(t)$ is the response when only the input $x_k(t)$ is driving the system and the other inputs are zero. The $y_k(t)$ are related to the $x_k(t)$ by the convolution integral

$$y_k(t) = \int_{-\infty}^{+\infty} h_k(\tau) x_k(t-\tau)\, d\tau \tag{B-4}$$

or equivalently

$$Y_k(j\omega) = H_k(j\omega)\, X_k(j\omega) \tag{B-5}$$

where $H_k(j\omega)$ and $h_k(t)$ are the transfer functions, in the frequency and time domains respectively, between the kth input and the output when all other inputs are zero.

If the inputs $x_1, x_2 \ldots x_N$ are random signals, the output power spectral density is given by (Davenport and Root, 1958)

$$S_y(\omega) = \sum_{k=1}^{N} \sum_{n=1}^{N} H_n^*(j\omega) H_k(j\omega) S_{nk}(\omega) \tag{B-6}$$

where $S_{nk}(\omega)$ is the cross spectral density between the inputs $x_n(t)$ and $x_k(t)$. $S_{nk}(\omega)$ can be expressed as

$$S_{nk}(\omega) = \int_{-\infty}^{+\infty} R_{x_n x_k}(\tau) e^{-j\omega\tau} d\tau \tag{B-7}$$

where $R_{x_n x_k}(t)$ is the cross correlation function of $x_n(t)$ and $x_k(t)$. If the inputs are uncorrelated, $S_{nk}(\omega) = 0$ and

$$S_y(f) = \sum_{n=1}^{N} |H_n(j\omega)|^2 S_{x_n}(\omega) \tag{B-8}$$

which the reader should compare with eq. (B-2).

A statement of the result given by (B-8) is as follows: The power spectral density of the output of a multiple input linear system driven by uncorrelated inputs is equal to the sum of the power spectral densities due to each input considering all other inputs to be zero.

We can apply the results of this appendix to the problem of lightning excitation of the earth-ionosphere cavity by assuming that the signals from the thunderstorms are stochastic in nature and that the different lightning strokes are independent. Hence, the signals from each discharge are uncorrelated. Raemer (1961) has pointed out that this approach is mathematically equivalent to the analysis of "shot noise" in vacuum tubes where it is usually assumed that the probability of the emission of an electron from the cathode is independent of the number of electrons emitted in the past (Davenport and Root, 1958).

REFERENCES

Abbas, M., "Hydromagnetic Wave Propagation and Excitation of Schumann Resonances", Planet. Space Science, Vol. 16, p. 831 (1968).

Balser, M. and Wagner, C. A., "Observation of Earth-Ionosphere Cavity Resonances", Nature, Vol. 188, p. 638 (1960).

Balser, M. and Wagner, C. A., "Diurnal Power Variations in the Earth-Ionosphere Cavity Modes and their Relationship to Worldwide Thunderstorm Activity", Jl. Geophys. Res., Vol. 67, No. 2, p. 619 (1962).

Bendat, J. and K. Piersol, The Measurement and Analysis of Random Data, Wiley, New York (1966).

Beyers, H. R., The Thunderstorm, U. S. Dept. of Commerce, Washington (1949).

Blackman, R. B. and Tukey, J. W., The Measurement of Power Spectra, Dover Publications, New York (1958).

Budden, K. G., The Wave-Guide Mode Theory of Wave Propagation, Prentice Hall (1961).

Chalmers, J. A., Atmospheric Electricity, Pergammon Press (1967).

Cole, R. K. and Pierce, E. T., "Electrification in the Earth's Atmosphere for Altitudes between 0 and 100 Kilometers", Jl. Geophys. Res., Vol. 70, No. 12, p. 2735 (1965).

Cooley, J. W. and Tukey, J. W., "An Algorithm for the Maching Calculation of Complex Fourier Series", Math. of Comput., Vol. 19 (1965).

Davenport, W. B. and Root, W. L., An Introduction to the Theory of Random Signals and Noise, McGraw-Hill, New York (1958).

Gage, B. P., Reynolds, D. K., and Rogers, James C., "Artificial Excitation of Schumann Resonances in the Earth-Ionosphere Cavity", Jl. Geophys. Res., Vol. 73, No. 13, p. 4416 (1968).

Galejs, J., "Terrestrial Extremely Low Frequency Noise Spectrum in the Presence of Exponential Ionospheric Conductivity Profiles", Jl. Geophys. Res., Vol. 66, No. 9, p. 2787 (1961a).

Galejs, J., "ELF Waves in the Presence of Exponential Ionospheric Conductivity Profiles", IRE Trans. Ant. Prop., Vol. AP-9, No. 6, p. 554 (1961b).

Galejs, J., "Terrestrial Extremely-Low-Frequency Propagation", pp. 205-260 in Natural Electromagnetic Phenomena Below 30 Kc/s. (D. F. Bleil, editor), Plenum Press, New York (1964).

Galejs, J., "ELF and VLF Fields of a Horizontal Electric Dipole", IEEE Trans. Ant. Prop., Vol. AP-16, No. 6, p. 689 (1968a).

Galejs, J., "Propagation of ELF and VLF Waves Below an Anisotropic Ionosphere with a Dipping Static Magnetic Field", Jl. Geophys. Res., Vol. 73, No. 1, p. 339 (1968b).

Galejs, J., "Propagation of ELF and VLF Waves Below a Generally Anisotropic Ionosphere", Radio Science, Vol. 3, p. 781 (1968c).

Harris, F. B. and Tanner. R. L., "A Method for the Determination of Lower Ionosphere Properties by Means of Field on Spherics", Jl. Res. Natl. Bur. Stan., Vol. 66D, No. 4, p. 463 (1962).

Hemmerle, W. J., Statistical Computations on a Digital Computer, Blaisdell Publishing Company (1967).

Herman, J. R., "A Sensitive Technique for Detecting Late-time Absorption Following High Altitude Nuclear Explosions", Radio Science, Vol. 3, No. 9, p. 964 (1968).

Heydt, G. and Volland, H., "Atmospheric Disturbances and their use for the Quantitative Analysis of Thunderstorm Activity" (in German), Zeitschrift für Meteorologie, Vol. 18, No. 11/12, p. 423 (1966).

Hinich, M. J. and Clay, C. S., "The Application of the Discrete Fourier Transform in the Estimation of Power Spectra, Coherence, and Bispectra of Geophysical Data", Reviews of Geophysics, Vol. 6, No. 3, p. 347 (1968).

Hughes, H. G., "Current Moments at ELF of Lightning Discharges Associated with a Mature Tropical Hurricane", Jl. Geomagn. Geoelec., Vol. 19, No. 4, p. 281 (1967).

Hughes, H. G., "Some Lightning Discharge Characteristics at Extremely Low Frequencies Determined from 'Slow Tail' Measurements" in Planetary Electrodynamics, Vol. 2, ed. by S. Coroniti and J. Hughes, Gordon and Breach Publishers, p. 93 (1969).

Jones, D. Llanwyn, "Schumann Resonances and e.l.f. propagation for inhomogeneous, isotropic ionosphere profiles", Jl. of Atm. and Terrestrial Physics, Vol. 29, p. 1037 (1967).

Jones, D. L., "Observation on the Propagation Constant of the Earth-Ionosphere Waveguide in the Frequency Band 8c/s to 16 kc/s", Radio Science, Vol. 1 (New Series), No. 11, p. 1273 (1966).

Jones, D. L. and Kemp, D. T., "Schumann Resonances Excited by Single Dipole Sources—Theory and Experiment" (1968 Fall A.G.U. Meeting), Trans. A.G.U., Vol. 49, No. 4, p. 687 (1968).

Jones, D. L. and Kemp, D. T., "Experimental and Theoretical Observations on the Impulse Excitation of Schumann Resonances" (unpublished manuscript) (1969).

Jordan, E. C., "Electromagnetic Waves and Radiating Systems", First Edition, Prentice-Hall, New York (1950).

Kealoha, J. H. S., Serebreny, S. M. and Smith, M. I., "Cloud Photo Interpretations of Selected Cyclones and Thunderstorms", Final Report on Stanford Research Institute Project 6806, (1968).

Keefe, T. J., Etzold, H., and Polk, C., "Characteristics of ELF (3 to 30 Hz) Spectra during Solar Proton Events and Some Geomagnetically Disturbed Periods", Abstract in Program, 1968 Spring URSI Meeting, Natl. Acad. of Sciences, Washington, D. C., p. 72 (1968).

Kimpara, A., "Electromagnetic Energy Radiated from Lightning" in Problems of Atmospheric and Space Electricity edited by S. C. Coroniti, Elsevier, New York (1965).

König, H., "Atmospheric Geringster Frequenzen", Zeitschr. Angew. Phys., Vol. 11, No. 7, p. 264 (1959).

Korn, G. A. and Korn, T. M., Mathematical Handbook for Scientists and Engineers, McGraw-Hill, New York (1968).

Large, D. B. and J. R. Wait, "Theory of Electromagnetic Coupling Phenomena in the Earth-Ionosphere Cavity", Jl. Geophys. Res., Vol. 73, No. 13, p. 4335 (1968).

Loeb, L. B., Fundamental Processes of Electrical Discharges in Gases, Wiley, New York (1939).

Madden, T. and Thompson, W., "Low-Frequency Electromagnetic Oscillations of the Earth-Ionosphere Cavity", Reviews of Geophysics, Vol. 3, No. 2, p. 211 (1965).

Magnus, W., Oberhettinger, F. and Soni, L., Formulas and Theorems for the Special Functions of Mathematical Physics, Springer-Verlag, Berlin (1966).

Mood, A. M. and Graybill, F. A., Introduction to the Theory of Statistics, Second Edition, McGraw-Hill, New York (1963).

Nelson, P. H., "Ionospheric Perturbations and Schumann Resonance Data", Ph.D. Thesis (M.I.T.), Project NR-371-401, Geophysics Lab., M.I.T. (1967).

Ogawa, T., Tanaka, Miura and Yasuhara, "Observations of Natural ELF Electromagnetic Noise by Using the Ball Antenna", Jl. Geomagn. and Geoelectr., Vol. 18, pp. 443-454 (1966).

Papoulis, A., The Fourier Integral and Its Applications, McGraw-Hill, New York (1962).

Pierce, E. T., "Atmospherics as Indicators of World Wide Thunderstorm Activity", Report of Meeting on Atmospheric Electricity during IGY at Aachen, May 11-12, 1956, p. 28-37 (1957).

Pierce, E. T., "Excitation of the Earth-Ionosphere Cavity by Lightning Flashes", Jl. Geophys. Res., Vol. 68., No. 13, p. 4125 (1963).

Pierce, E. T., "Progress in Radio Noise of Terrestrial Origin" Radio Science, Vol. 4, No. 7, p. 661 (1969a).

Pierce, E. T., "Monitoring of Global Thunderstorm Activity" in Planetary Electrodynamics, Vol. 2, edited by S. Coroniti and J. Hughes, Gordon and Breach Publishers, p. 3 (1969b).

Polk, C., "Relation of ELF Noise and Schumann Resonances to Thunderstorm Activity" in Planetary Electrodynamics, Vol. 2, edited by S. Coroniti and J. Hughes, Gordon and Breach Publishers, p. 55 (1969).

Raemer, H. R., "On the Spectrum of Terrestrial Radio Noise at Extremely Low Frequencies", Jl. Res. Natl. Bur. Stan., Vol. 65D, No. 6, p. 581, (1961).

Rycroft, M. J., "Low Frequency Disturbances of Natural Origin of the Electric and Magnetic Fields of the Earth", Ph.D. thesis, University of Cambridge (1963).

Rycroft, M. J., "Resonances of the Earth-Ionosphere Cavity Observed at Cambridge, England", Radio Science, Jl. of Research Natl. Bur. Stan./ USNC-URSI, Vol. 69D, No. 8, p. 1071 (1965).

Schonland, B. F. J., "Atmospheric Electricity", Second Edition. Methnen - John Wiley and Sons, New York (1953).

Schonland, B. F. J., "The Lightning Discharge" in Handbuch der Physik, Springer-Verlag, Berlin (1956).

Schonland, B. F. J., The Flight of Thunderbolts, Clarendon Press, Oxford (1964).

Schumann, W. O., "On the Characteristic Oscillations of a Conducting Sphere which is Surrounded by an Air Layer and an Ionospheric Shell", (in German) Z. Naturforsch., Vol. 71, (1952a).

Schumann, W. O., "On the Damping of Electromagnetic Characteristic Oscillations of the Earth-Ionosphere Cavity" (in German); Z. Naturforsch., Vol. 72, (1952b).

Smith, L. G., "Atmospheric Electricity" in Handbook of Geophysics, Revised Edition. The Macmillan Co., New York (1961).

Solov'jev, V. A., "Thunderstorm Activity According to the Data of Atmospherics Direction Finding", in Problems of Atmospheric and Space Electricity, edited by Samuel C. Coroniti, Elsevier (1965).

Sommerfeld, A., Partial Differential Equations in Physics, Academic Press, New York (1949).

Toomey, J. P., "Analysis of VLF Data as a Means for Determining Diurnal Variation of World-Wide Thunderstorm Activity", M. S. Thesis, University of Rhode Island (1966).

Wait, James R., "Terrestrial Propagation of Very-Low-Frequency Radio Waves", Jl. Res. Natl. Bur. Stan., Vol. 64D, p. 153 (1960).

Wait, James R., "Electromagnetic Waves in Stratified Media", Pergamon Press - The Macmillan Co., New York (1962).

Watt, A. D., "ELF Electric Fields from Thunderstorms", Jl. Res. Natl. Bur. Stan., Vol. 64D, No. 5, p. 425 (1960).

Watt, A. D., VLF Radio Engineering, Pergamon Press, New York (1967).

Weinberger, H. F., Partial Differential Equations, Blaisdell Publishing Co., Waltham, Mass. (1965).

Williams, J. C., "Thunderstorms and VLF Radio Noise", Ph.D. Thesis, Harvard University (1959).

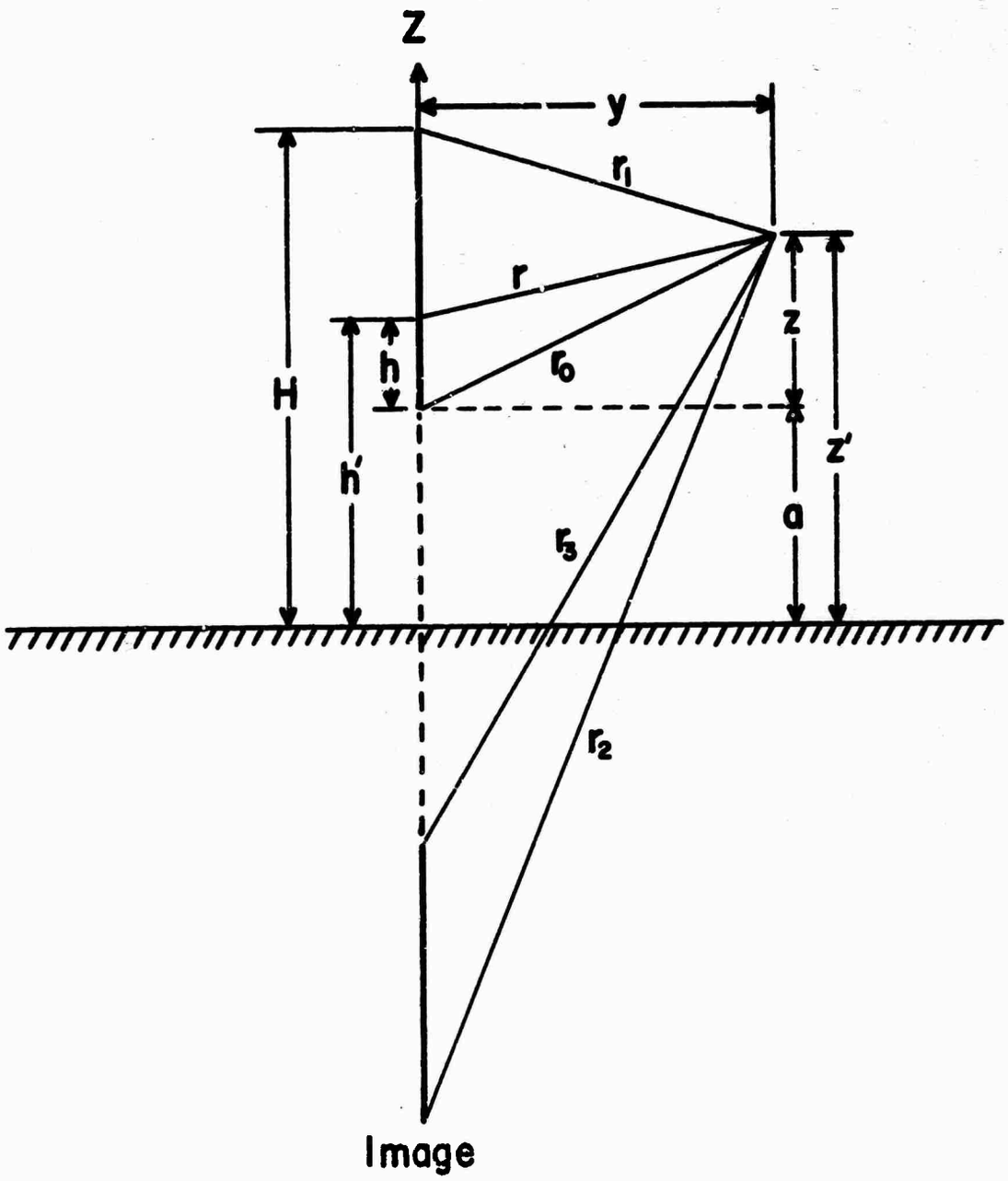

Figure 1.1. Diagram of calibrating antenna (Identification of symbols).

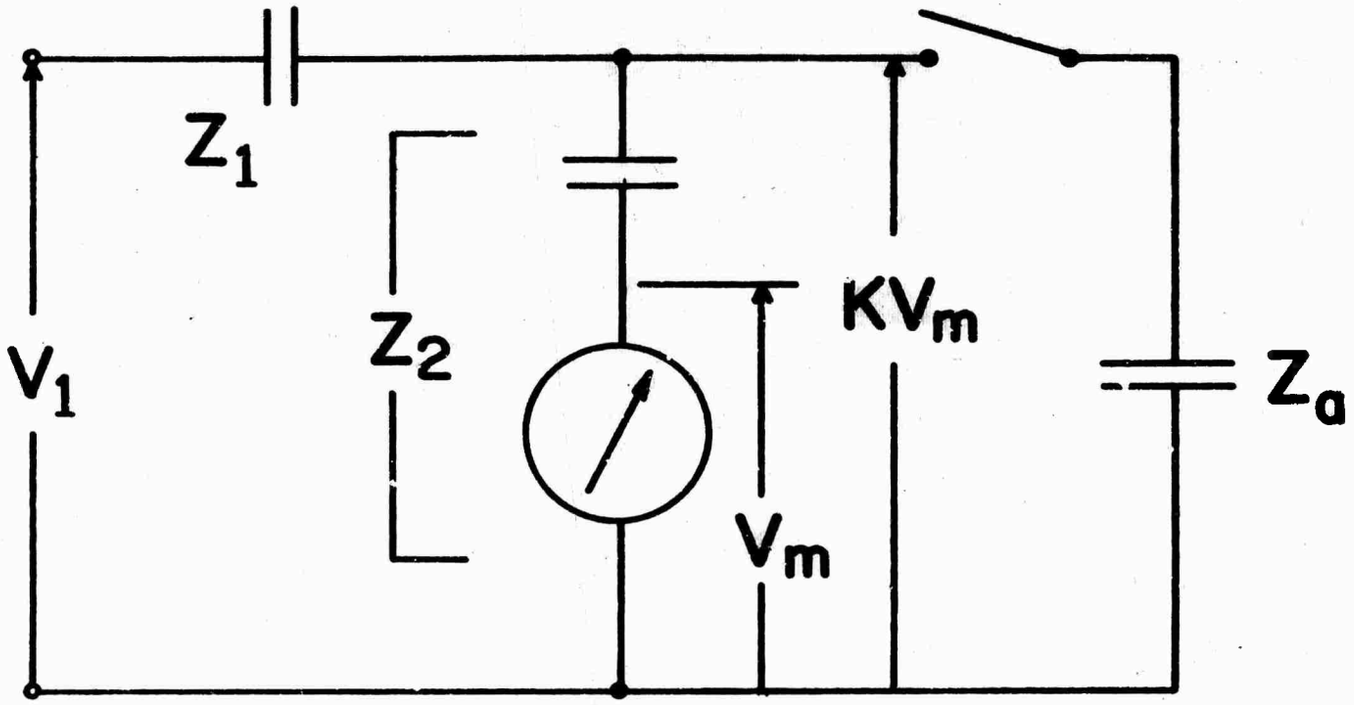

Figure 1.2. Circuit for measuring input capacitance of short vertical antenna. (Identification of symbols used in text)

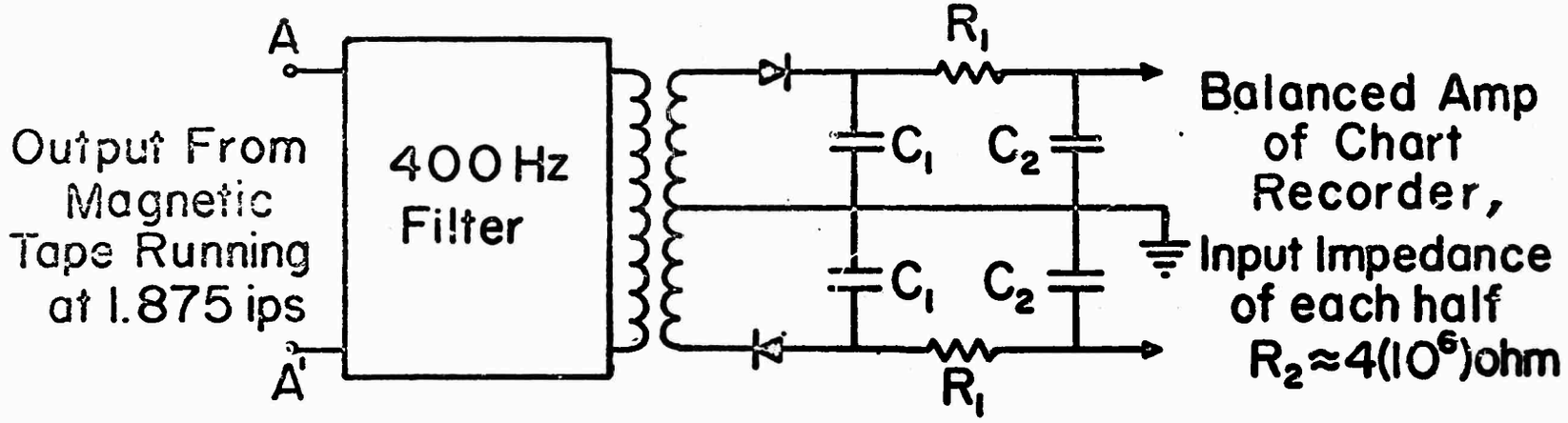

Figure 1.3 - Filter and Smoothing Network Between Magnetic Tape Recorder and Chart Recorder for "summary records".

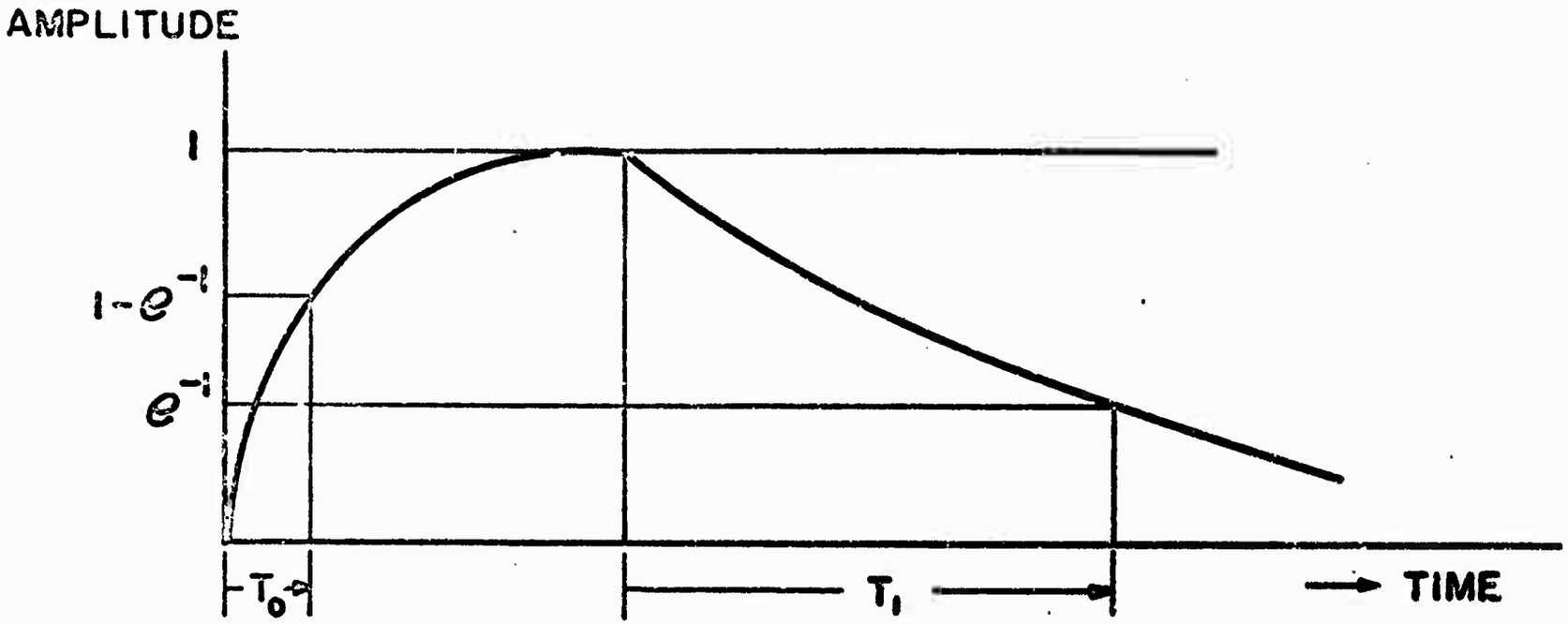

Figure 1.4 - Response of Network in Figure 1.3 to Application and Disconnection of a Constant 400 Hz signal

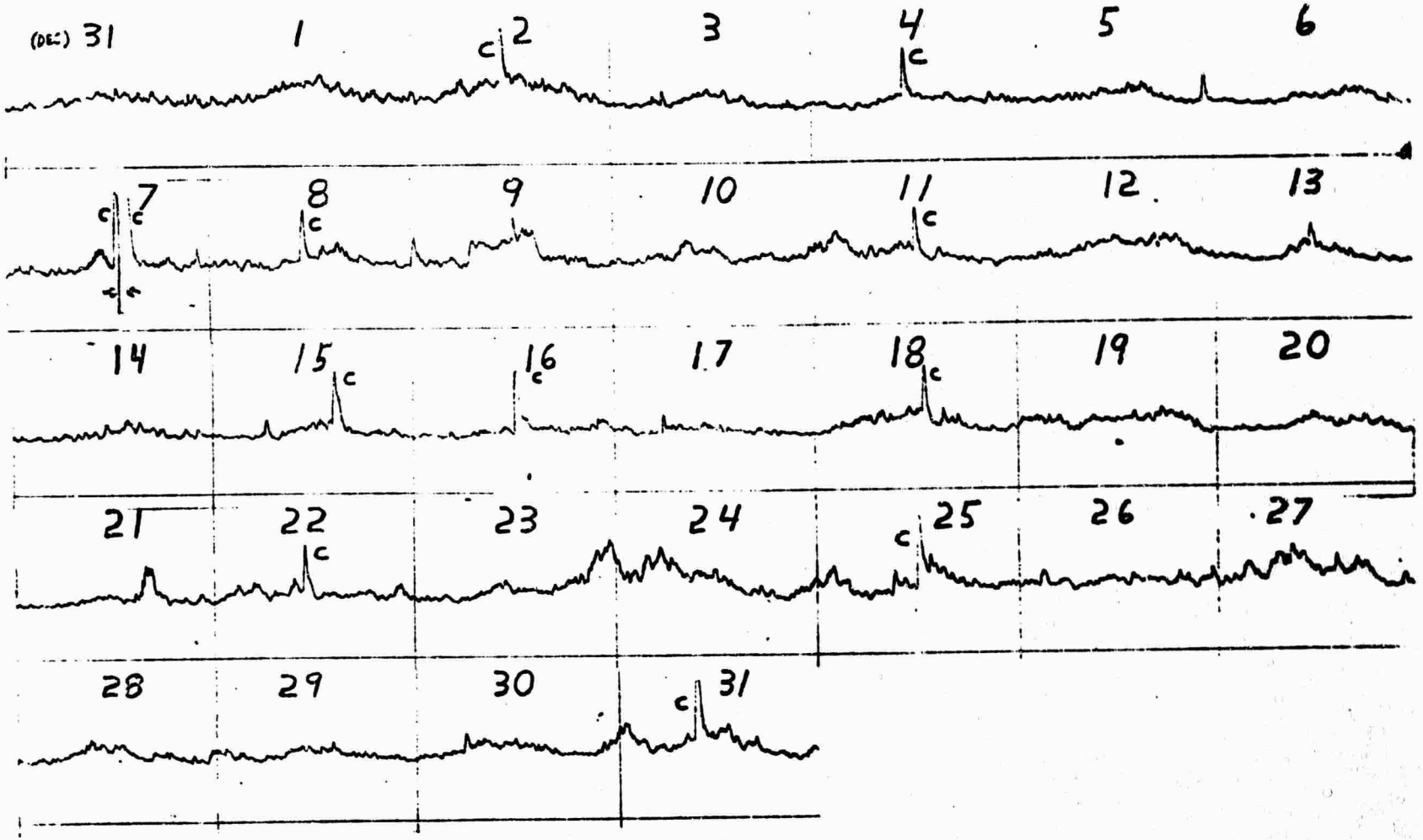

Fig. 1.5. Typical ELF "Summary data"

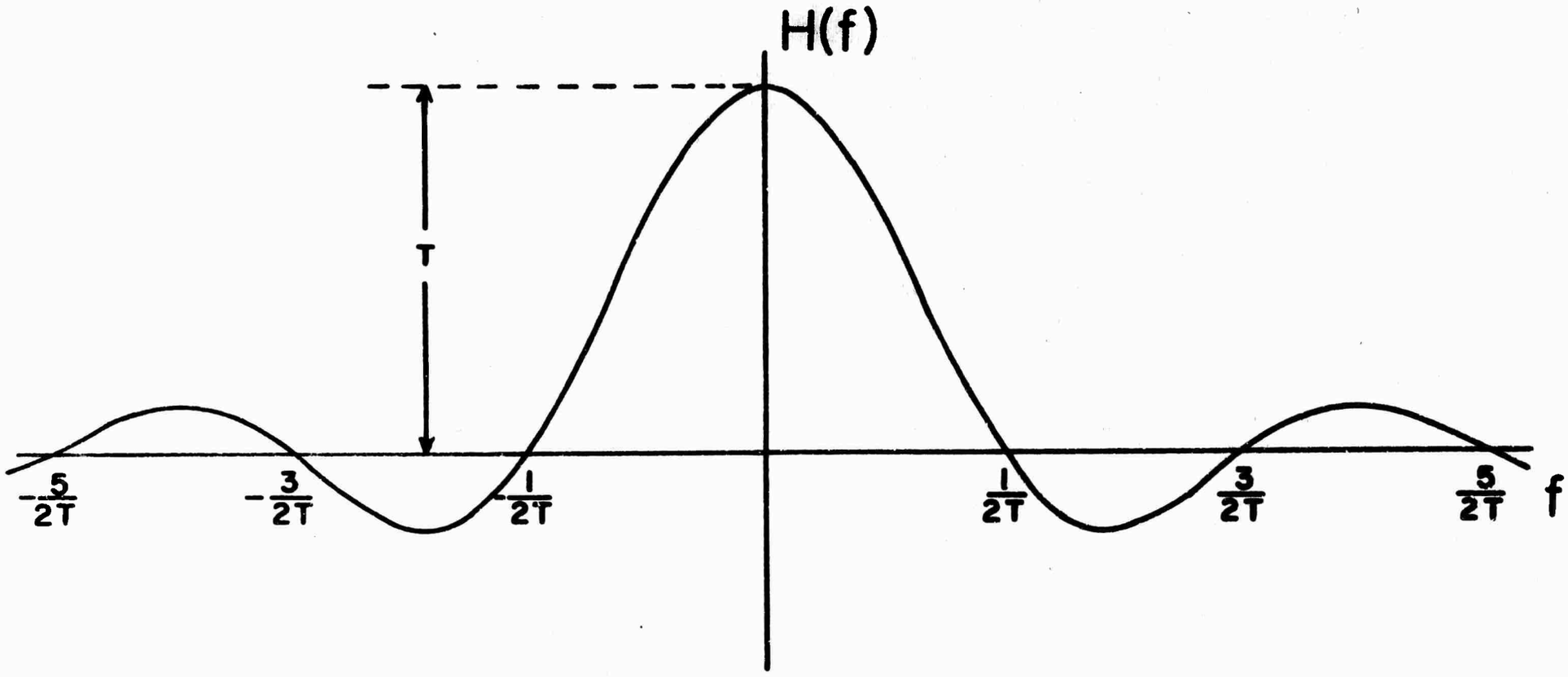

SPECTRAL WINDOW CORRESPONDING TO RECTANGULAR DATA WINDOW

Figure 2.1 Spectral window corresponding to rectangular data window.

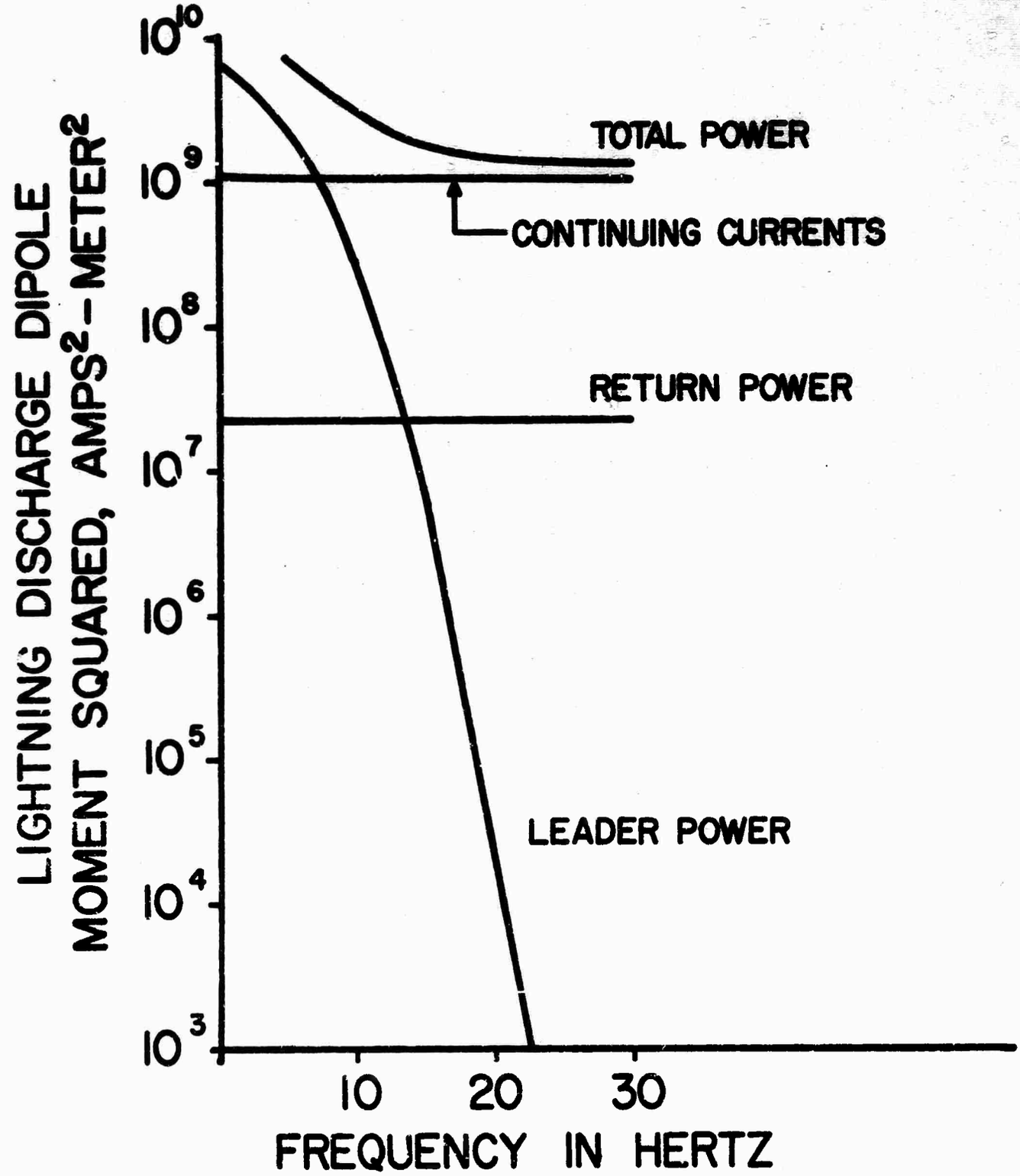

Figure 4.1. Lightning spectrum of Pierce.

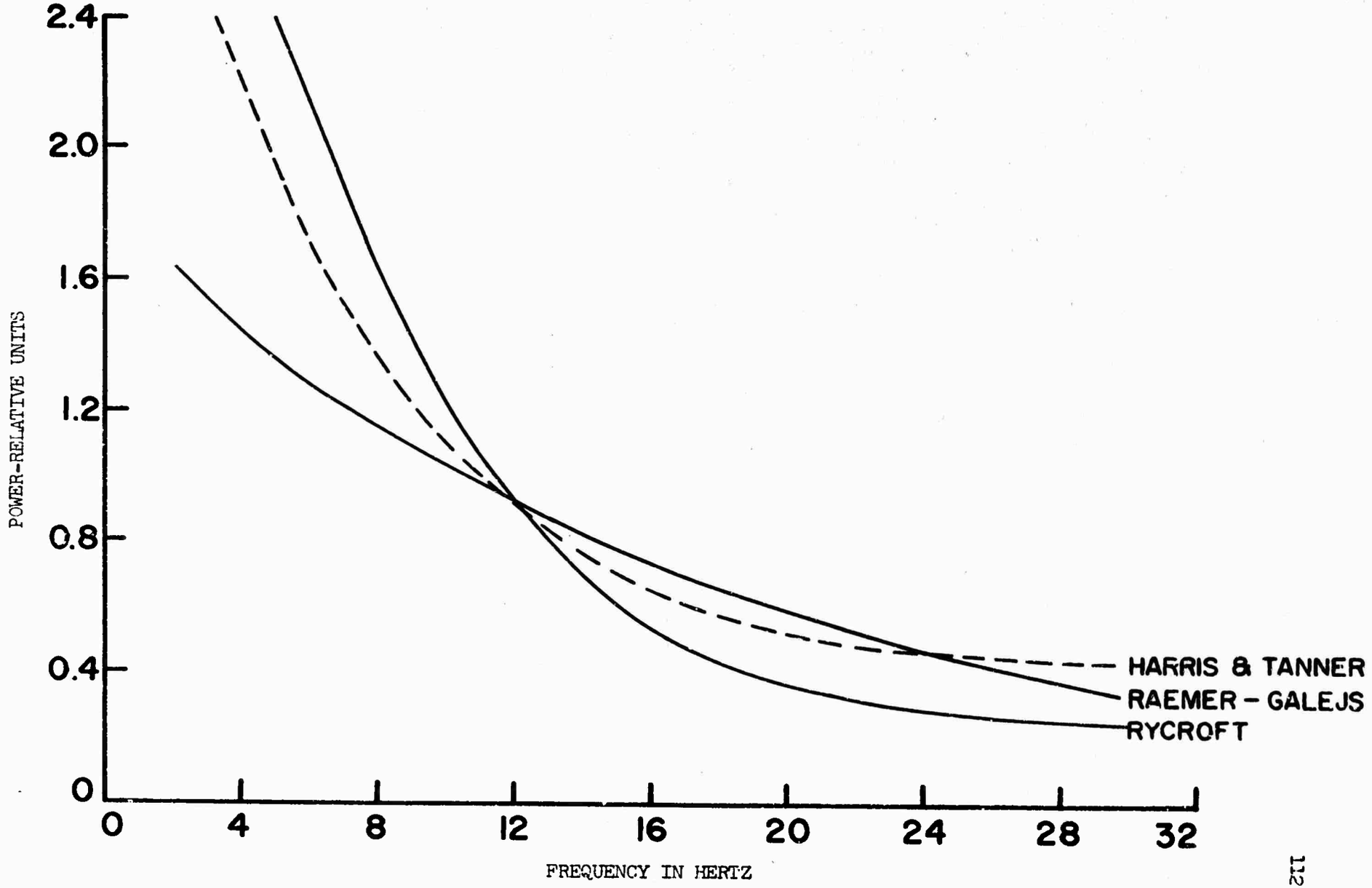

Figure 3.2. Spectra of square of lightning dipole moment.

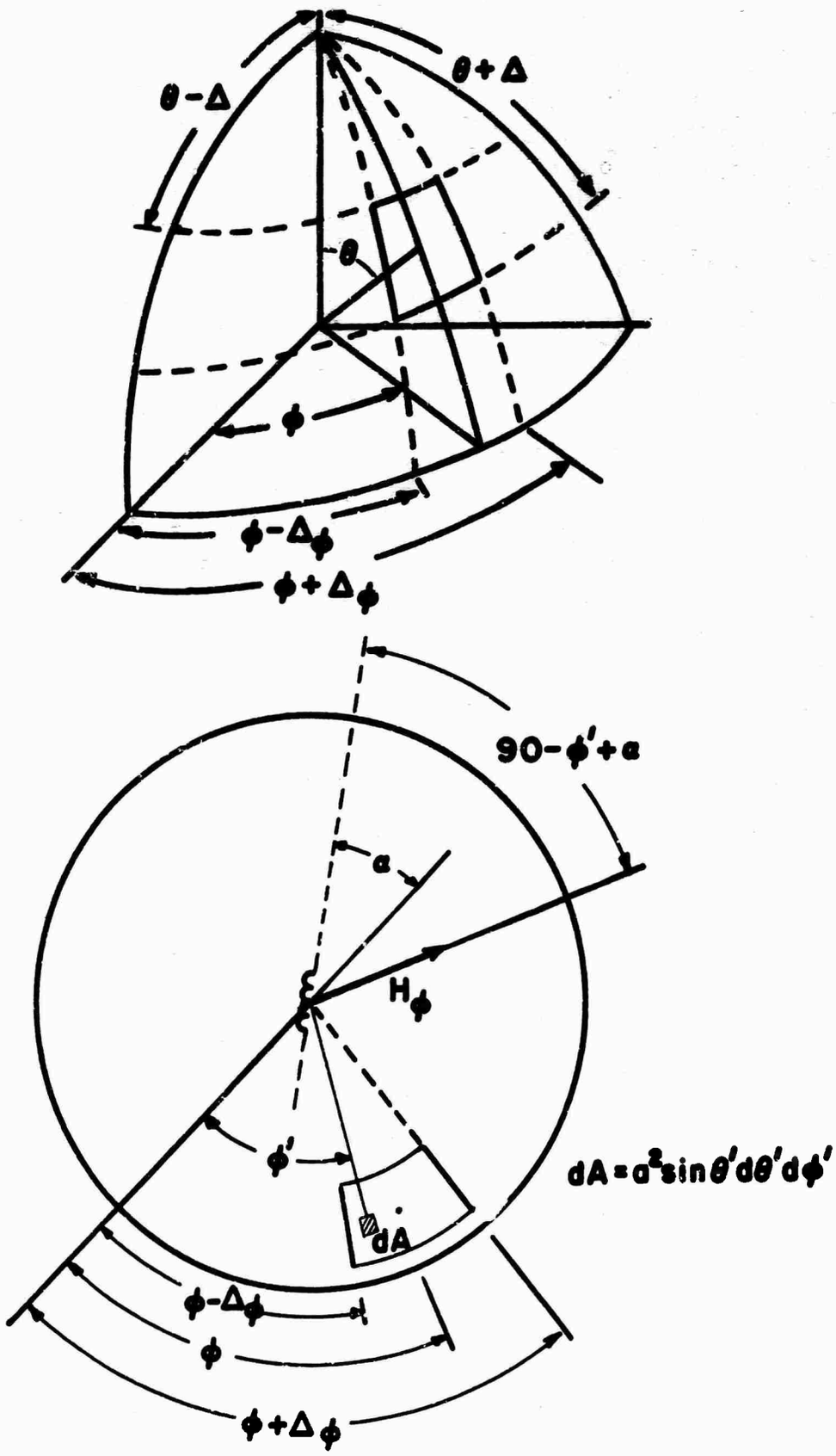

Figure 4.1. Source geometry.

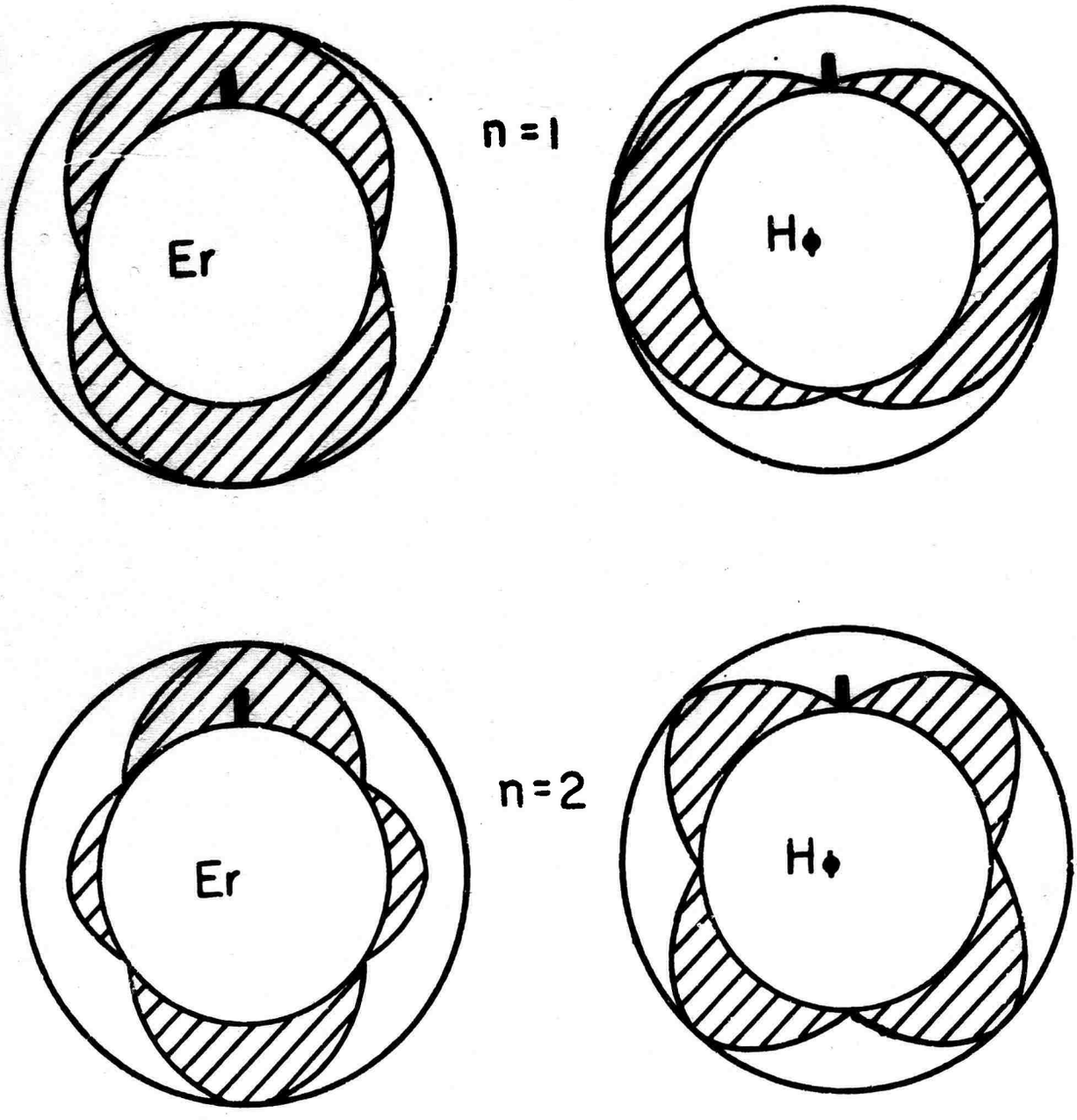

Figure 5.1. Amplitude distributions for first and second modes (single source).

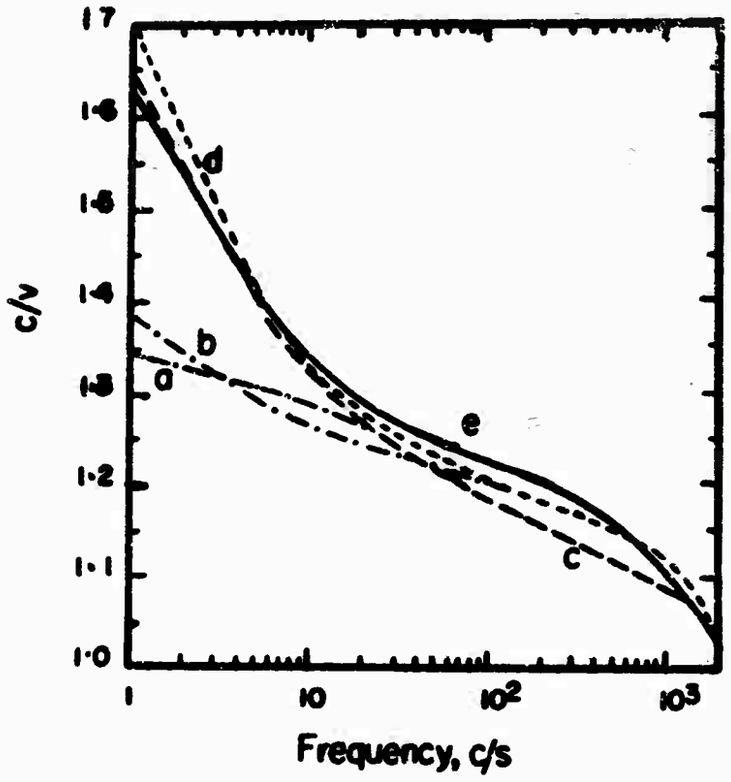

Figure 5.2. **ELF phase velocities,**
D. L. Jones (1967).

a) Pierce and Cole ionosphere profile omitting data below 56 km

b) Deeks ionosphere profile (B. R. May, J. Atmosph. Terr. Phys., 28, 553, 1966)

c) Cole and Pierce (1965) ionosphere profile including heavy ion region down to 30 km altitude

d) Profile (b) continued to lower altitudes by profile (c)

e) Chapman-Jones (1964) two-layer profile.

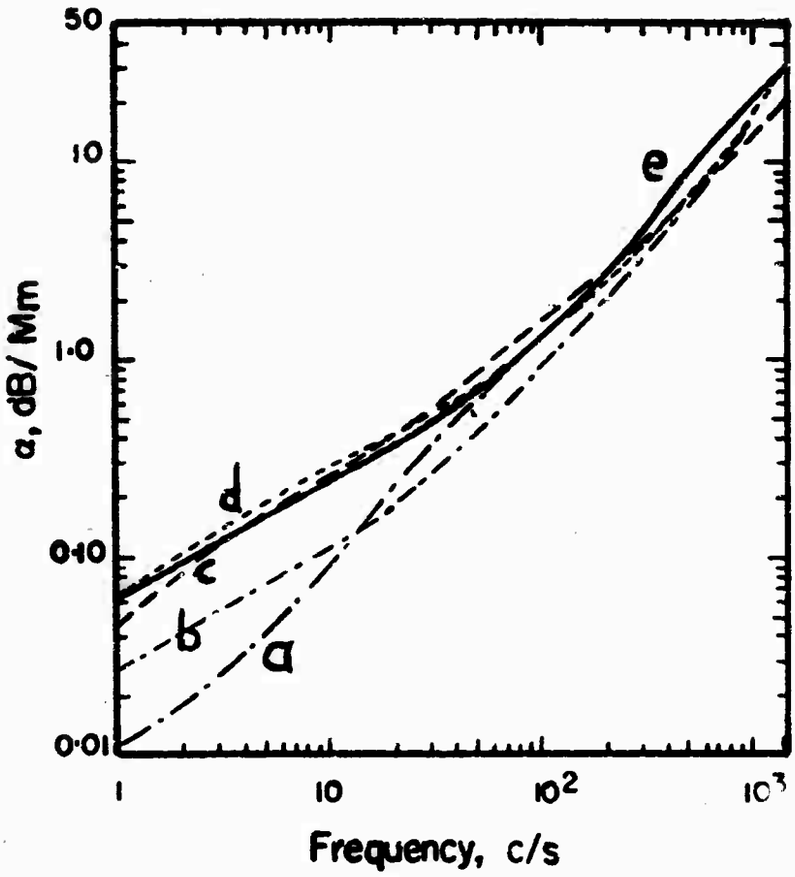

Figure 5.3. ELF attenuation,
D. L. Jones (1967).

a) Pierce and Cole ionosphere profile omitting data below 56 km

b) Deeks ionosphere profile (B. R. May, J. Atmosph. Terr. Phys., 28, 553, 1966)

c) Cole and Pierce (1965) ionosphere profile including heavy ion region down to 30 km altitude

d) Profile (b) continued to lower altitudes by profile (c)

e) Chapman-Jones (1964) two-layer profile.

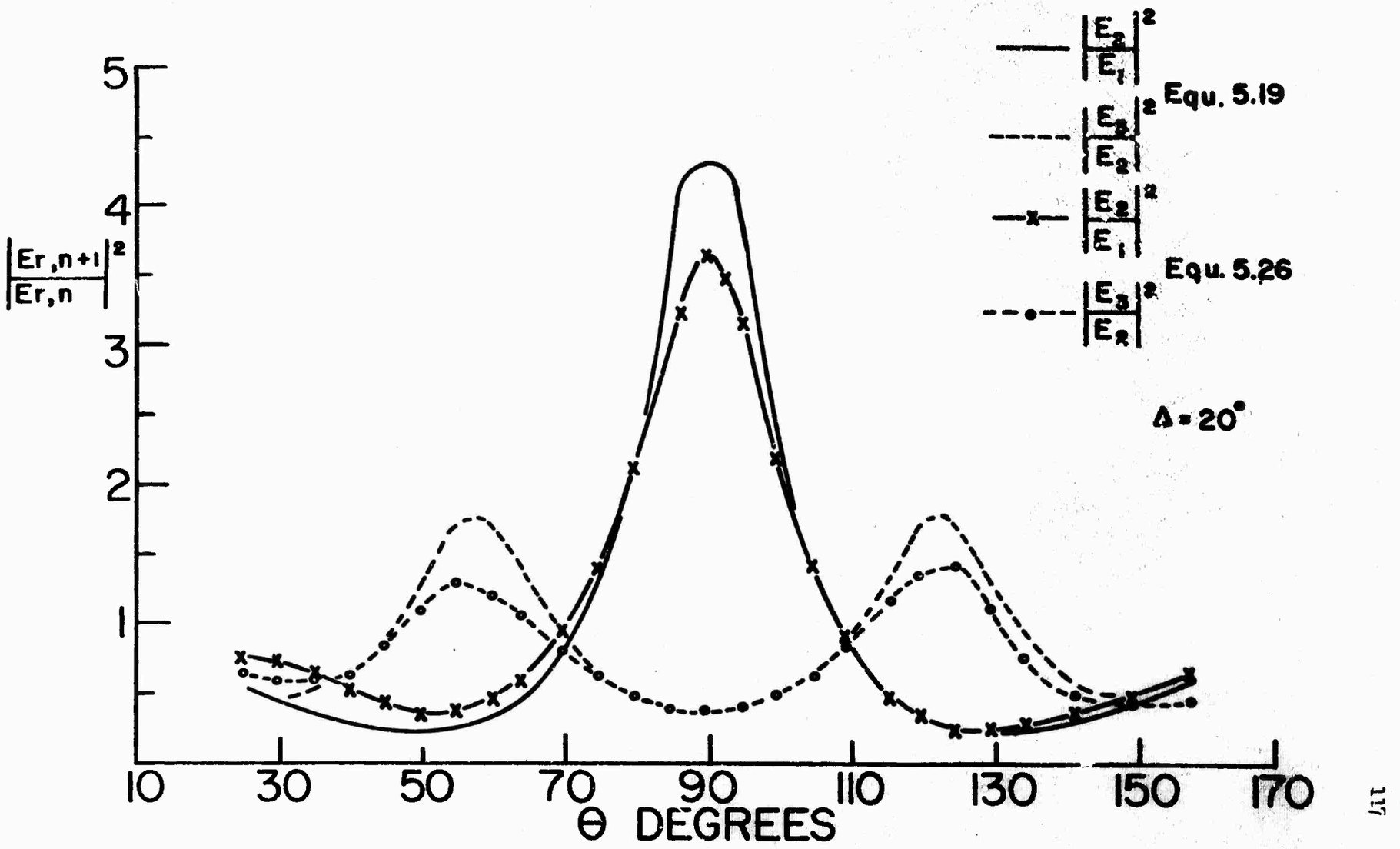

Figure 5.4. Ratio of resonant peaks; sources at $\theta - \Delta$ to $\theta + \Delta$. Results of approximation, equation (5.19), and results of numerical integration employing equations (5.26) and using ν based on Cole-Pierce profile.

Figure 5.5. Ratio of resonant peaks; magnetic field; sources at $\theta - \Delta$ to $\theta + \Delta$. Results of approximation, equation (5.20) and results of numerical integration of (5.27); ν based on Cole-Pierce profile.

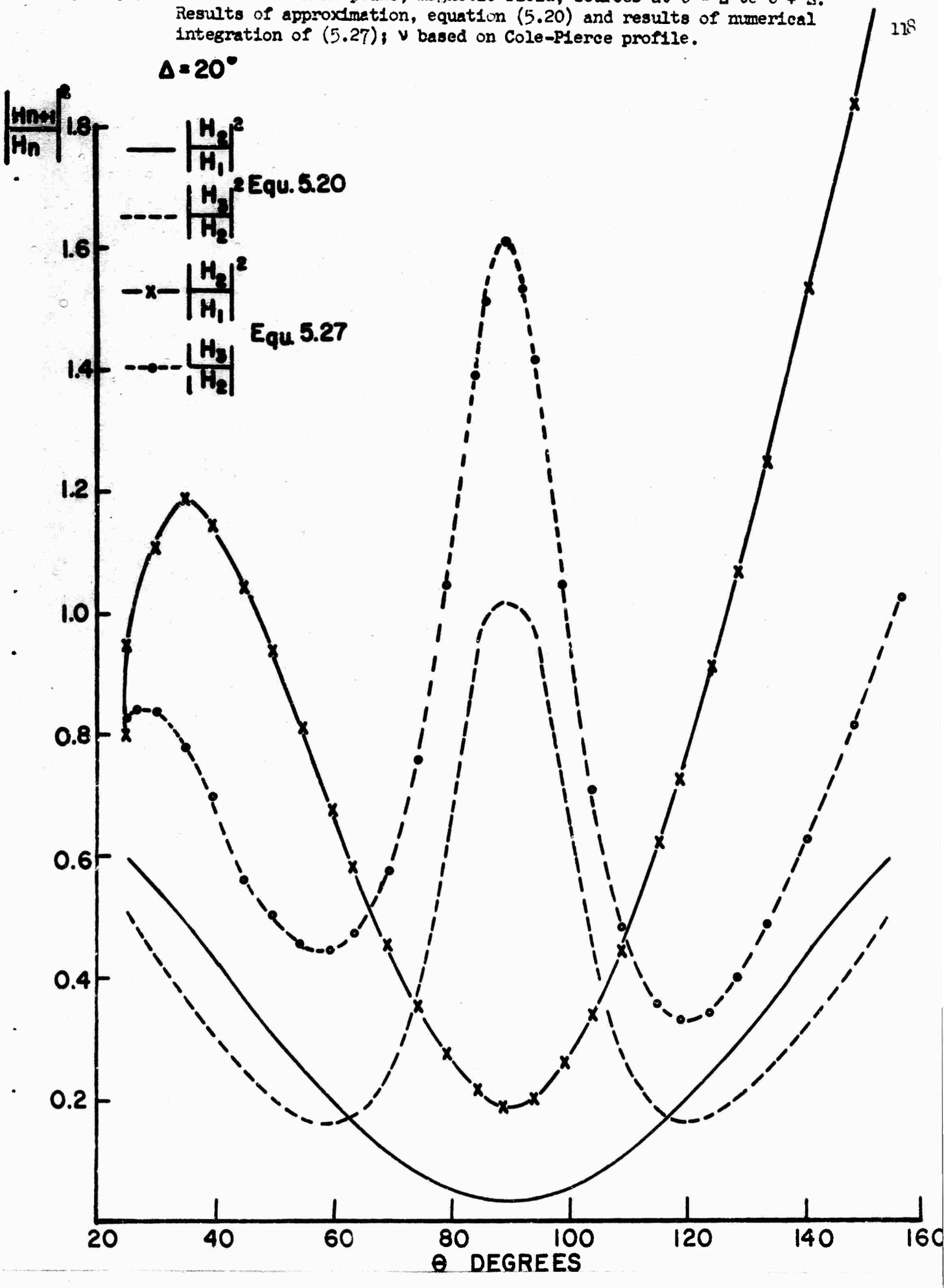

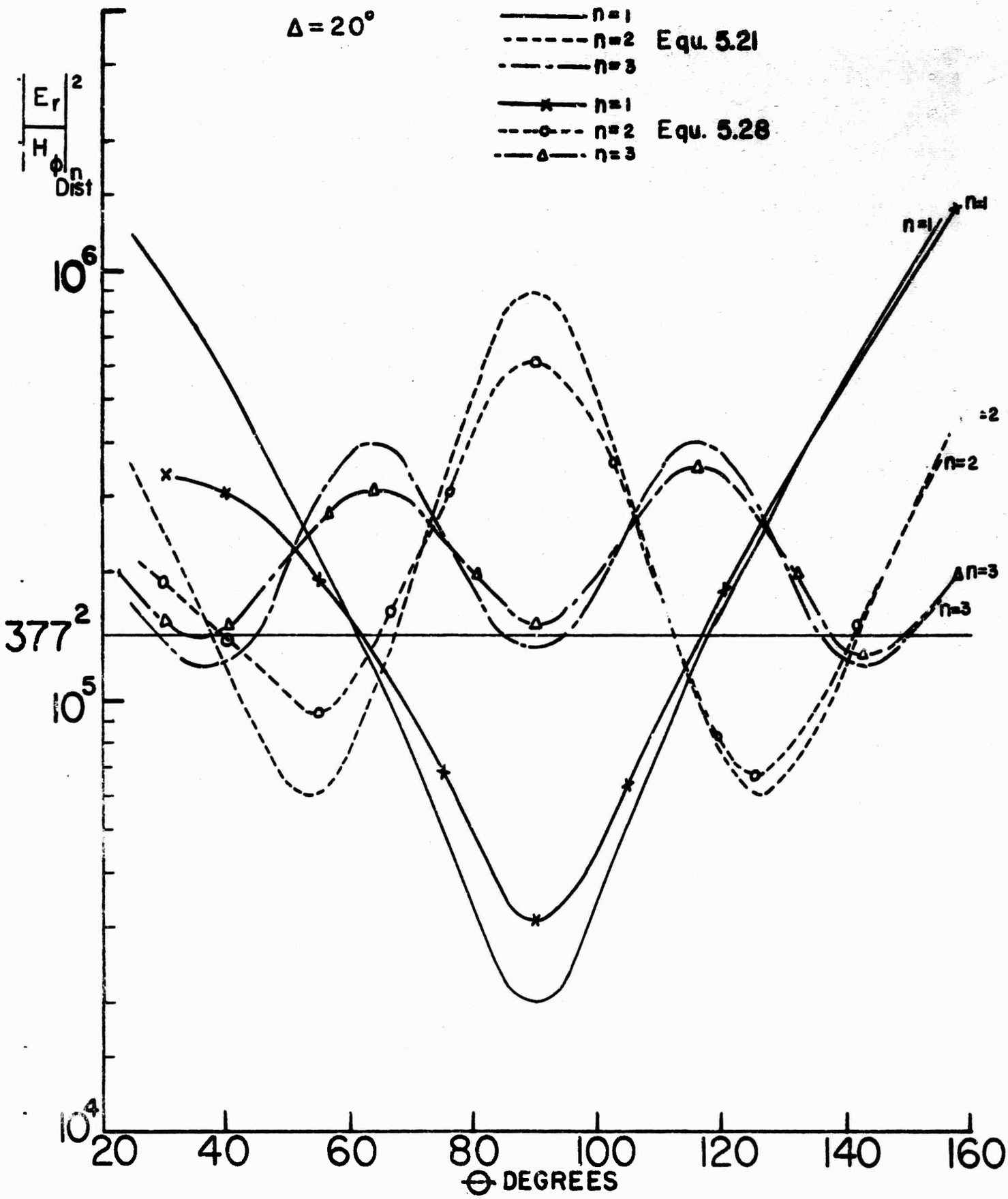

Figure 5.6. Ratio of electric to magnetic fields.

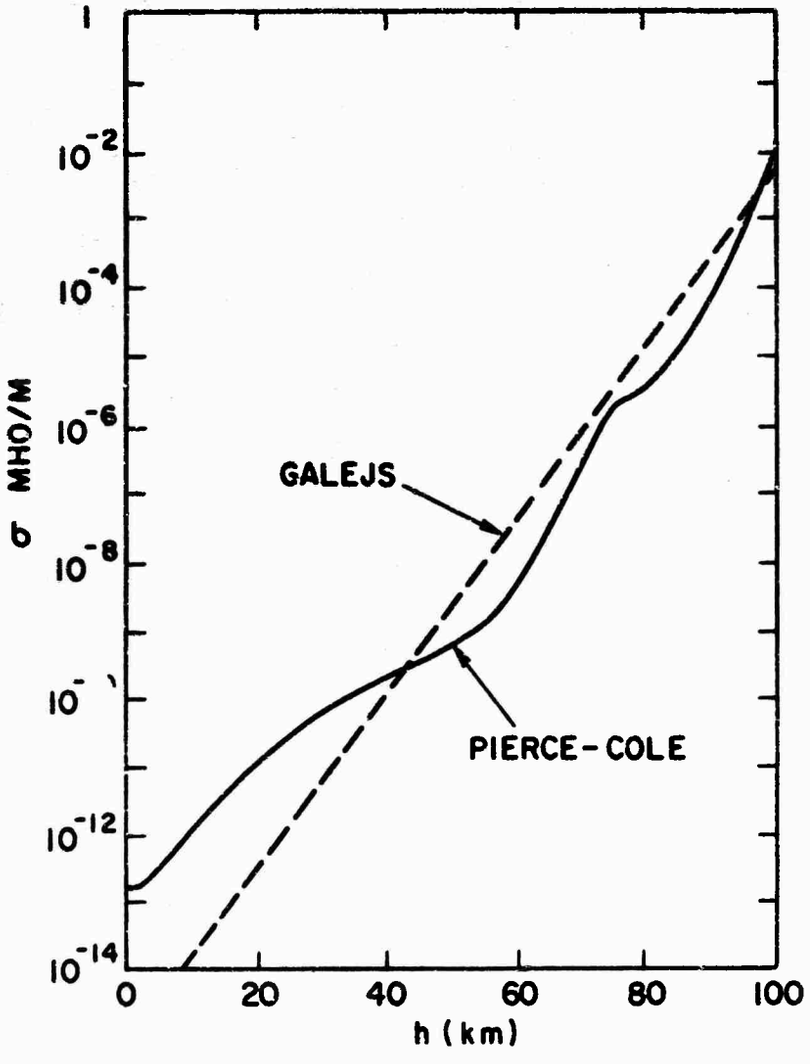

Figure 5.7. Effective ionospheric conductivity.

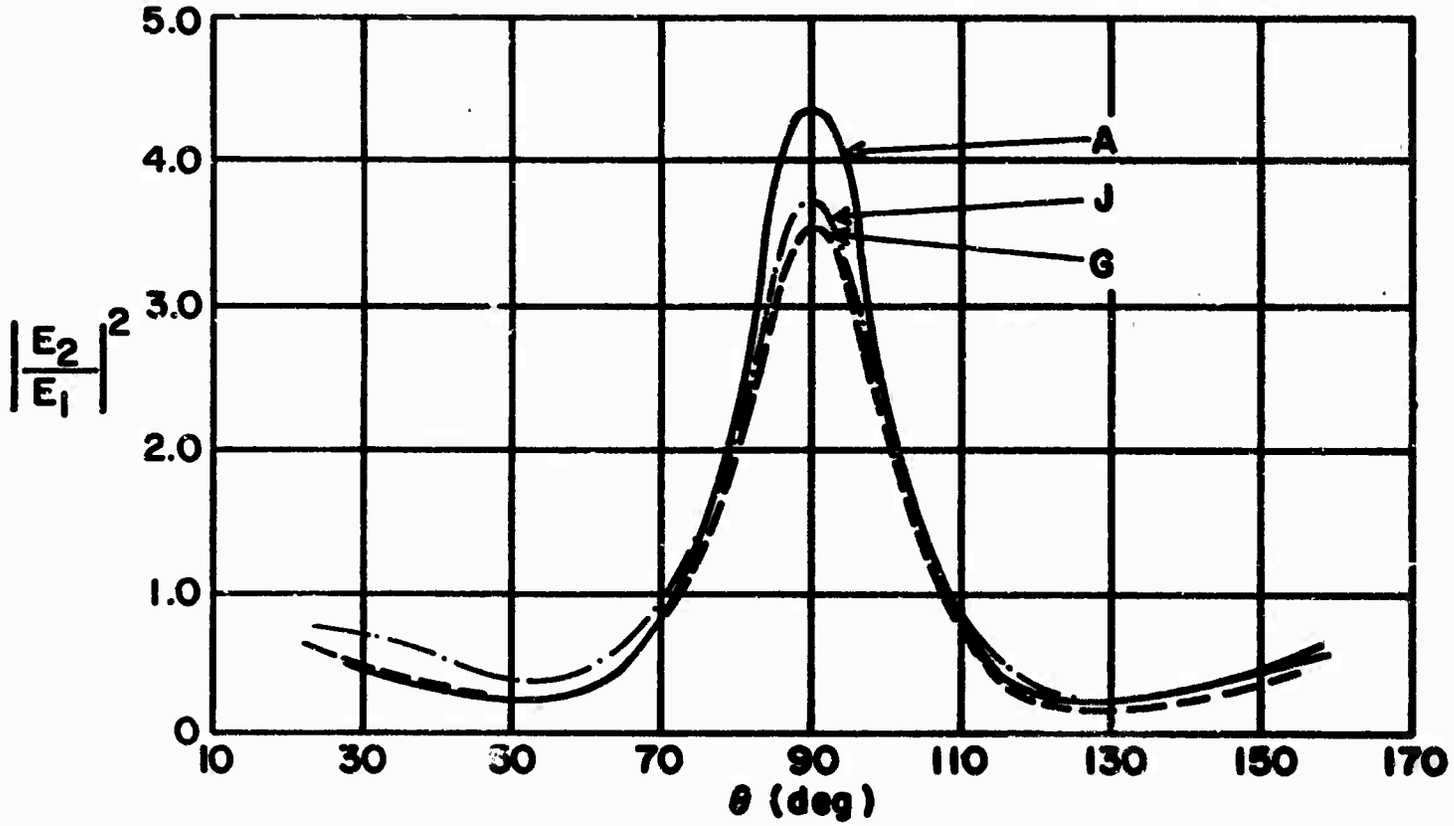

A: High Q cavity
J: Pierce-Cole Profile
G: Galejs Profile

Figure 5.8. Ratios for different ionosphere models.

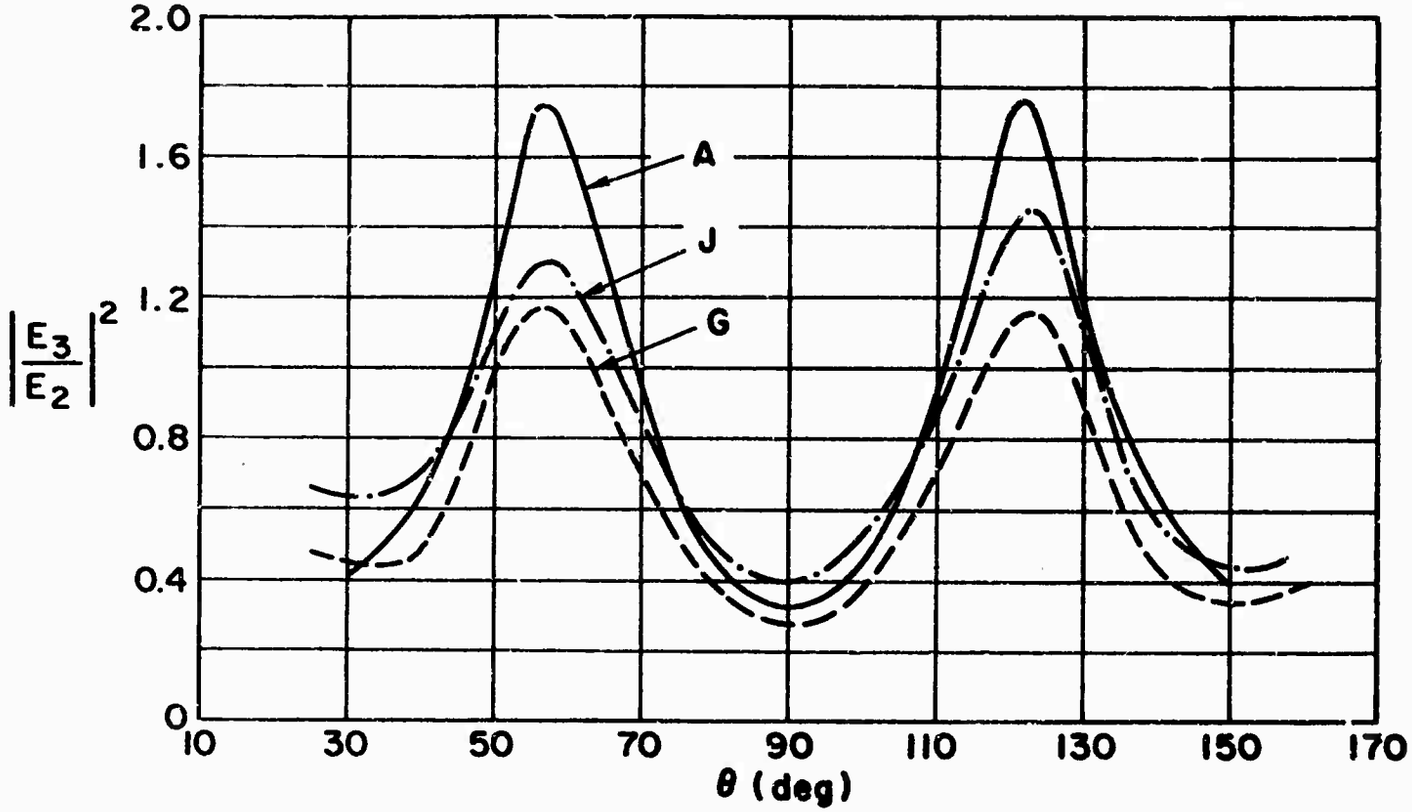

A: High Q cavity

J: Pierce-Cole profile

G: Galejs profile

Figure 5.9. Electric field ratios for different ionosphere models.

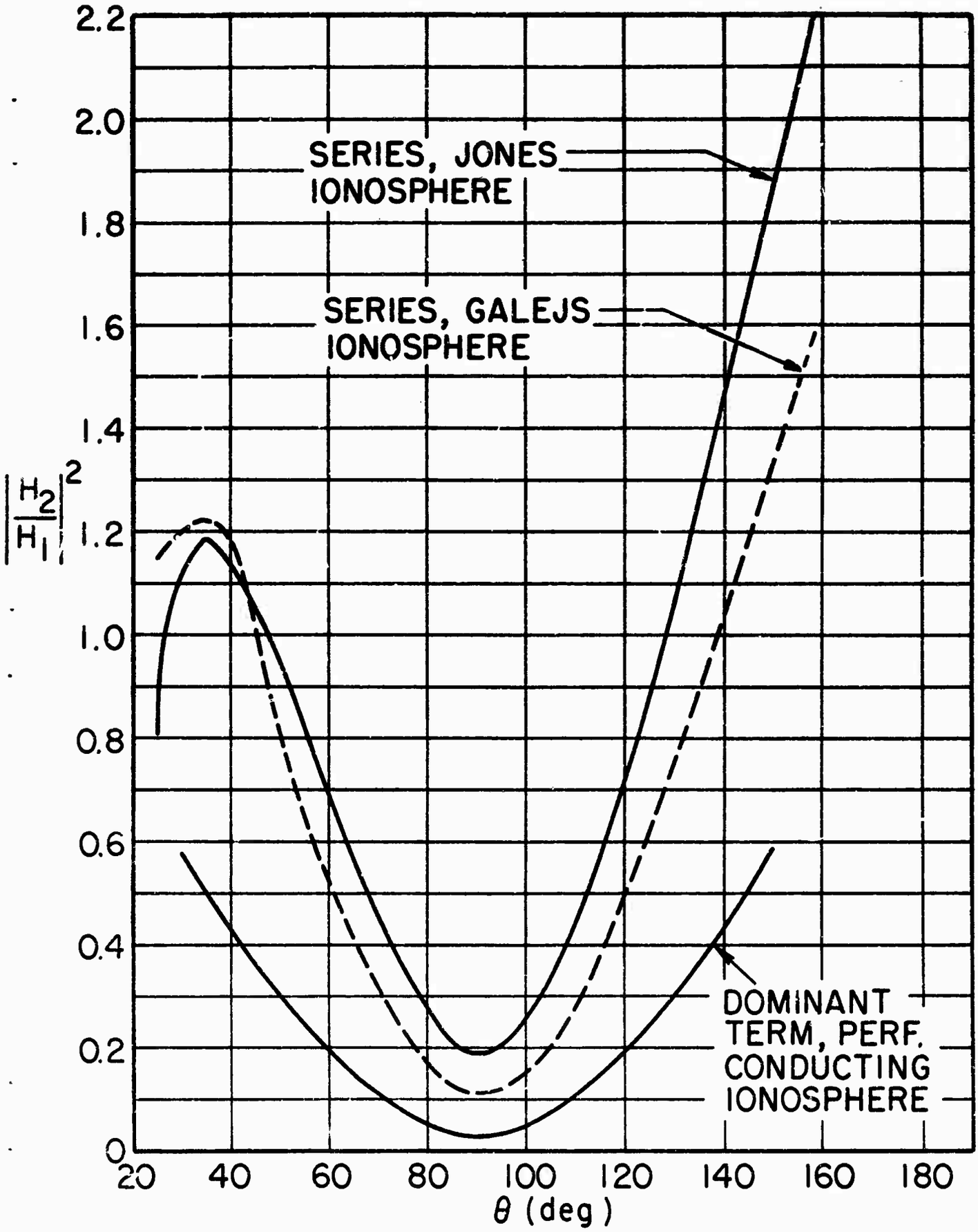

Figure 5.10. Magnetic field ratios for different ionosphere models.

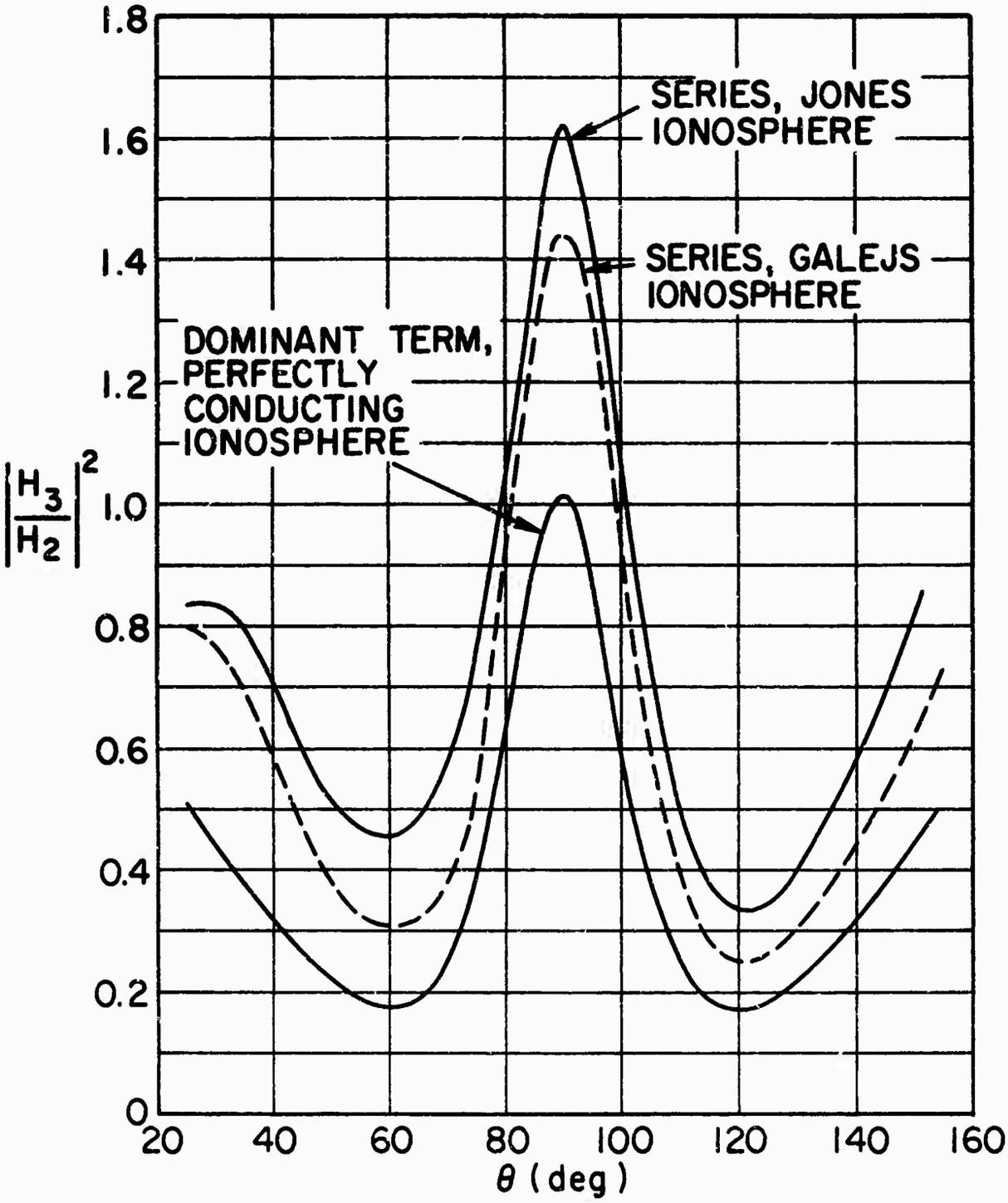

Figure 5.11. Magnetic field ratios for different ionosphere models.

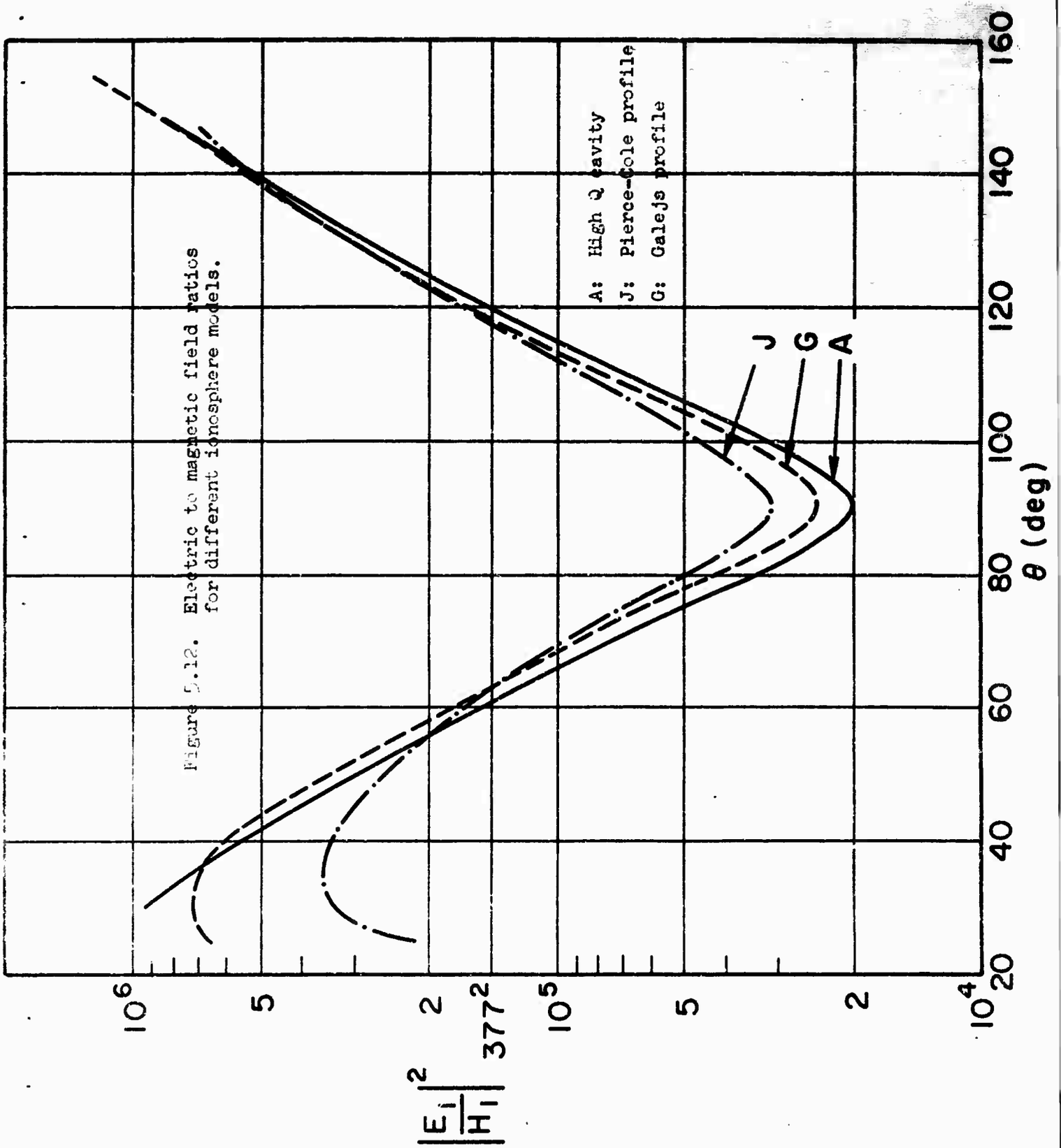

Figure 5.12. Electric to magnetic field ratios for different ionosphere models.

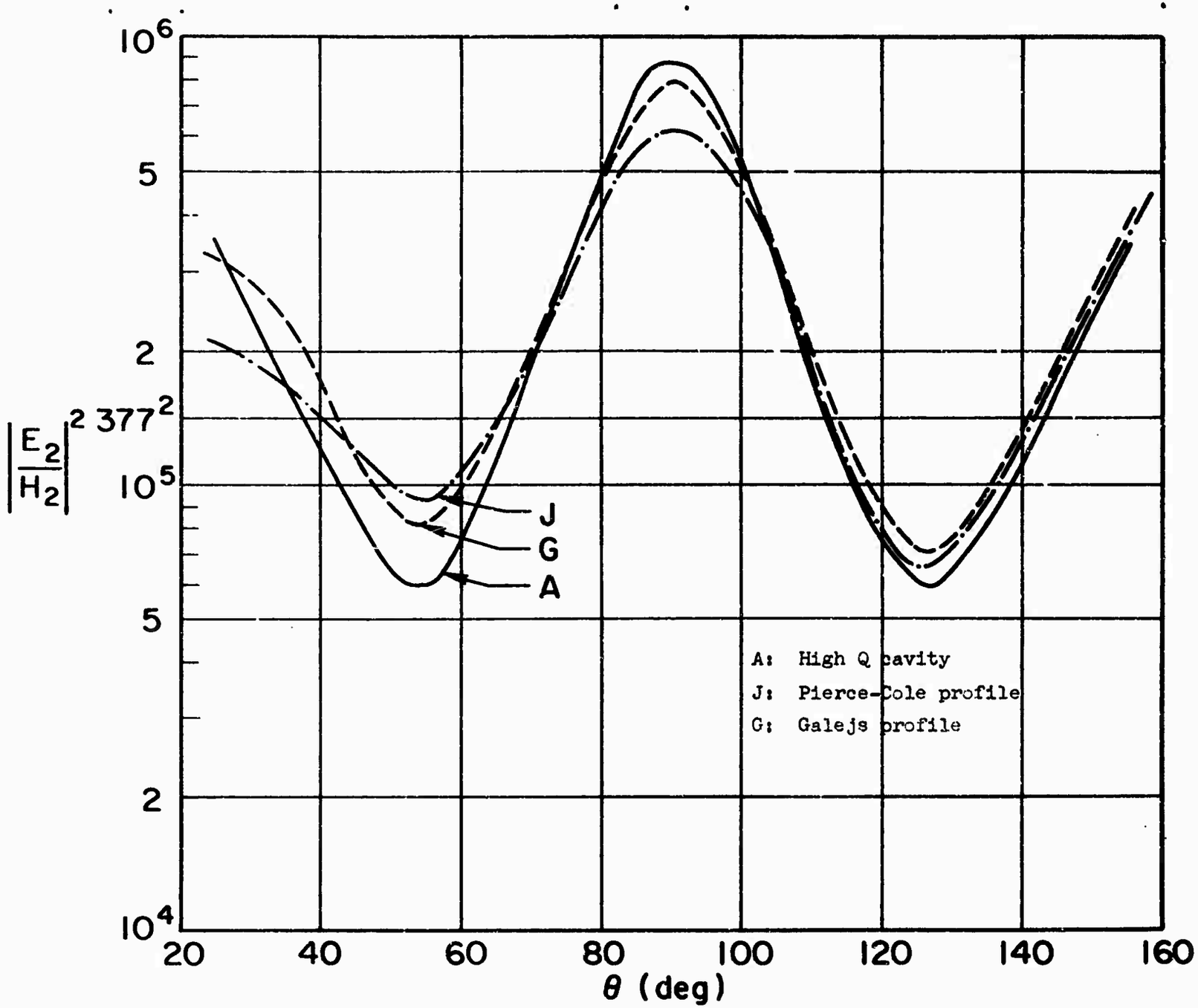

Figure 3.14. Electric to magnetic field ratios for different ionosphere profiles.

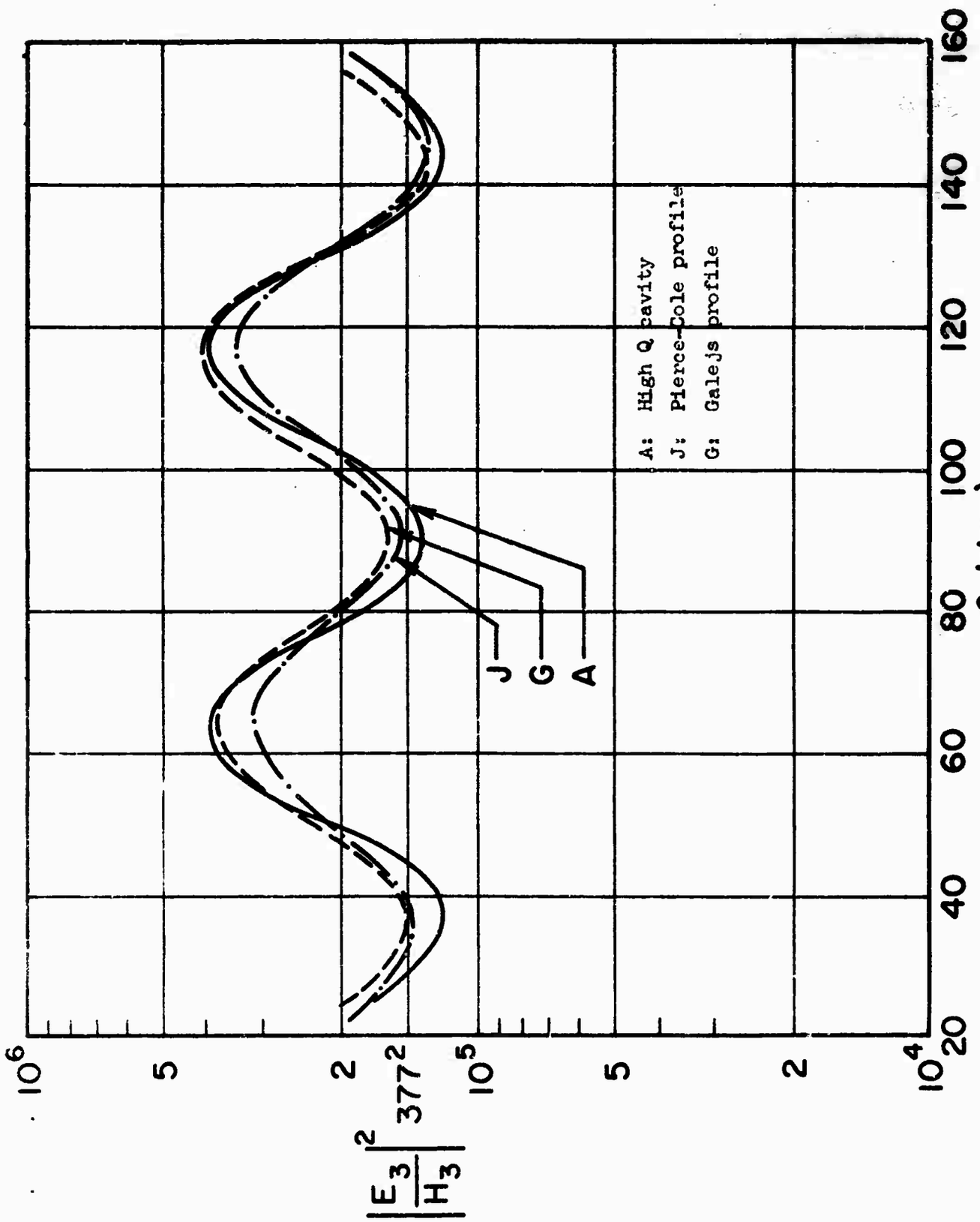

Figure 5.2-. Electric to magnetic field ratios for different ionosphere models.

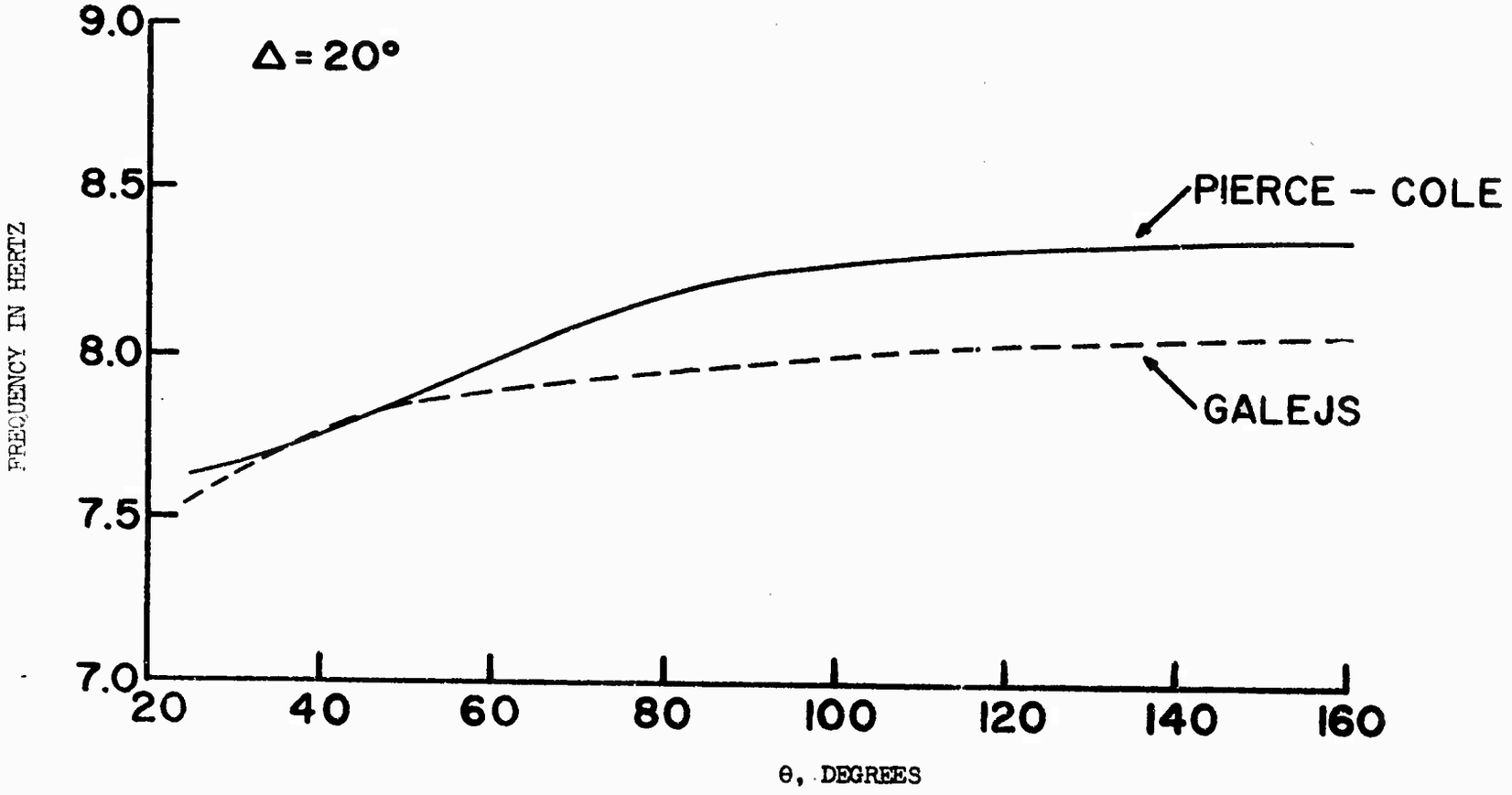

Figure 5.15. Variation of magnetic field first resonant frequency with source distance for two different ionosphere profiles.

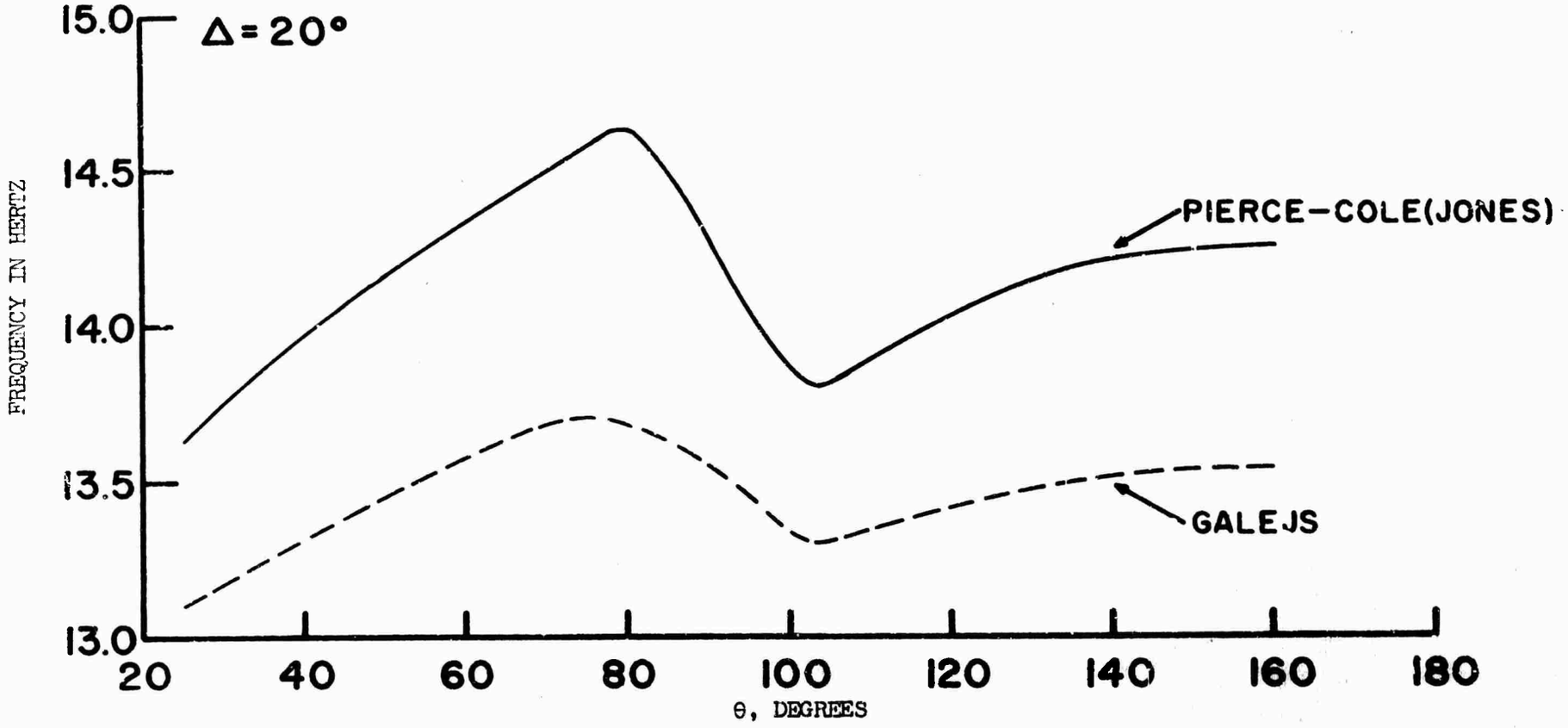

Figure 5.16. Variation of magnetic field second resonant frequency with source distance for two different ionosphere profiles.

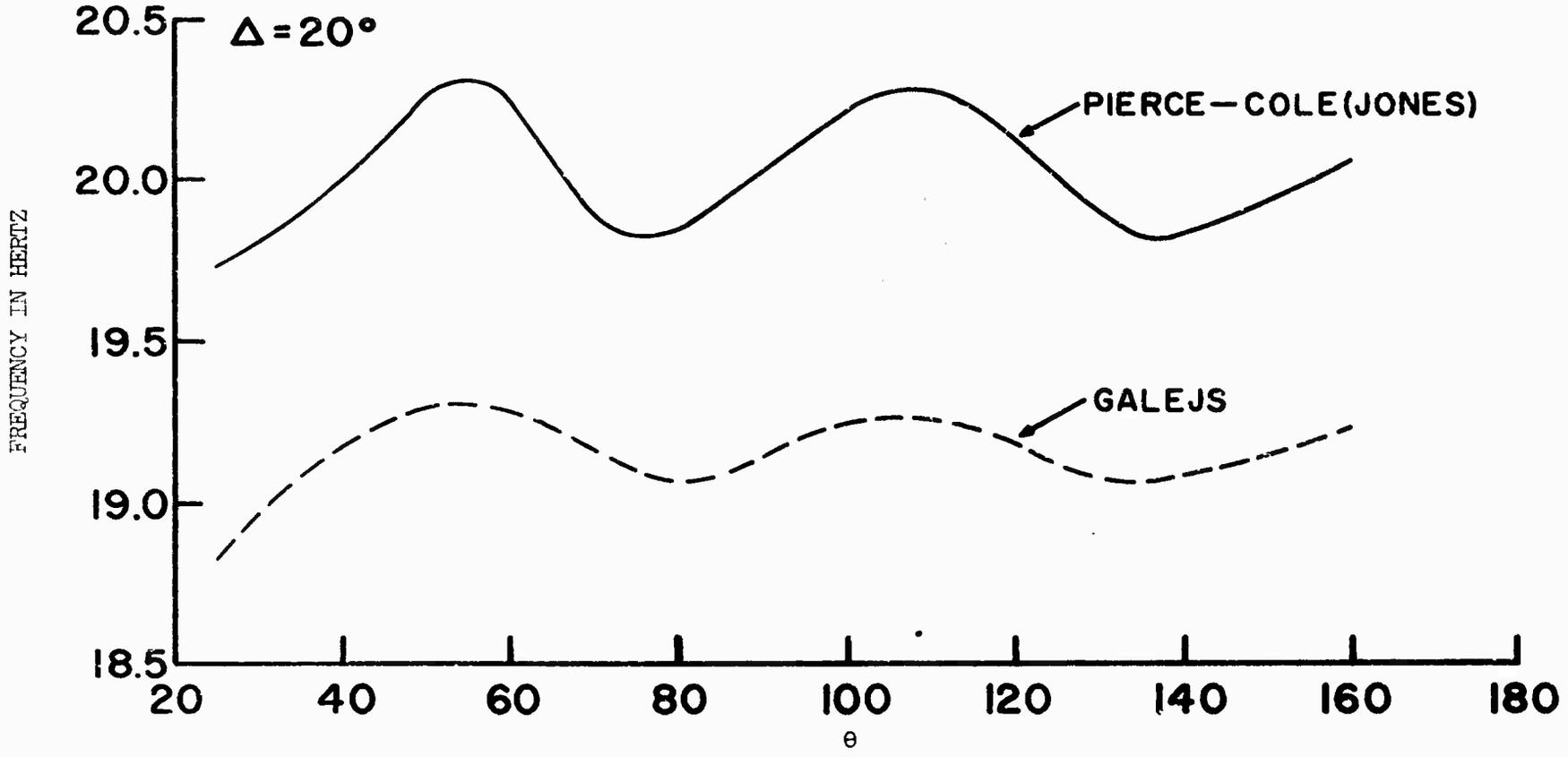

Figure 5.17. Variation of magnetic field third resonant frequency with source distance for two different ionosphere profiles.

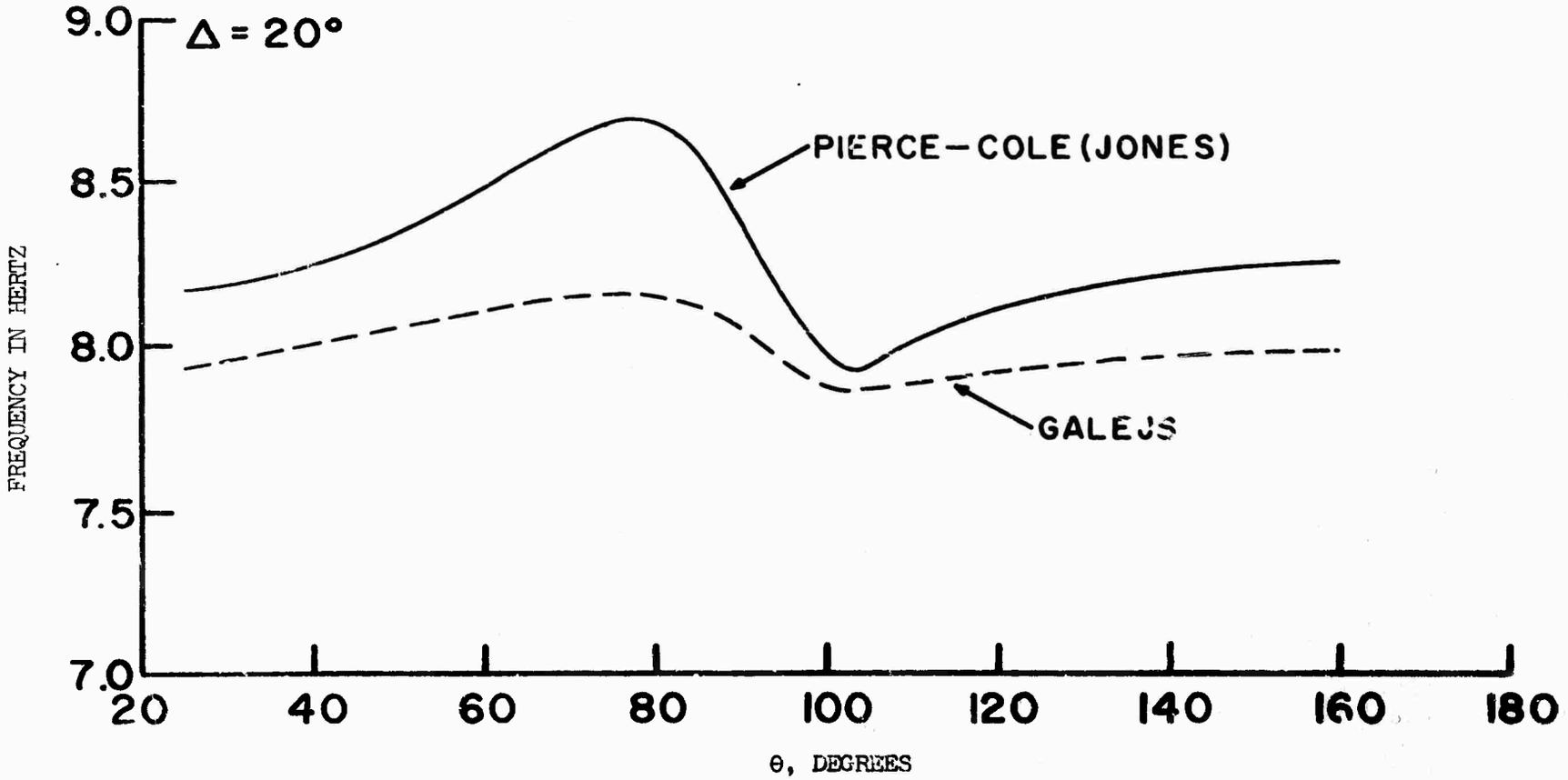

Figure 5.18. Variation of electric field first resonant frequency with source distance for two different ionosphere profiles.

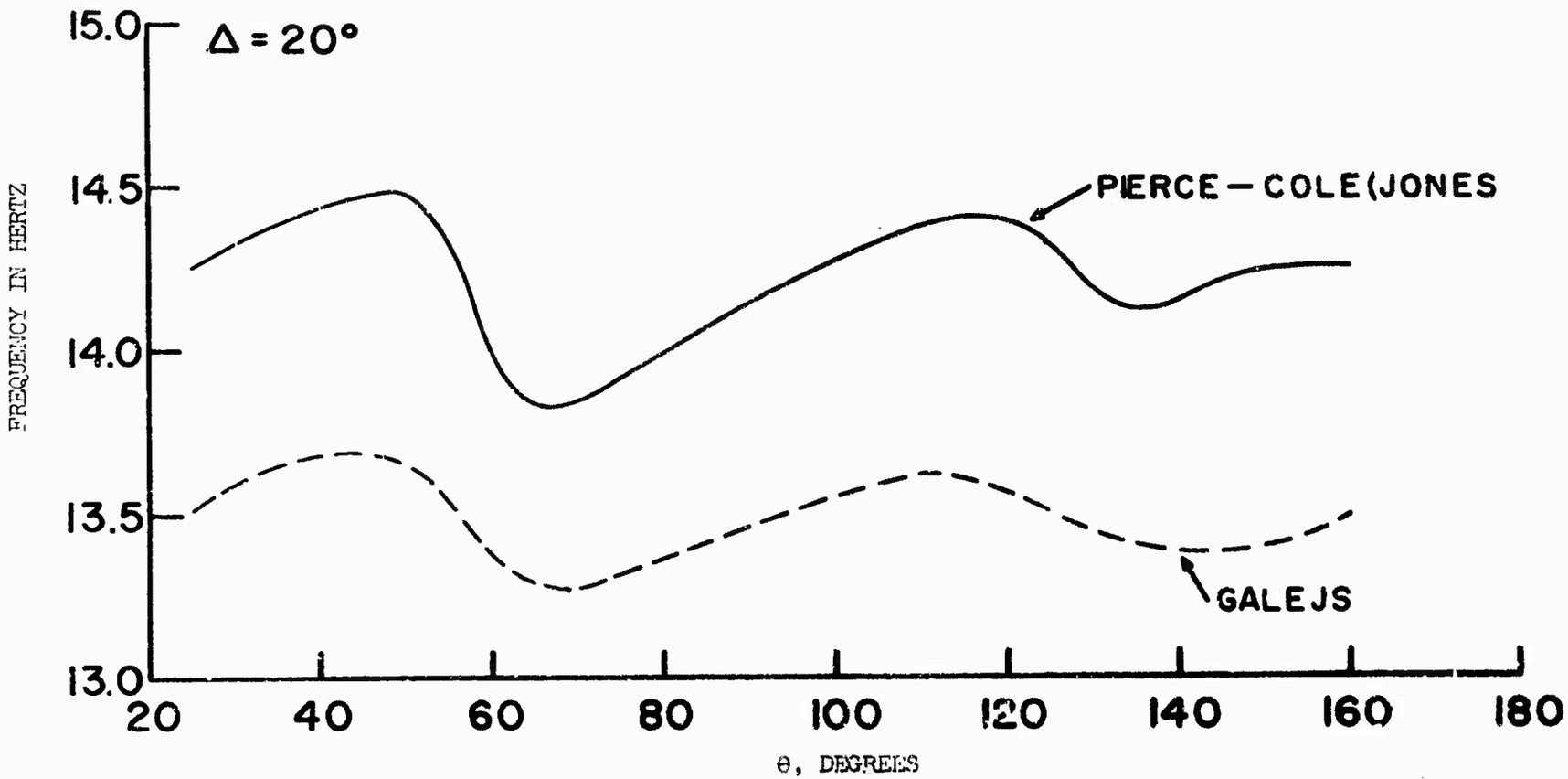

Figure 5.19. Variation of electric field second resonant frequency with source distance for two different ionosphere profiles.

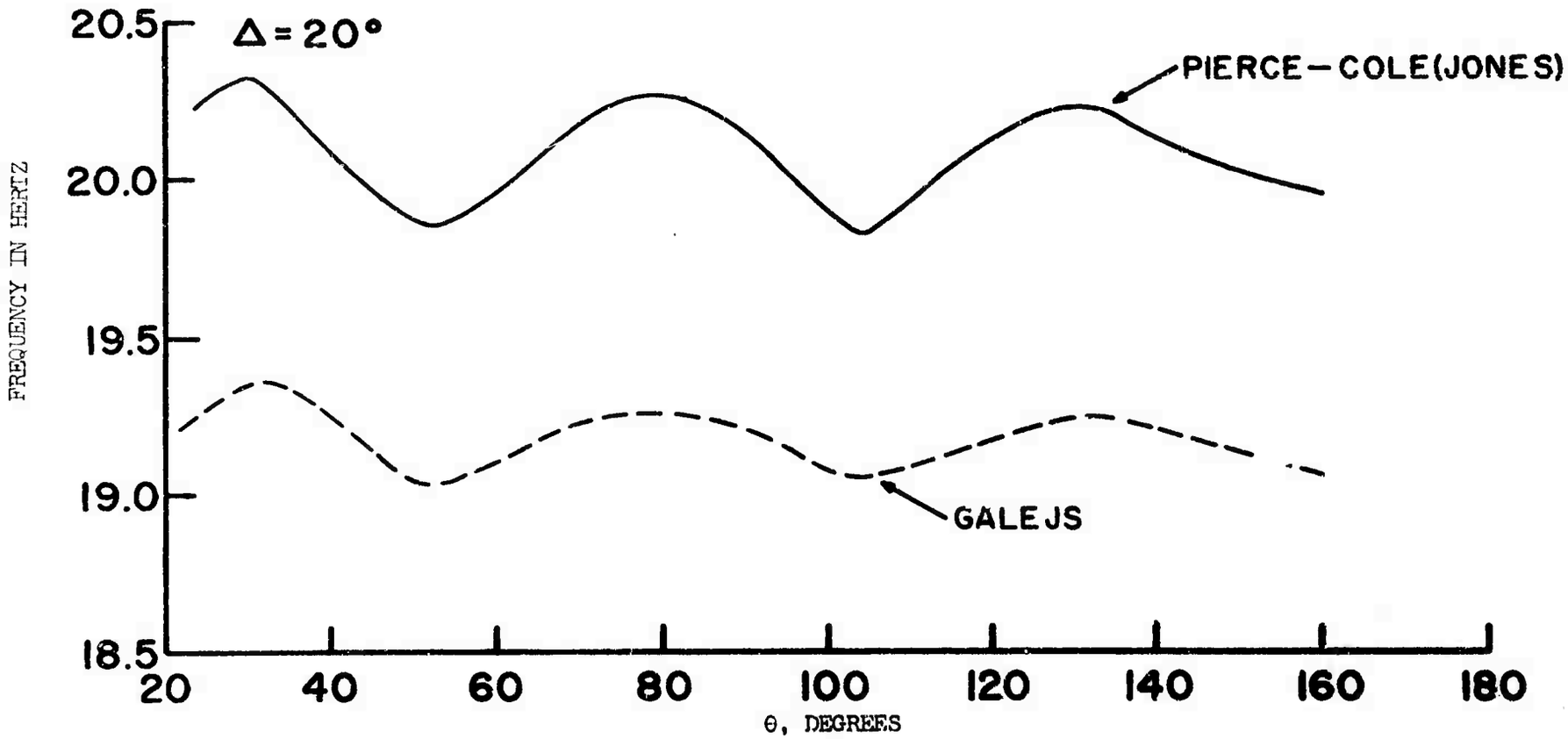

Figure 5.20. Variation of electric field third resonant frequency with source distance for two different ionosphere profiles.

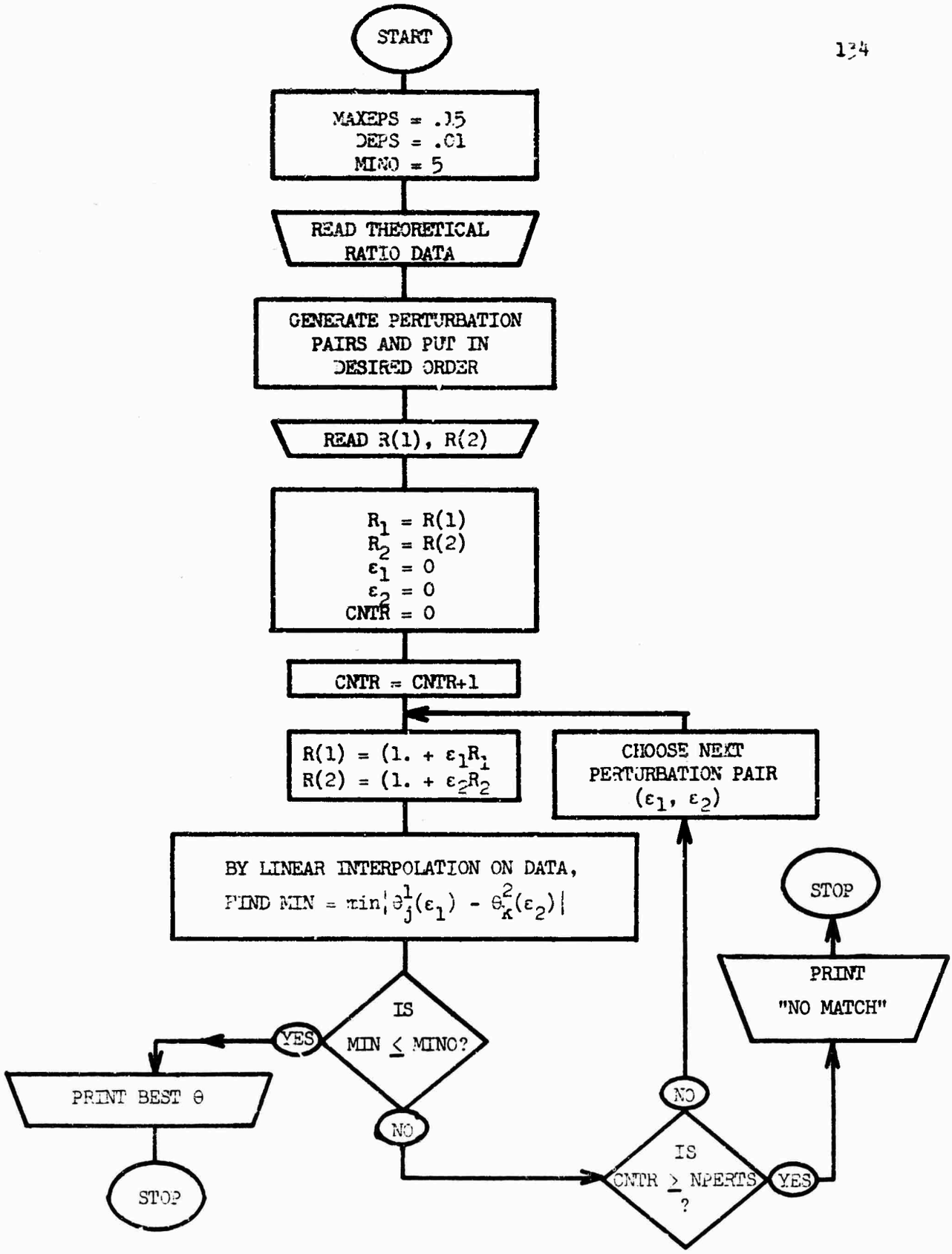

Figure 6.1. Flowchart describing method for determining best distance estimate for two measured ratio values.

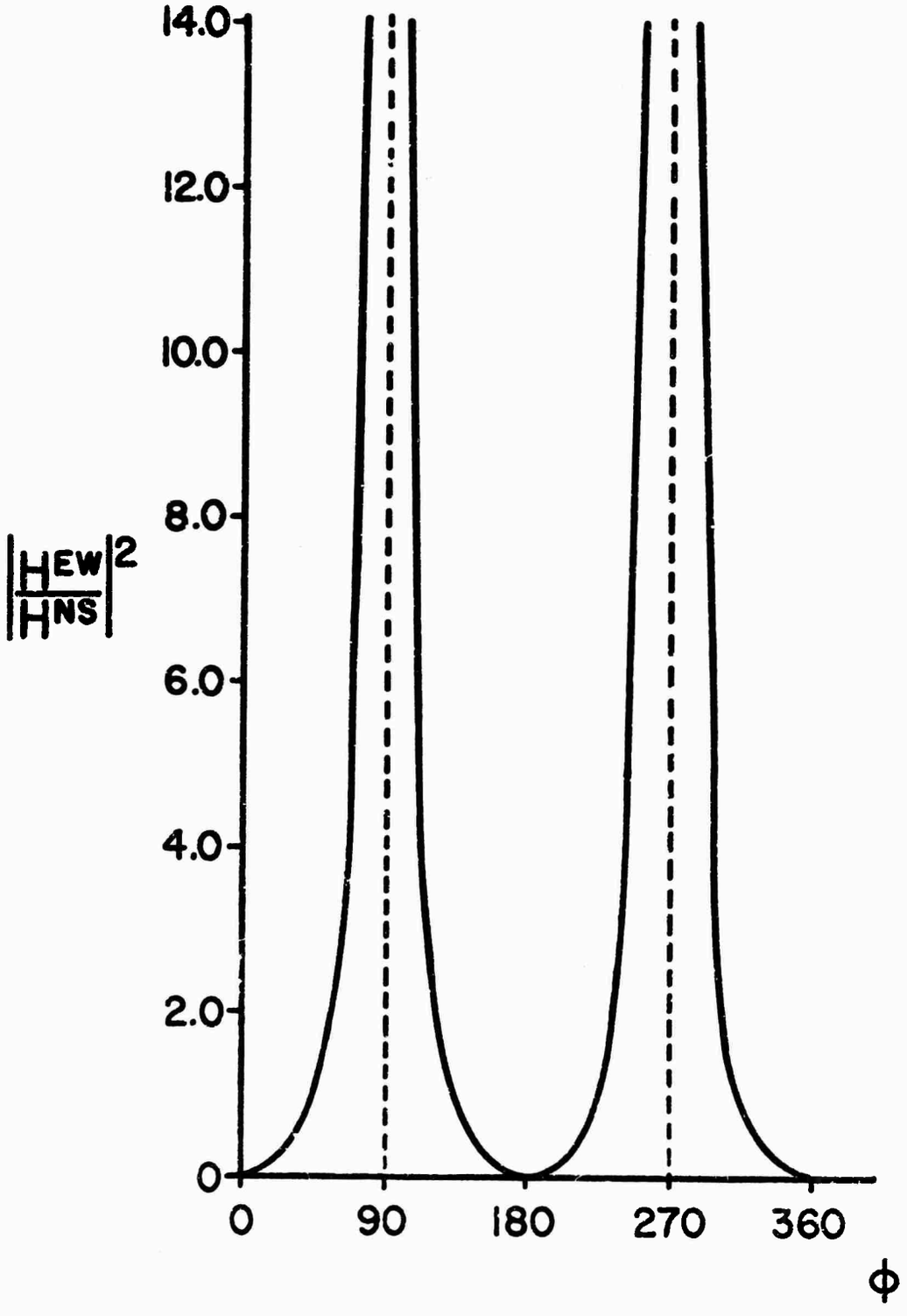

Figure 3.2. Relative response of two orthogonal coils for varying source azimuth, Φ.

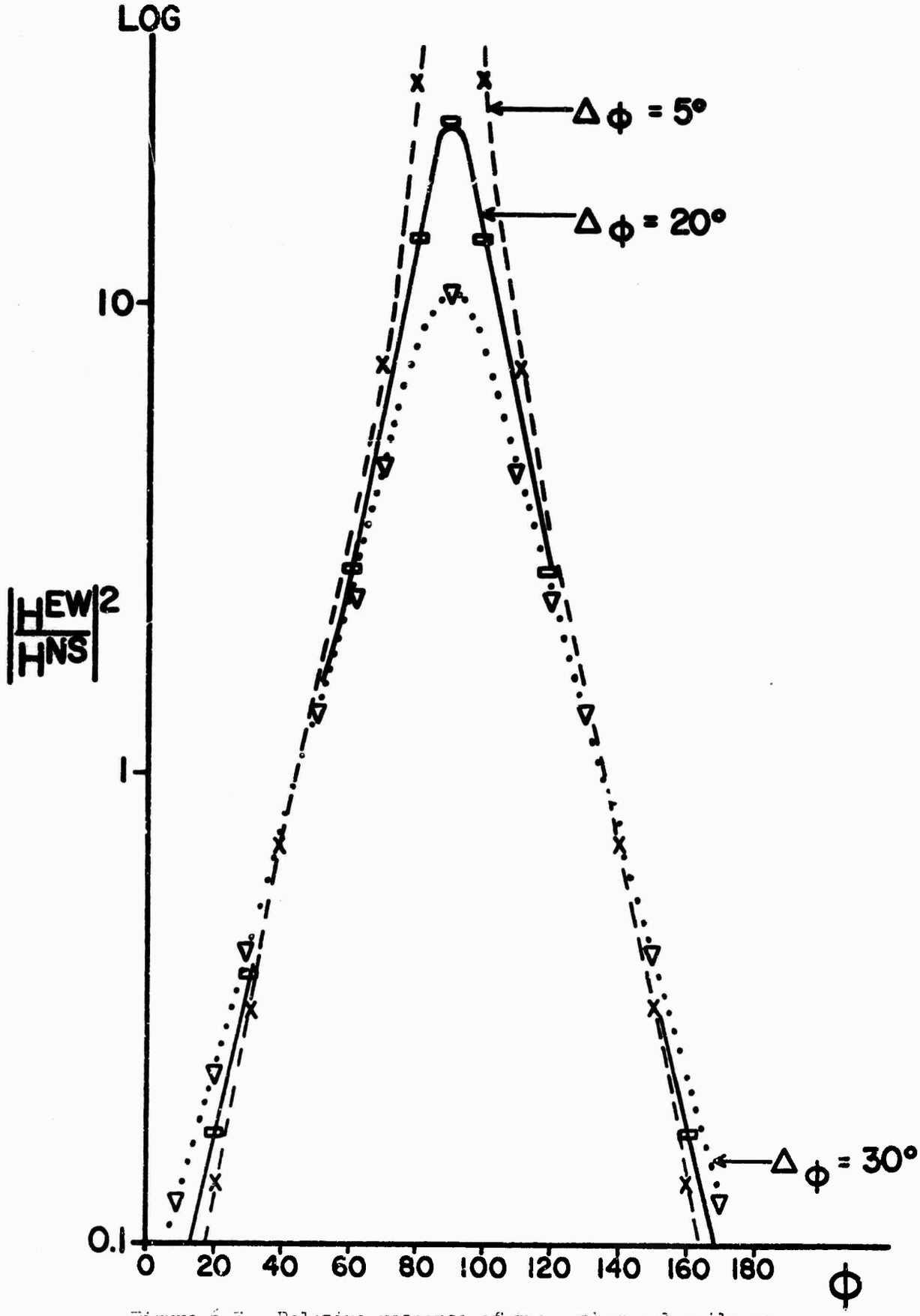

Figure 6.3. Relative response of two orthogonal coils vs source azimuth for different Δ_ϕ.

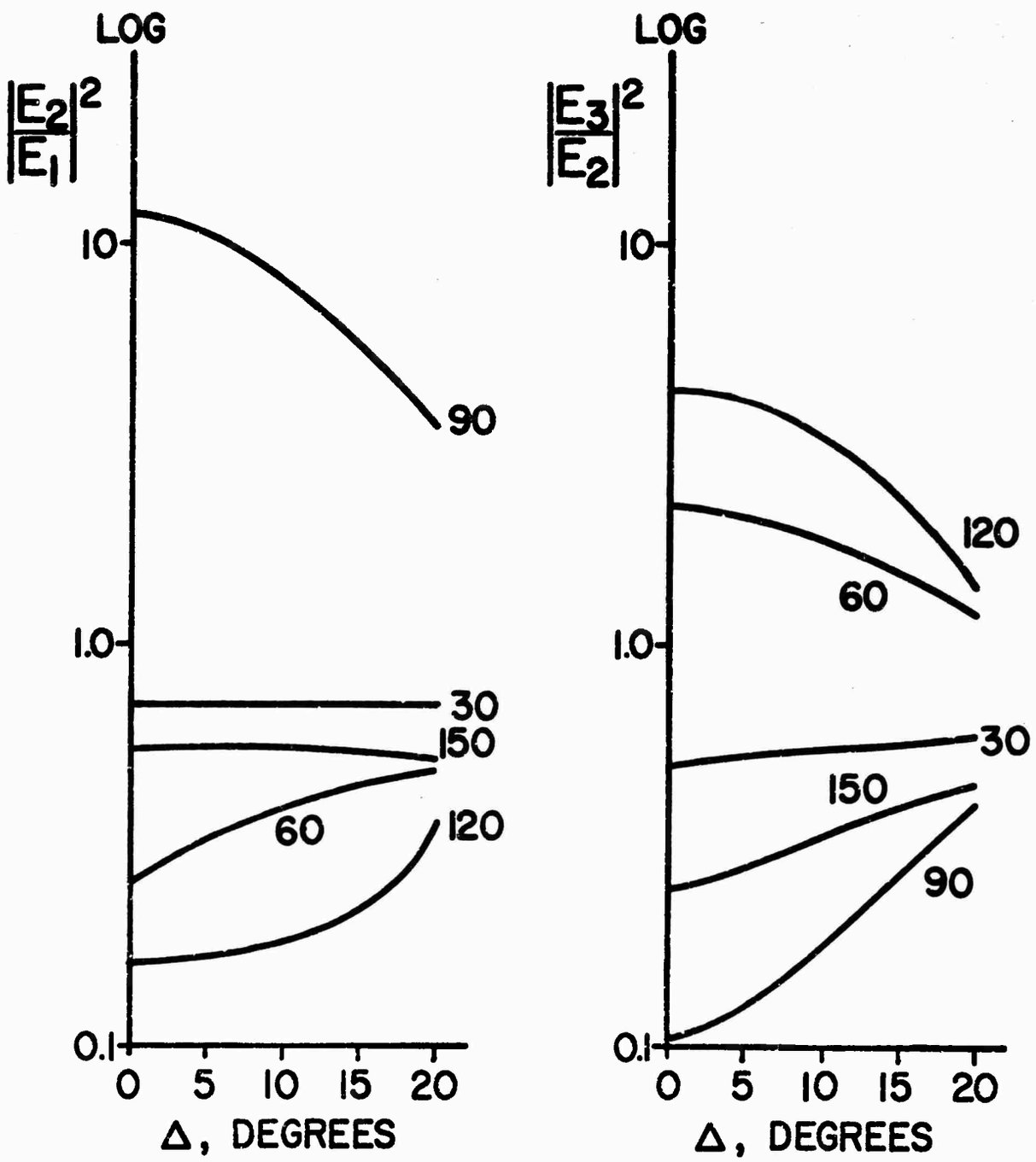

Figure 7.1. Variation of electric field ratios with Δ, parametric in source location, θ.

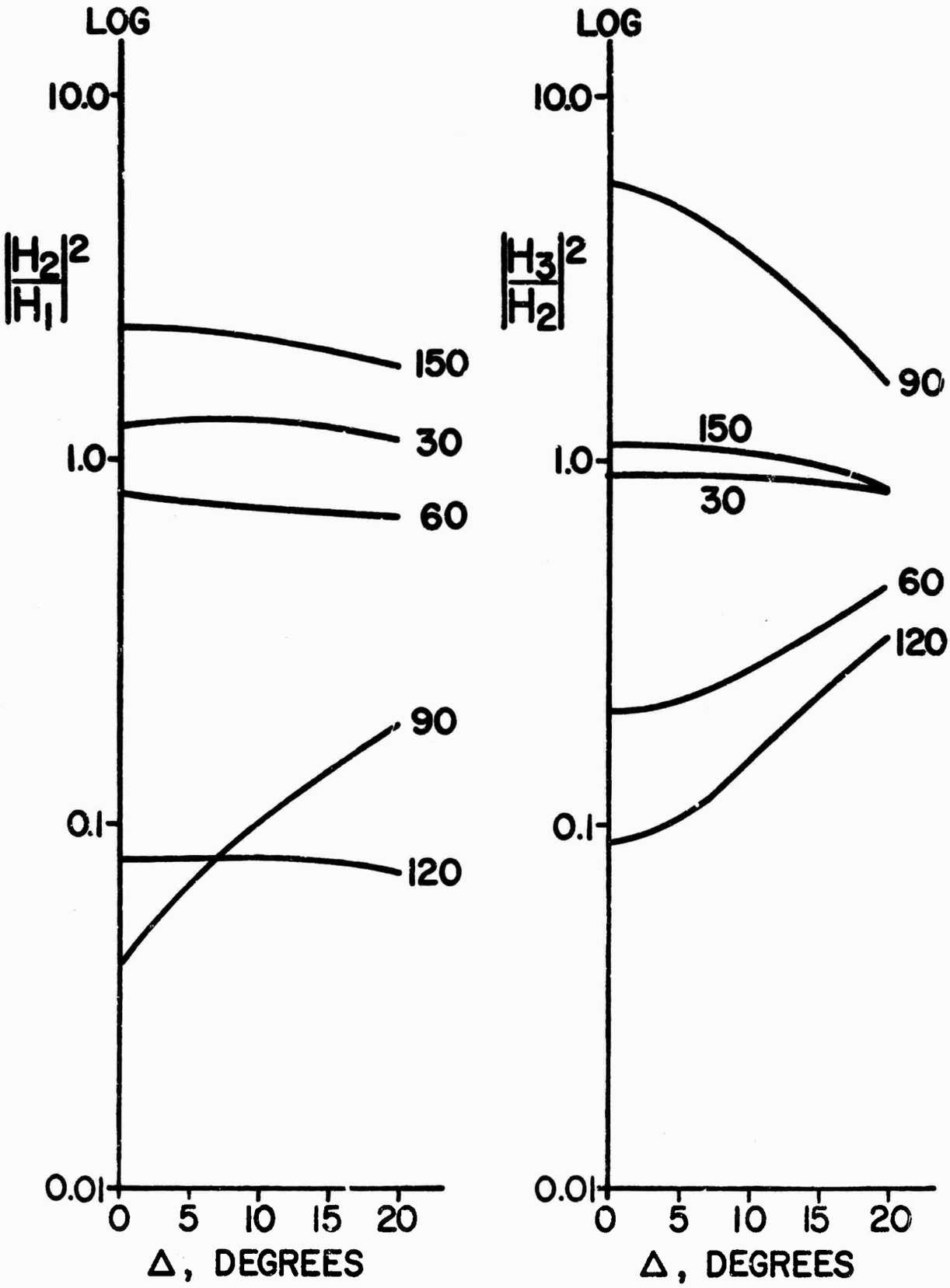

Figure 7.2. Variation of magnetic field ratios with Δ, parametric in source location, θ.

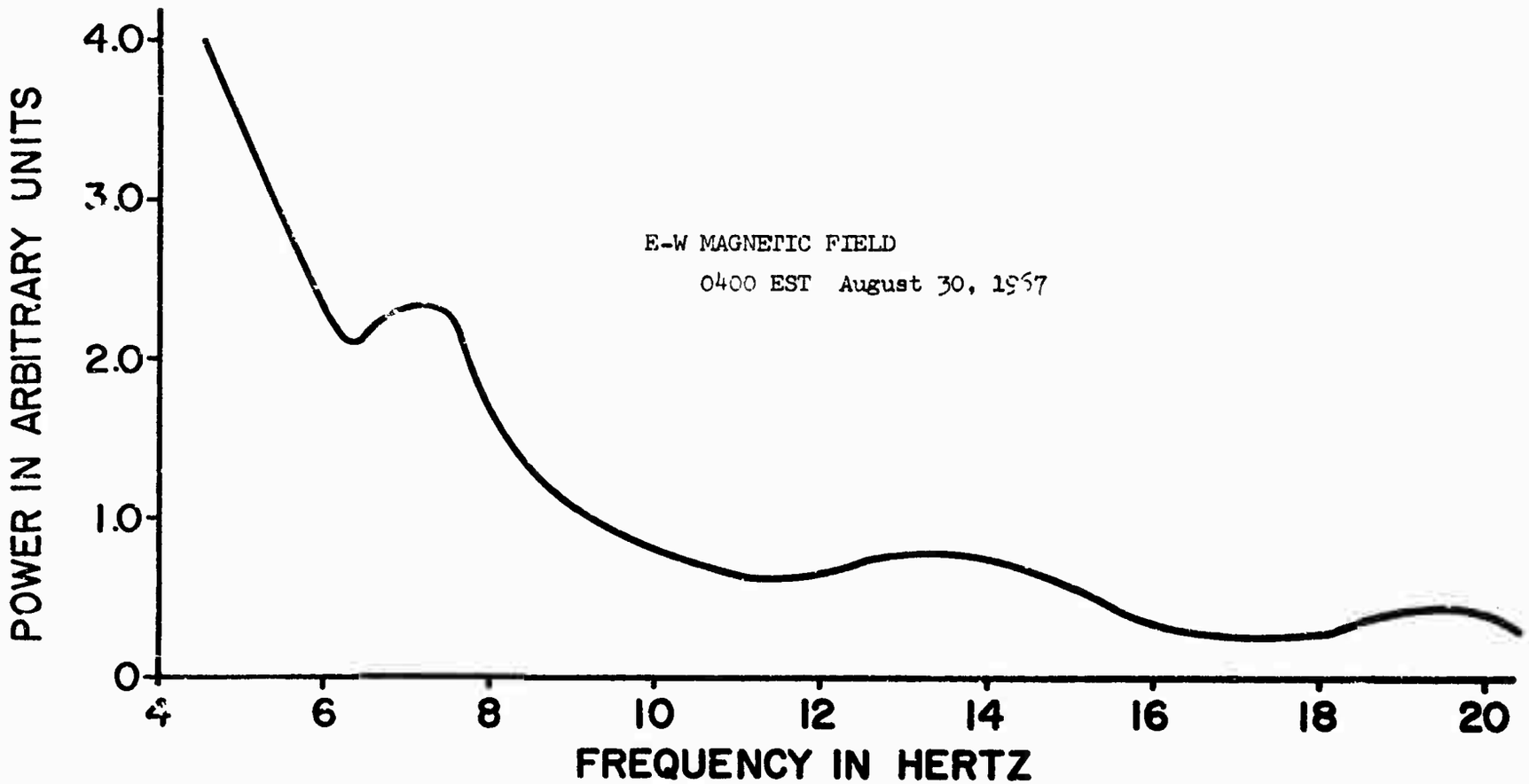

Figure 8.1. East-West magnetic field spectrum in Rhode Island at 0400 EST August 30, 1967. An illustration of cosmic noise contamination.

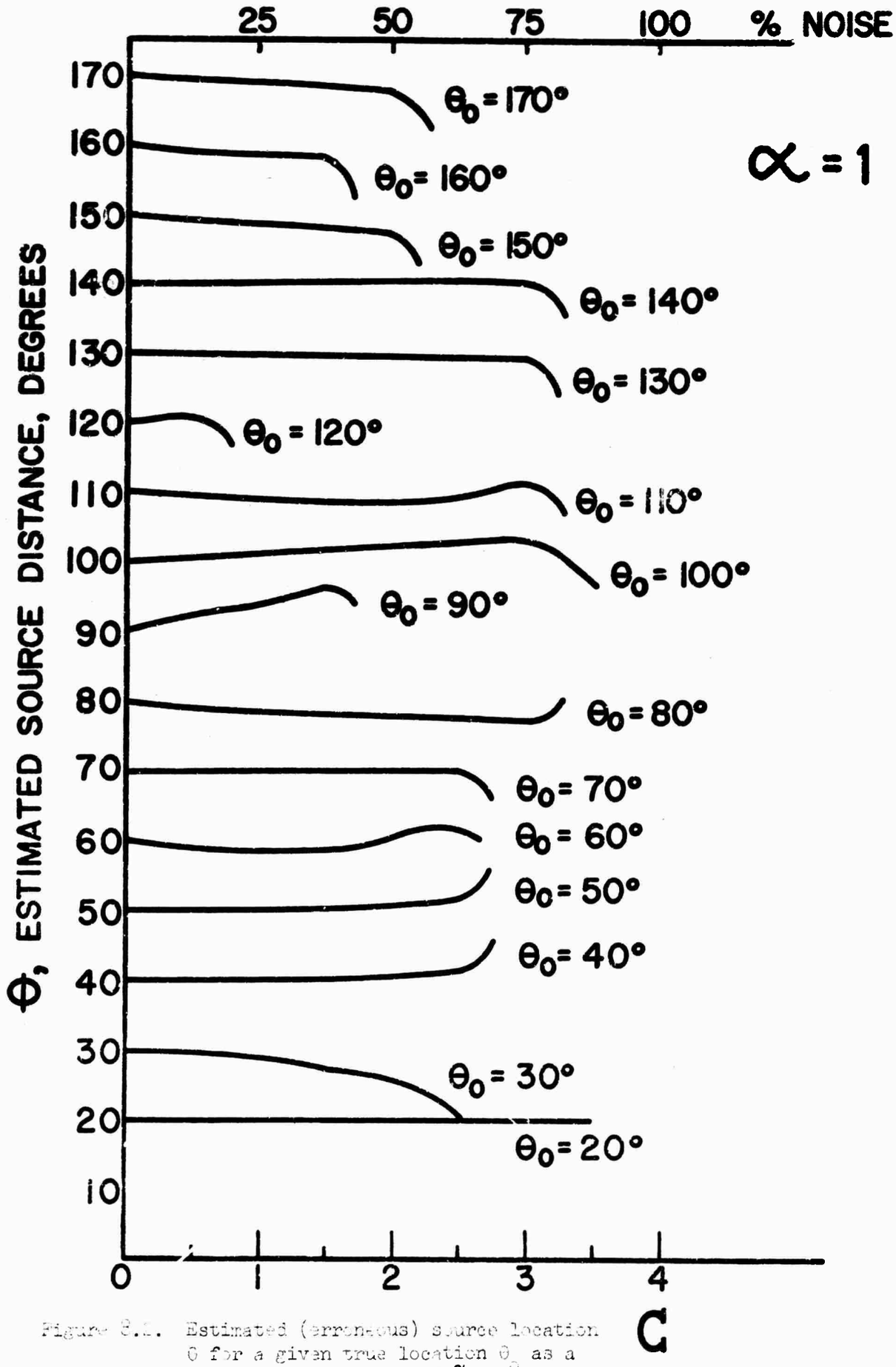

Figure 8.1. Estimated (erroneous) source location θ for a given true location θ_0 as a function of additive $Af^{-\alpha}$ noise ($\alpha = 1$).

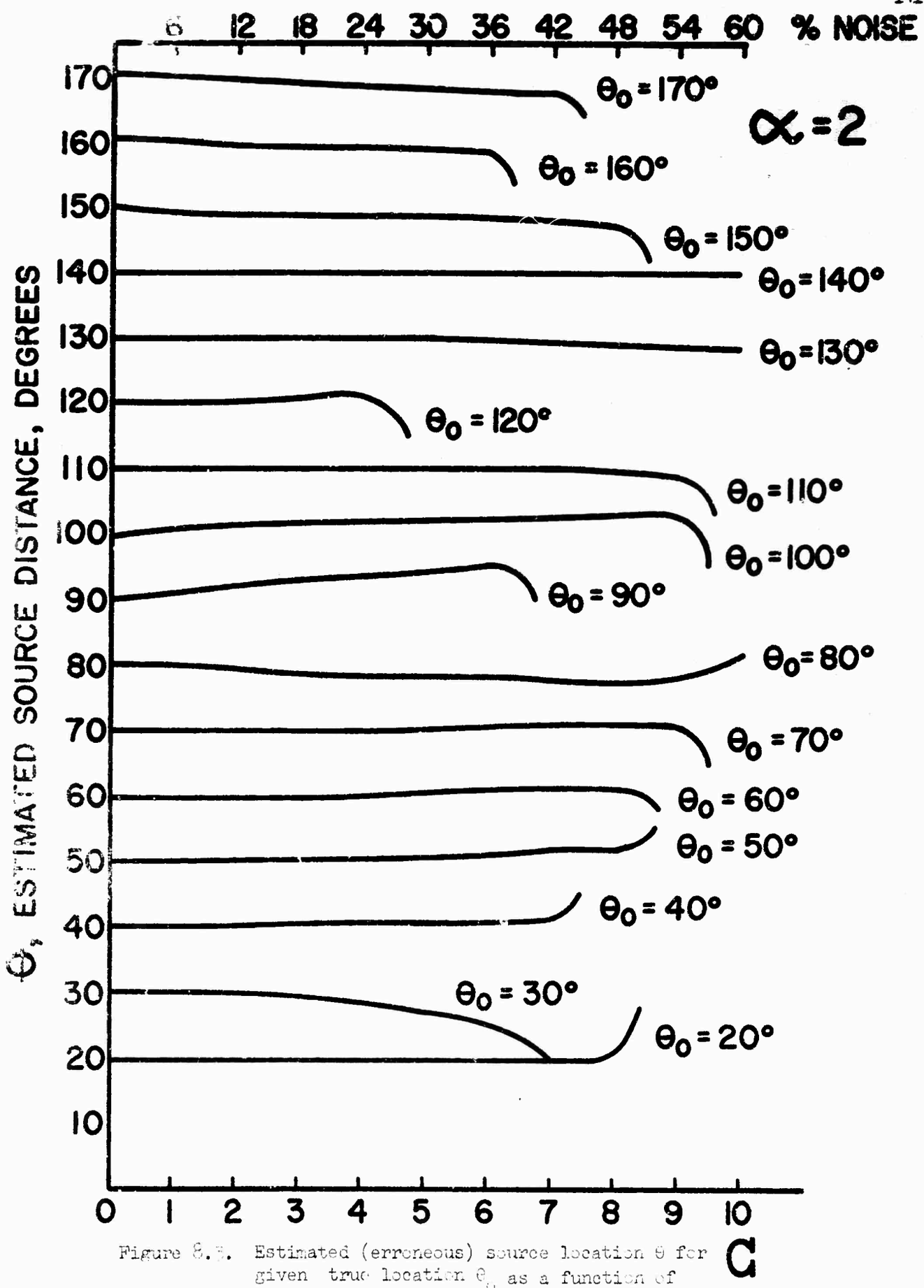

Figure 8.3. Estimated (erroneous) source location θ for given true location θ_0 as a function of additive $Af^{-\alpha}$ noise ($\alpha = 2$).

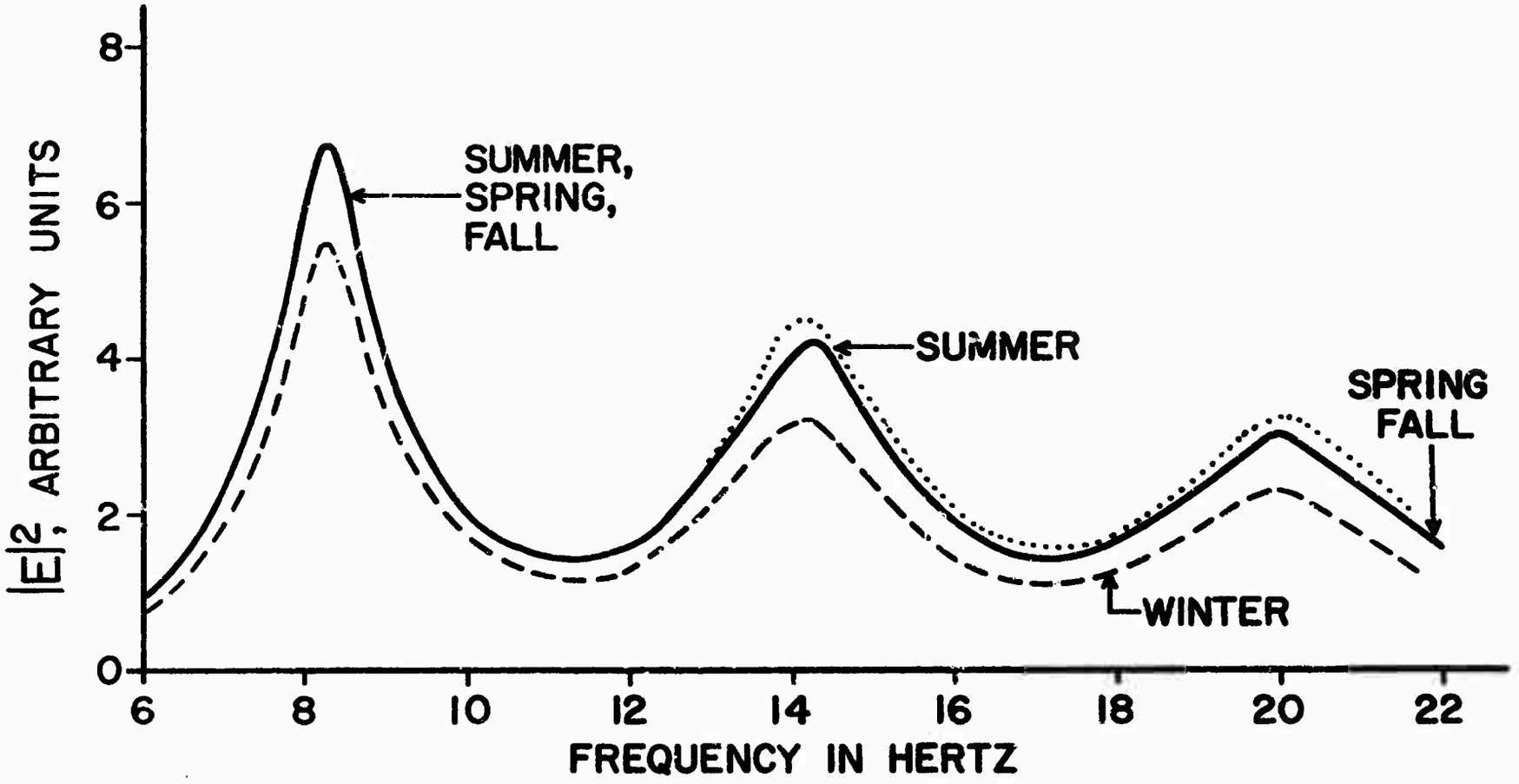

Figure 8.4. Estimated electric field spectra for uniform lightning distribution: summer 10°S to 60°N, winter 40°S to 10°N, fall-spring 30°S to 30°N.

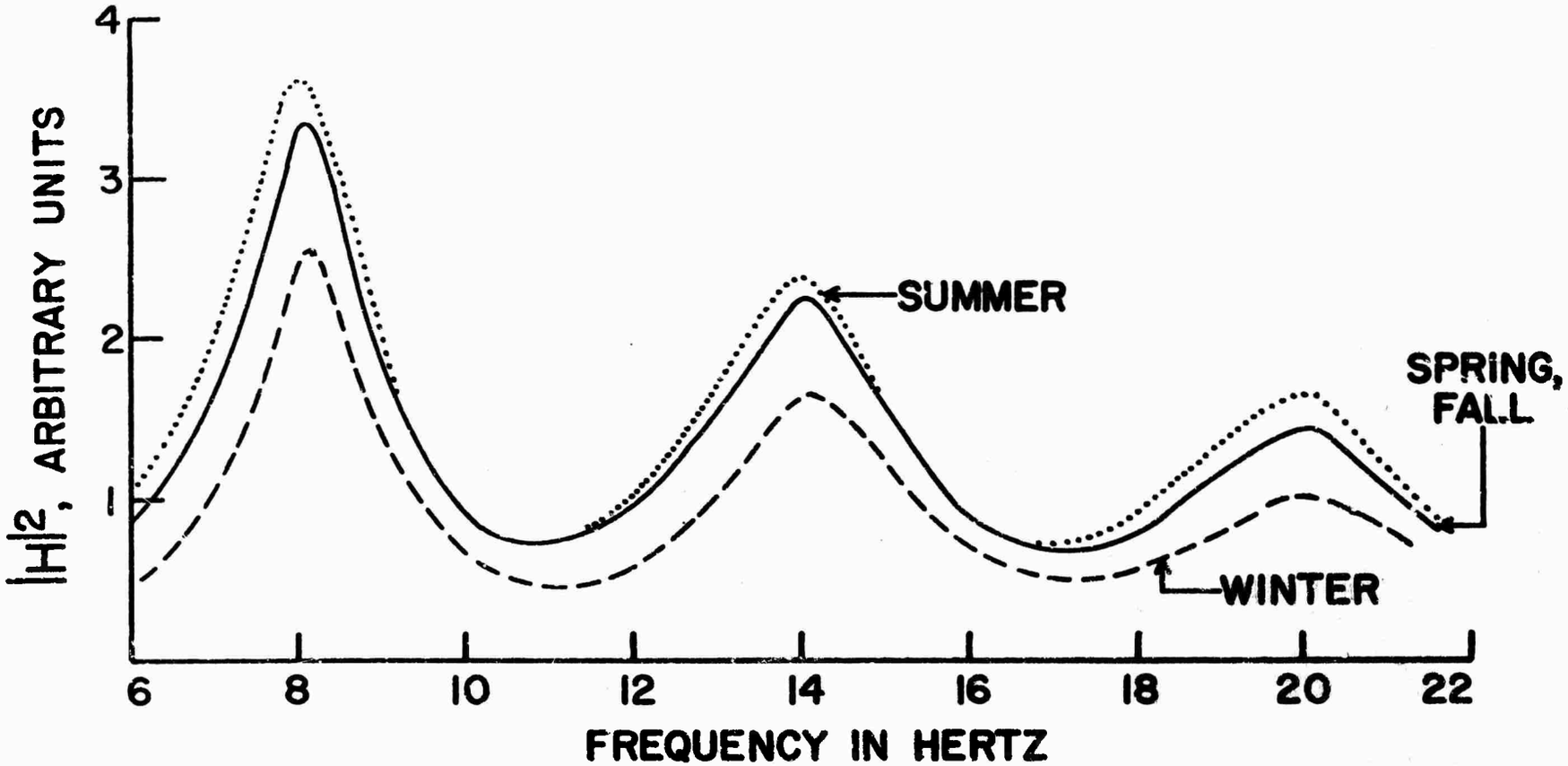

Figure 8.5. Estimated magnetic field spectra for uniform lightning distribution: summer 10°S to 60°N, winter 40°S to 10°N, fall-spring 30°S to 30°N.

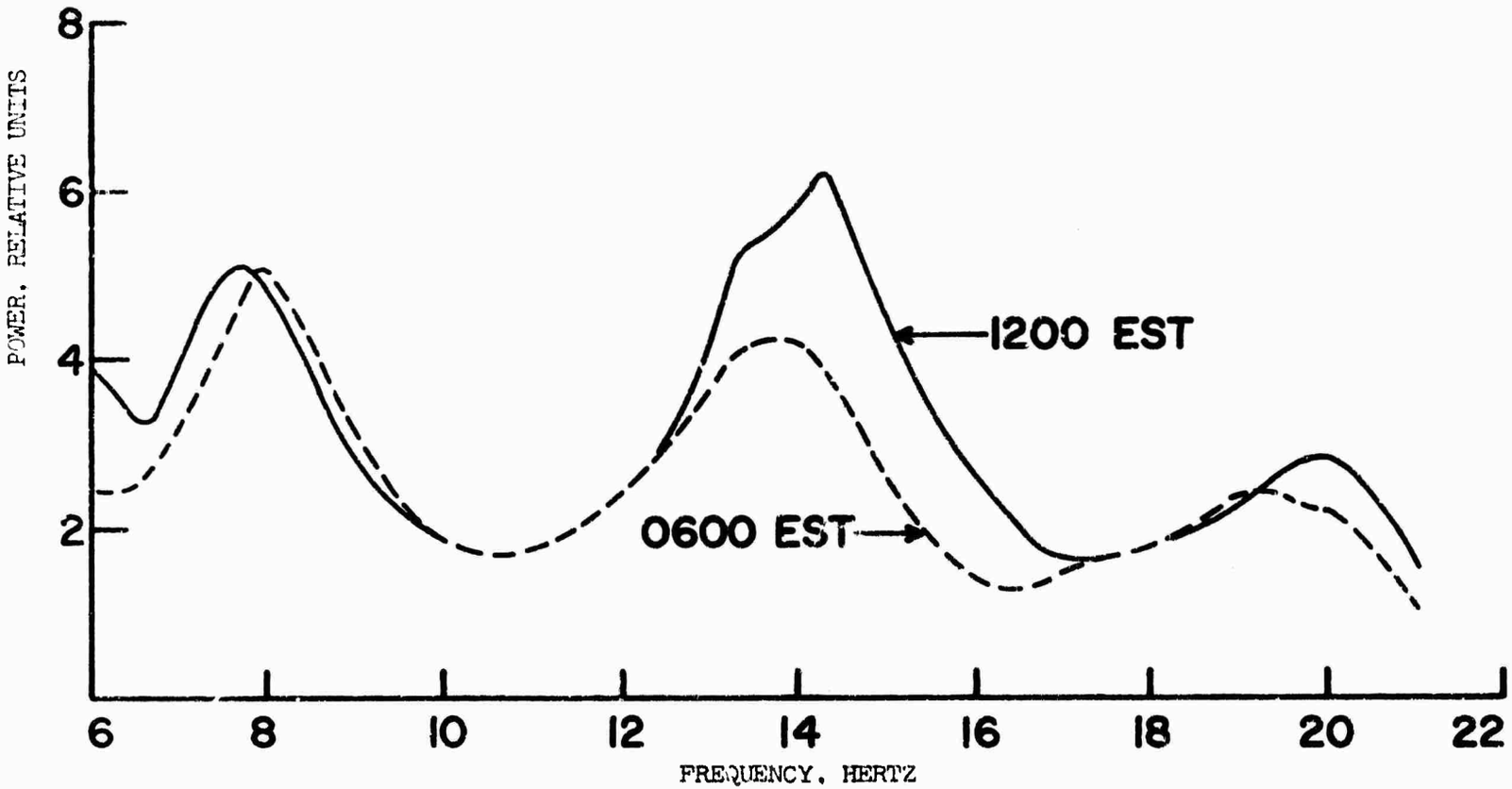

Figure 8.6. E-W magnetic field, February 19, 1957.

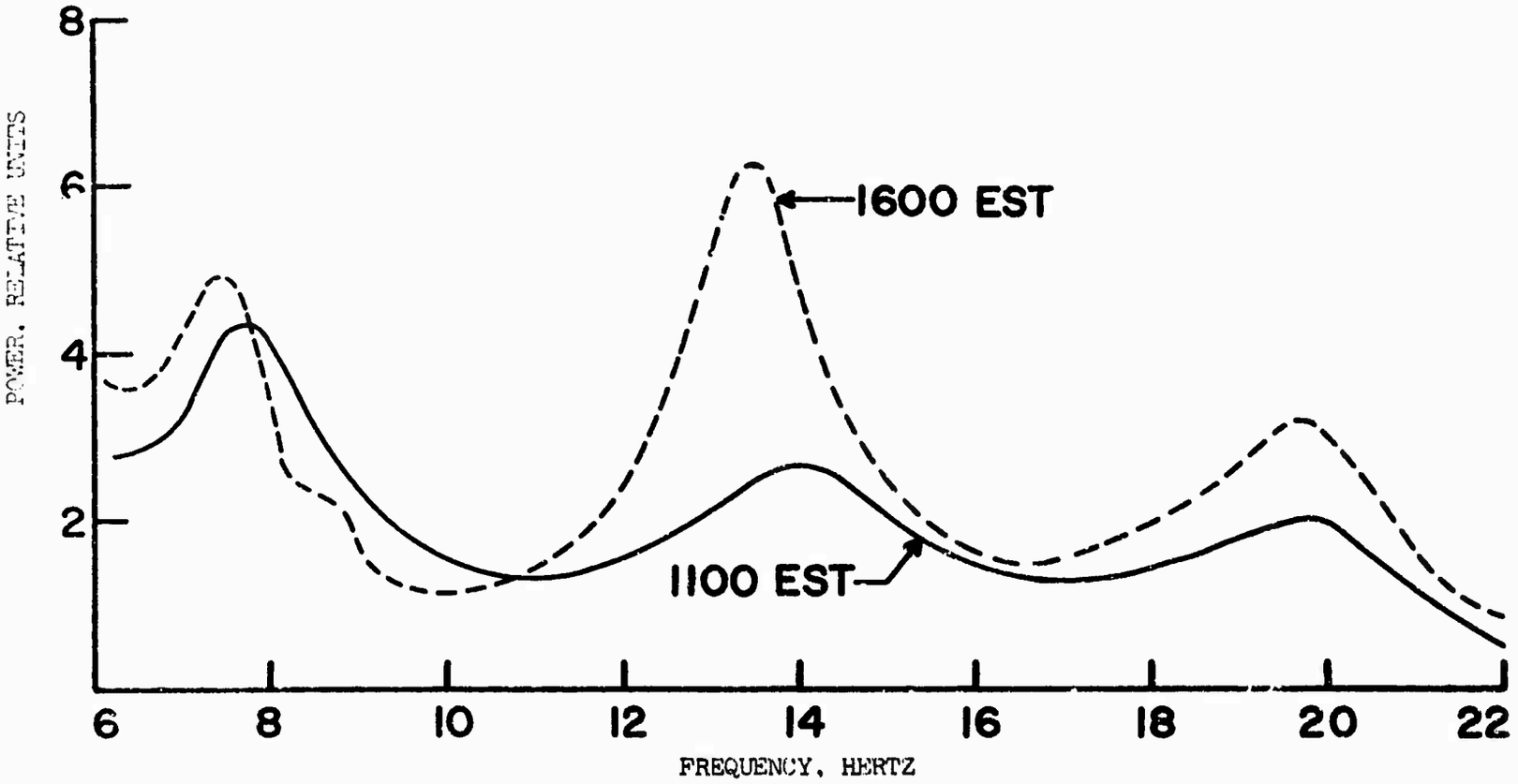

Figure 8.7. E-W magnetic field, March 23, 1967.

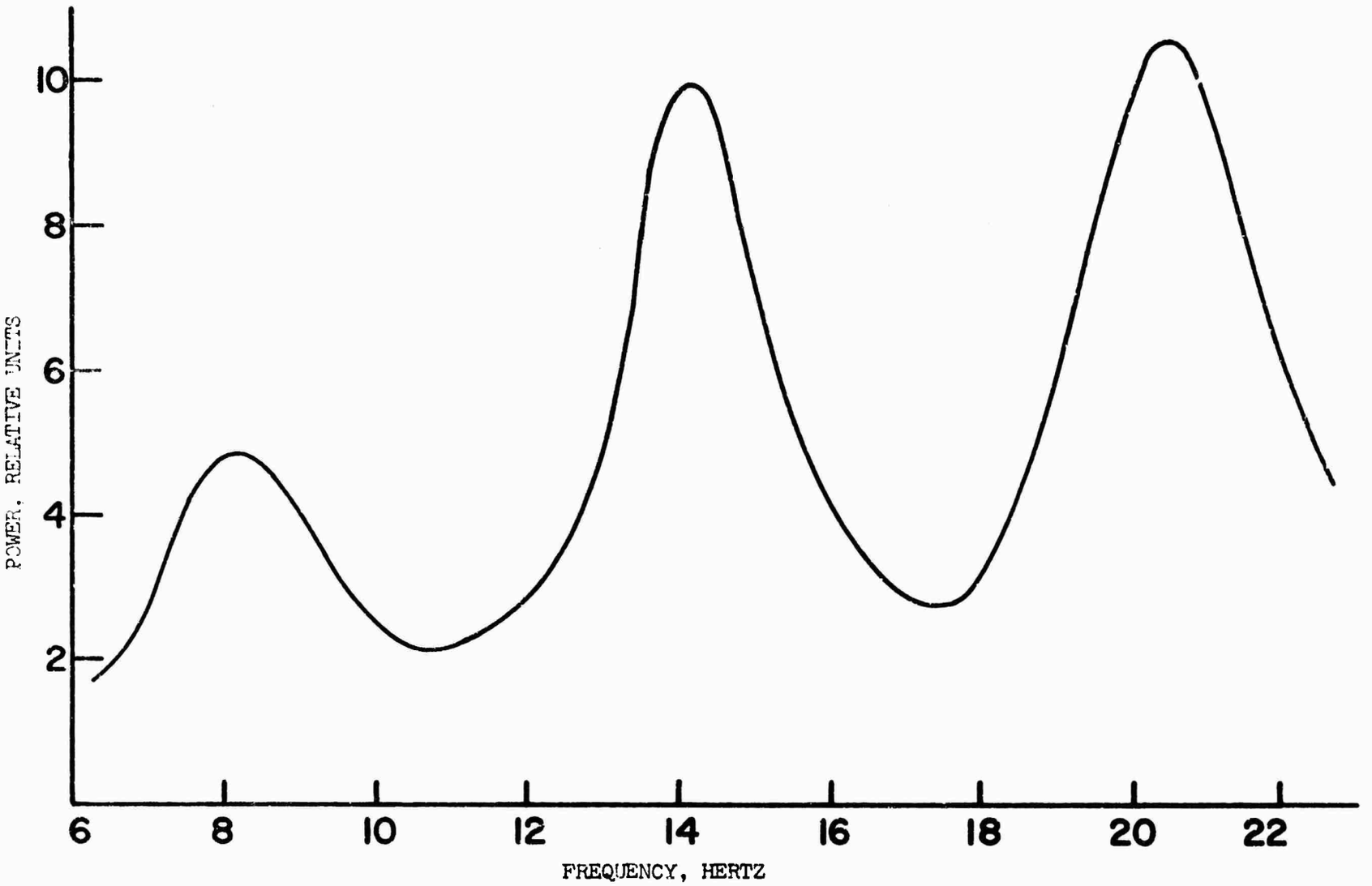

Figure 8.8. Vertical electric field, August 14, 1969, 1400 EST.

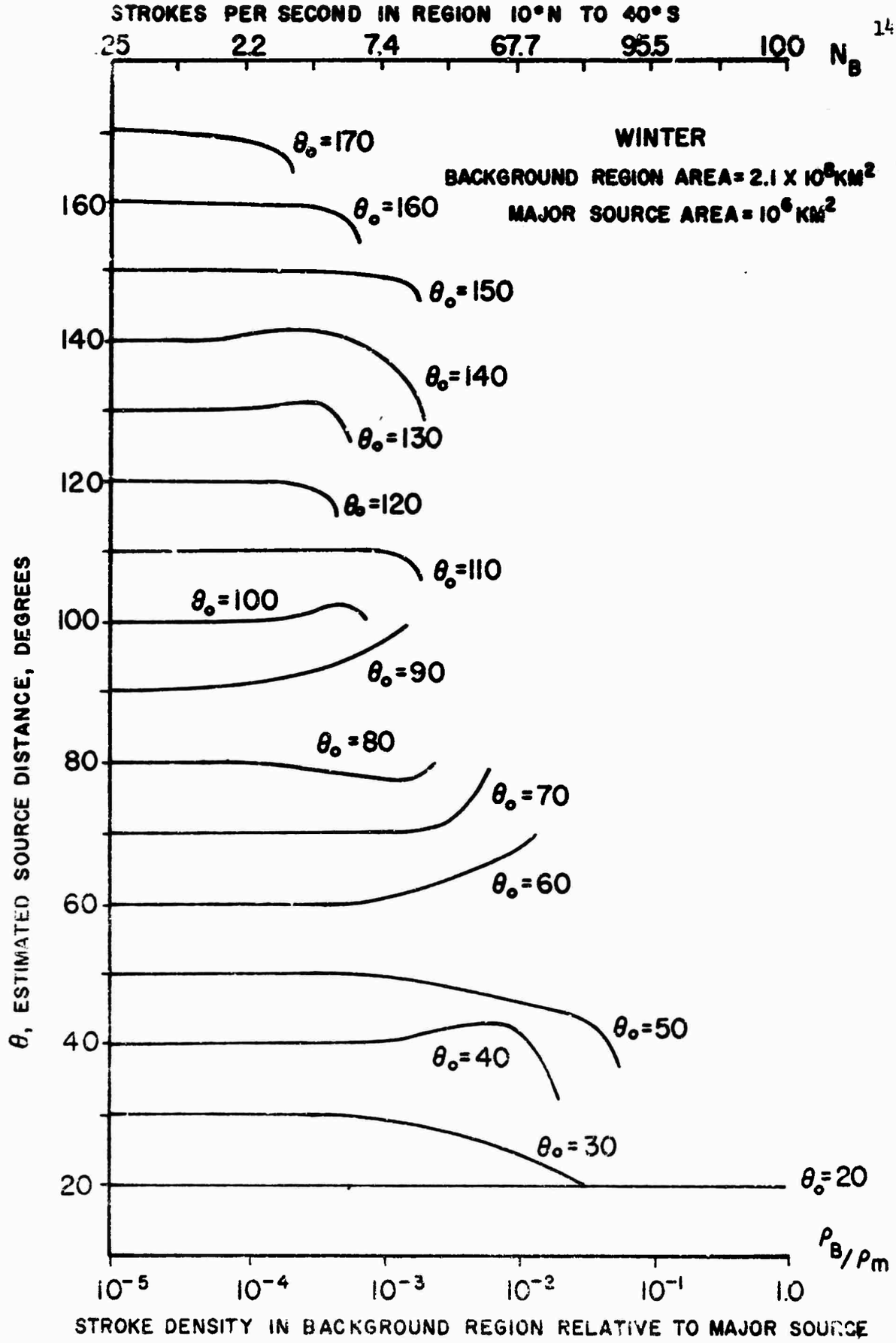

Figure 6.9. Effect of winter background noise on location estimates.

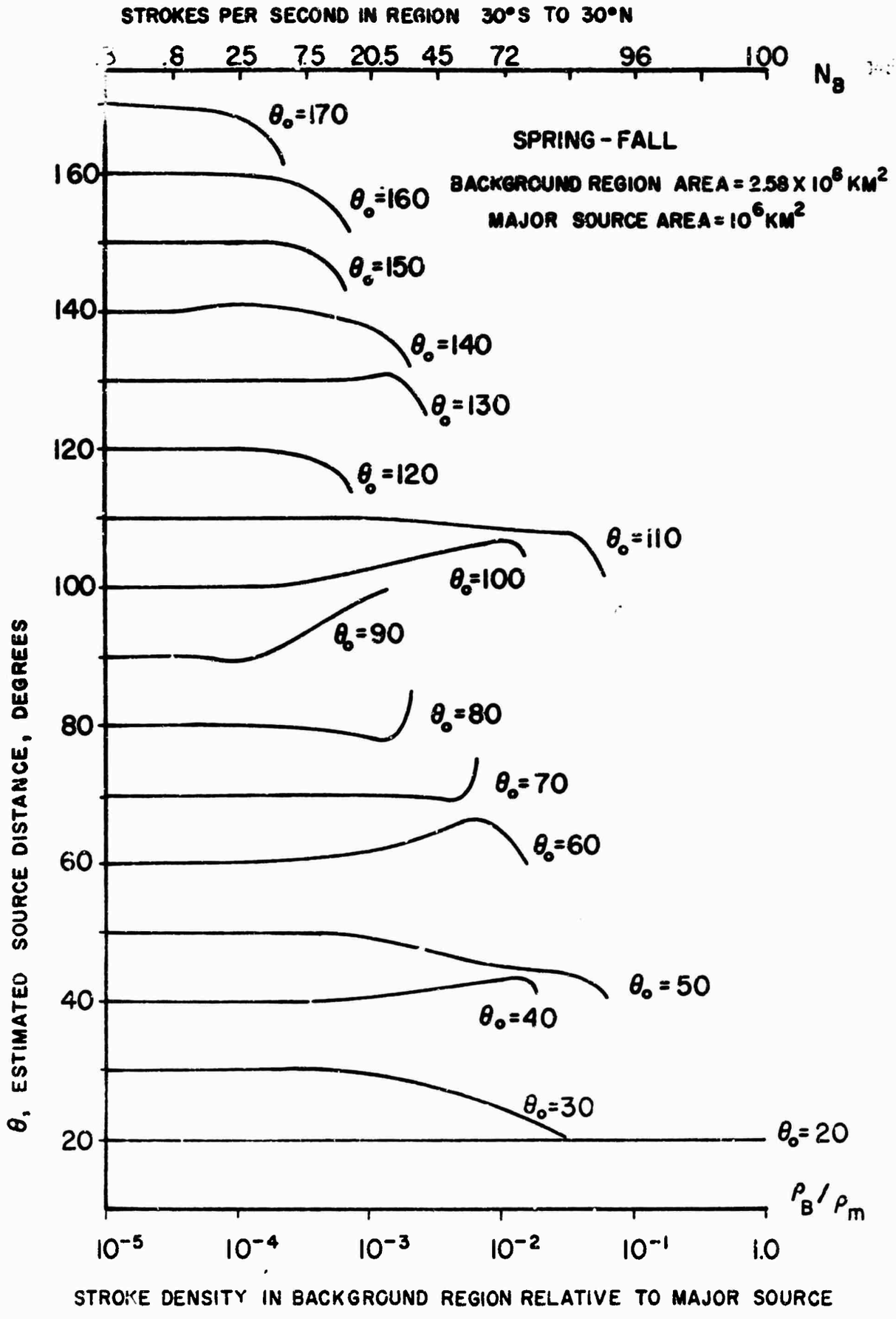

Figure 8.10. Effect of spring-fall background noise on location estimates.

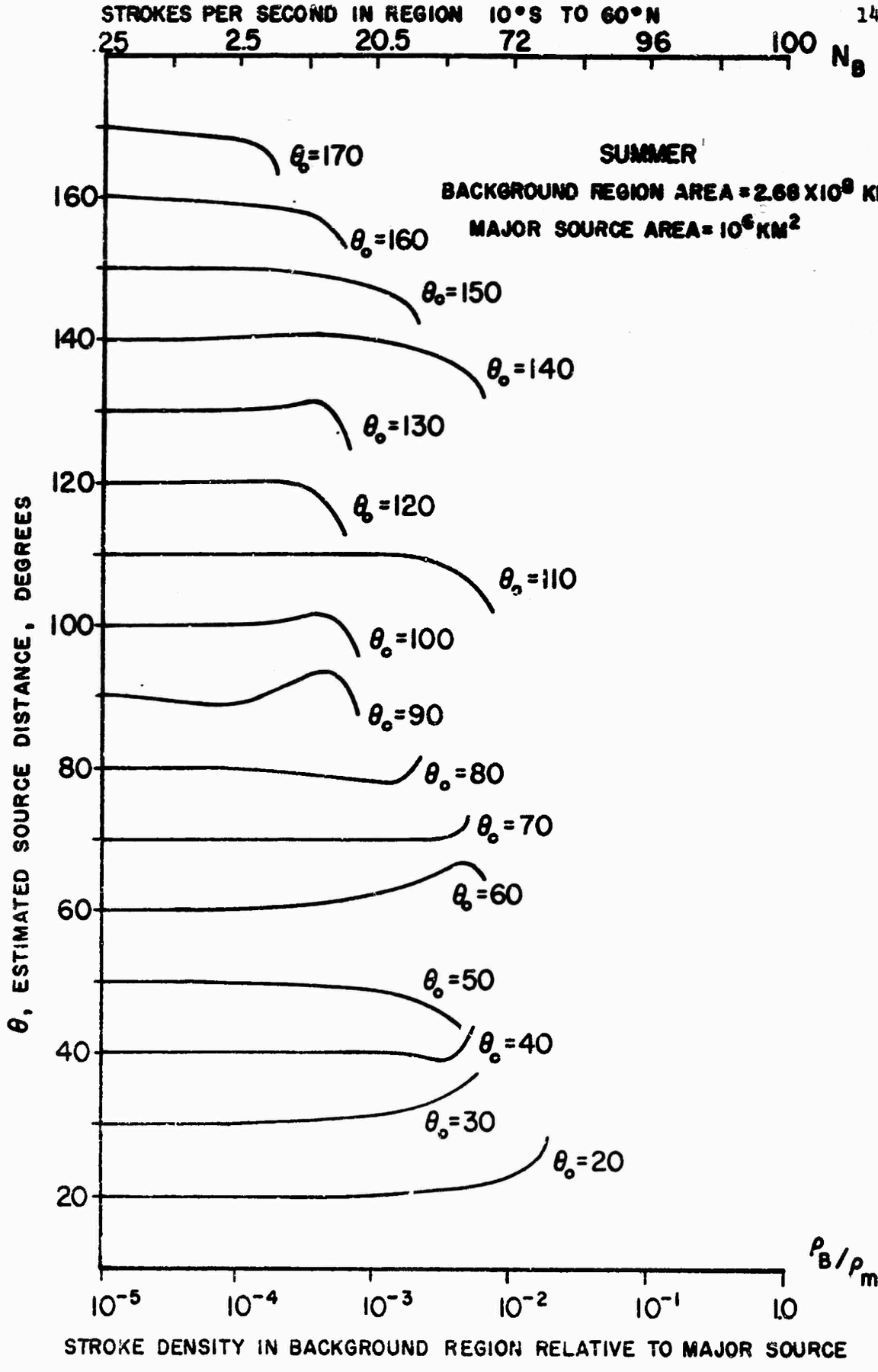

Figure 6.11. Effect of summer background noise on location estimates.

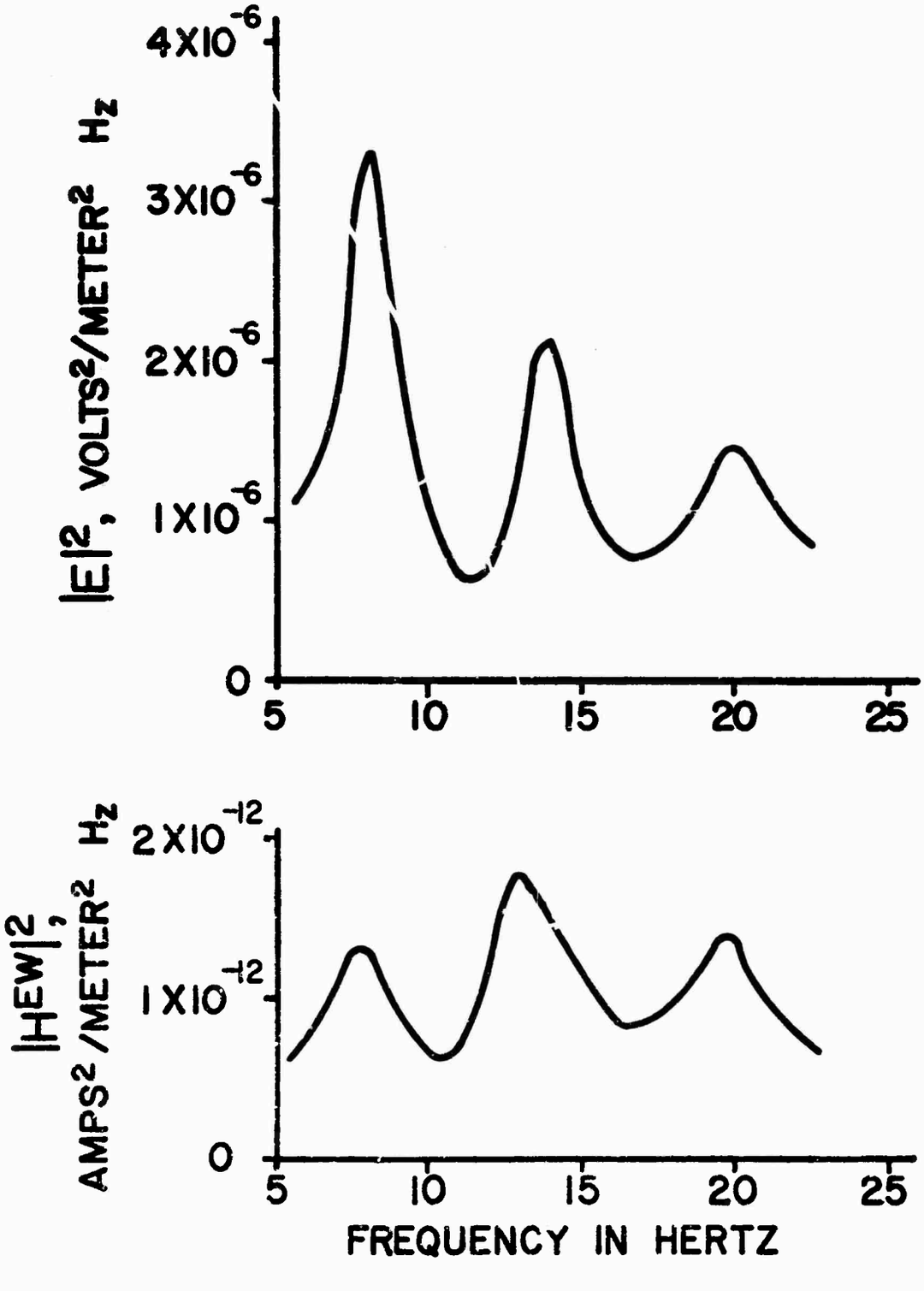

Figure 9.1. Power spectra in Rhode Island at 1700 EST June 6, 1967.

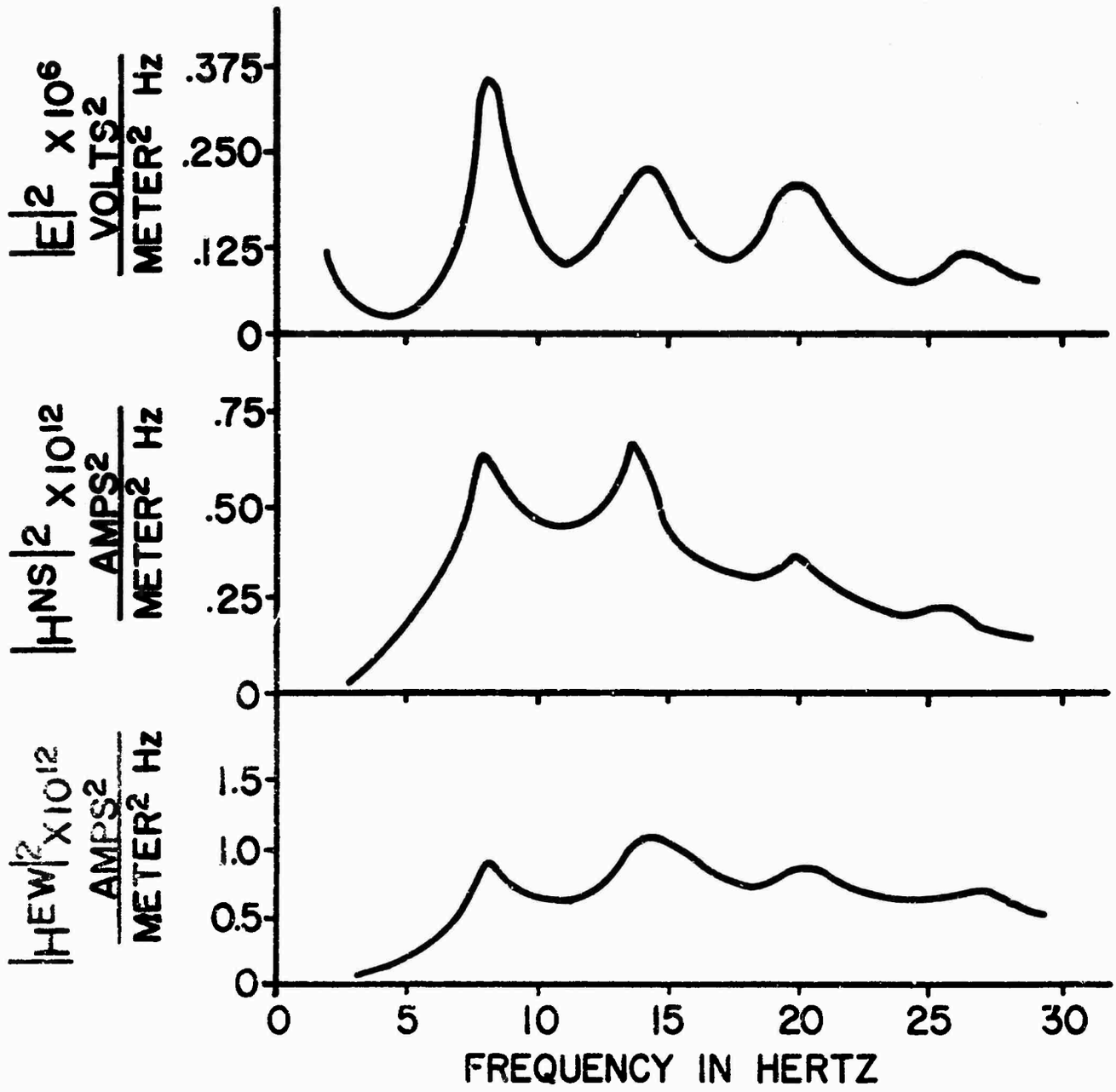

Figure 9.2. Power spectra measured in Rhode Island at 1720-1729 GMT January 1, 1970.

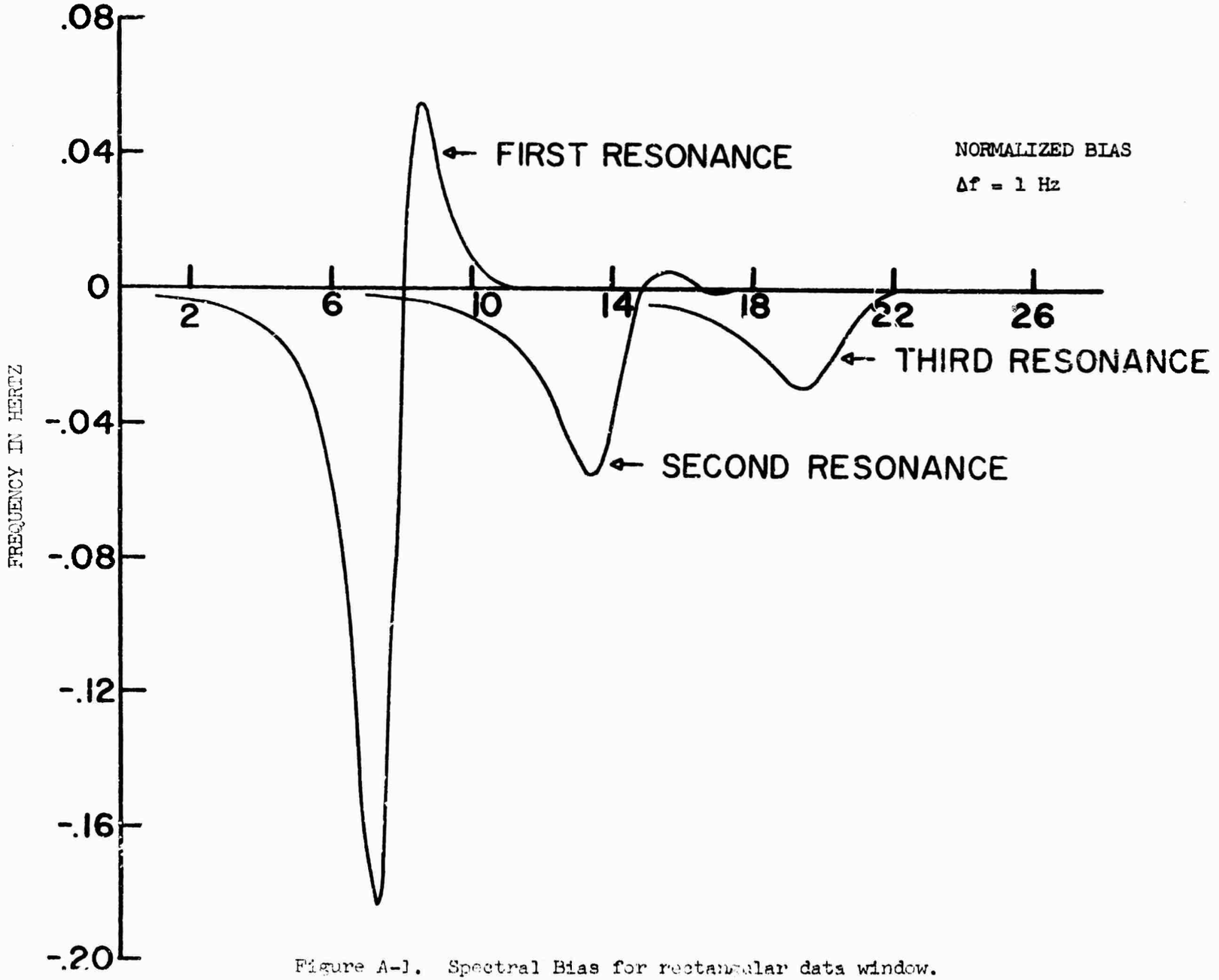

Figure A-1. Spectral Bias for rectangular data window.

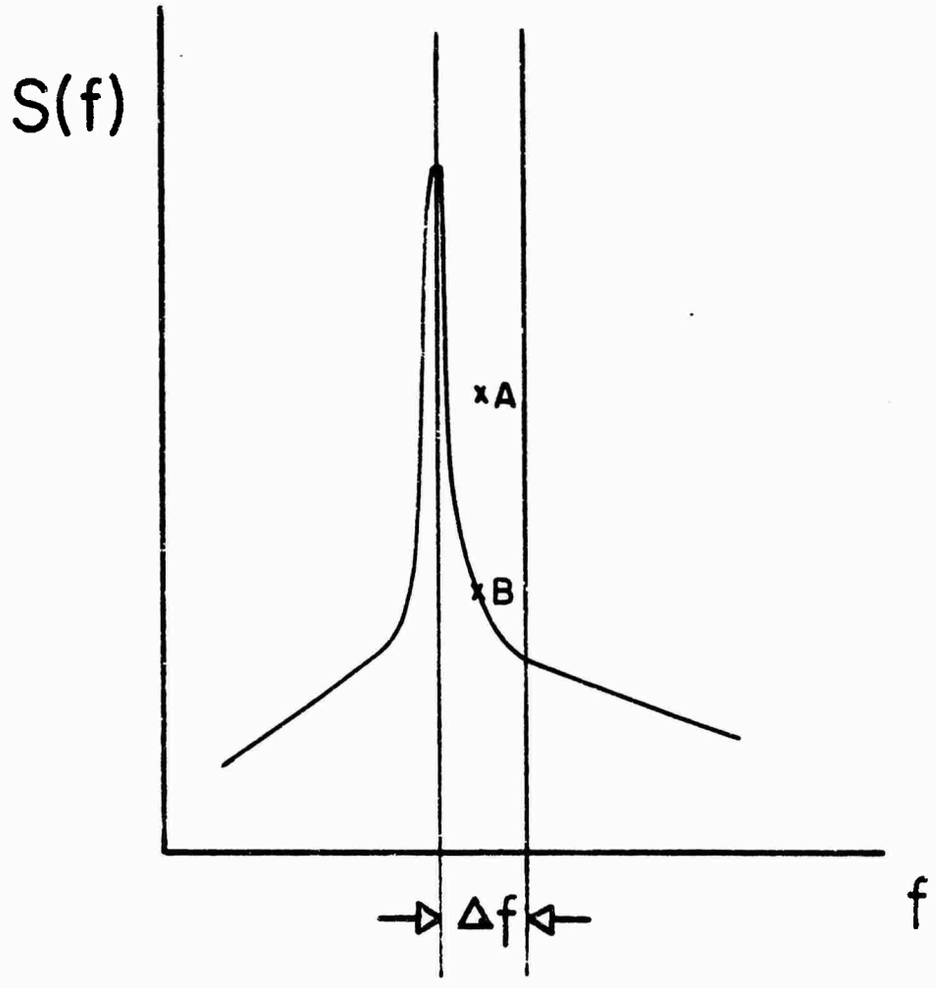

Figure A-2. Bias of a high Q resonance

A-Average power in bandwidth Δf
B-Actual power at center of band

Unclassified
Security Classification

DOCUMENT CONTROL DATA - R & D

(Security classification of title, body of abstract and indexing annotation must be entered when the overall report is classified)

1. ORIGINATING ACTIVITY (Corporate author) University of Rhode Island (Department of Electrical Engineering) Kingston, Rhode Island 02881	2a. REPORT SECURITY CLASSIFICATION Unclassified 2b. GROUP

3. REPORT TITLE
RESEARCH ON EXTREMELY LOW FREQUENCY PROPAGATION WITH PARTICULAR EMPHASIS ON SCHUMANN RESONANCE AND RELATED PHENOMENA PART II: LOCATION OF SOURCES

4. DESCRIPTIVE NOTES (Type of report and inclusive dates)
Scientific. Final. 15 January 1965 to 15 November 1969 Approved 6 May 1970

5. AUTHOR(S) (First name, middle initial, last name)
John Toomey
Charles Polk

6. REPORT DATE	7a. TOTAL NO. OF PAGES	7b. NO. OF REFS
April 1, 1970	168	66

8a. CONTRACT OR GRANT NO.	9a. ORIGINATOR'S REPORT NUMBER(S)
AF 19(628)-4950 b. PROJECT, Task, Work Unit Nos. 5631-10-01 c. DoD Element 61102F d. DoD Subelement 681310	4950/4 Final Report (Part II) 9b. OTHER REPORT NO(S) (Any other numbers that may be assigned this report) AFCRL-70-0226

10. DISTRIBUTION STATEMENT
This document has been approved for public release and sale; its distribution is unlimited. No. 1

11. SUPPLEMENTARY NOTES	12. SPONSORING MILITARY ACTIVITY
TECH, OTHER	Air Force Cambridge Research Laboratories (CRP) L. G. Hanscom Field Bedford, Massachusetts 01730

13. ABSTRACT

Experimental techniques for the measurement of natural extremely low frequency (ELF) electromagnetic noise are described, including methods for absolute calibration of magnetic and electric field sensors in this frequency range (3 to 30 Hz). After a review of the theory applicable to earth-ionosphere cavity resonances a method is developed which permits location of two simultaneously active, major thunderstorm regions on the surface of the earth by analysis of ELF spectra. In particular use is made of electric to magnetic field ratios and of ratios involving the power spectrum magnitudes at adjacent resonant peaks. Limitations of the method are analyzed, particularly those related to $f^{-\alpha}$ background noise (f = frequency) and to quasi-uniformly distributed, minor lightning activity which adds to the noise originating in the major thunderstorm regions. Appropriate methods of spectral analysis—appropriate frequency resolutions and integration times—are determined and the method is illustrated by experimental data. It is also indicated how the source location procedure—in conjunction with exact data (± 0.25 Hz) describing the position of the resonant peaks—may be used to evaluate Ionospheric conductivity profiles extending downward to about 40 km.

DD FORM 1 NOV 65 1473 REPLACES DD FORM 1473, 1 JAN 64, WHICH IS OBSOLETE FOR ARMY USE.

Unclassified
Security Classification

14. KEY WORDS	LINK A		LINK B		LINK C	
	ROLE	WT	ROLE	WT	ROLE	WT
Earth-Ionosphere cavity resonator						
ELF propagation						
Ionosphere, lower						
Lightning location						
Low frequencies						
Power spectrum analysis						
Schumann resonances						
Thunderstorm location						
Waves, electromagnetic						